Materials Horizons

ROYAL SOCIETY OF CHEMISTRY

REVIEW

View Article Online
View Journal | View Issue

Cite this: *Mater. Horiz.*, 2023, **10**, 4083

Porous organic polymers (POPs) for environmental remediation†

Sahel Fajal, ‡[a] Subhajit Dutta ‡[a] and Sujit K. Ghosh *[ab]

Modern global industrialization along with the ever-increasing growth of the population has resulted in continuous enhancement in the discharge and accumulation of various toxic and hazardous chemicals in the environment. These harmful pollutants, including toxic gases, inorganic heavy metal ions, anthropogenic waste, persistent organic pollutants, toxic dyes, pharmaceuticals, volatile organic compounds, *etc.*, are destroying the ecological balance of the environment. Therefore, systematic monitoring and effective remediation of these toxic pollutants either by adsorptive removal or by catalytic degradation are of great significance. From this viewpoint, porous organic polymers (POPs), being two- or three-dimensional polymeric materials, constructed from small organic molecules connected with rigid covalent bonds have come forth as a promising platform toward various leading applications, especially for efficient environmental remediation. Their unique chemical and structural features including high stability, tunable pore functionalization, and large surface area have boosted the transformation of POPs into various macro-physical forms such as thick and thin-film membranes, which led to a new direction in advanced level pollutant removal, separation and catalytic degradation. In this review, our focus is to highlight the recent progress and achievements in the strategic design, synthesis, architectural-engineering and applications of POPs and their composite materials toward environmental remediation. Several strategies to improve the adsorption efficiency and catalytic degradation performance along with the in-depth interaction mechanism of POP-based materials have been systematically summarized. In addition, evolution of POPs from regular powder form application to rapid and more efficient size and chemo-selective, "real-time" applicable membrane-based application has been further highlighted. Finally, we put forward our perspective on the challenges and opportunities of these materials toward real-world implementation and future prospects in next generation remediation technology.

Received 3rd May 2023,
Accepted 10th July 2023

DOI: 10.1039/d3mh00672g

rsc.li/materials-horizons

Wider impact

The environmental release and accumulation of numerous poisonous and hazardous substances has been continuously expanding as a result of modern global industrialisation and the ever-increasing population expansion. Anthropogenic activities such as industrialization and its concomitant adverse effects, are among the forerunners of environmental degradation. In this regard, porous organic polymers (POPs) have emerged as a new class of multifunctional porous materials and received tremendous research attention from both academia and industry. Typically, POPs are constructed from versatile organic small molecules with diverse linkages through strong covalent bonds which result in exciting features like high surface area and porosity, low density, high stability *etc.* Because of such diverse material properties, POPs have been proven to be an excellent platform with exciting opportunities for environmental remediation applications. Consequently, considerable efforts have been devoted to preparation and exploration of POPs with an emphasis on their environmental applications. In this review, we have highlighted the current status and recent advances of various types of POPs towards diverse environmental applications. In addition, different synthetic strategies, functionalization methods and applications of POPs toward environmental remediation have been discussed in detail. This review provides a complete overview of current developments in POP materials from the standpoint of material design approach, synthetic methods, and their applicability in environmental remediation.

[a] *Department of Chemistry, Indian Institute of Science Education and Research, Dr Homi Bhabha Road, Pashan, Pune 411008, India.*
E-mail: sghosh@iiserpune.ac.in; Web: https://skg-lab.acads.iiserpune.ac.in/home; Tel: +91 20 2590 8076
[b] *Centre for Water Research, Indian Institute of Science Education and Research, Dr Homi Bhabha Road, Pashan, Pune 411008, India*

† Electronic supplementary information (ESI) available. See DOI: https://doi.org/10.1039/d3mh00672g

‡ These authors contributed equally.

1. Introduction

The last century has witnessed a rapid upsurge in the global population which has led to immense expansion in industrial and agricultural sectors. Such extensive anthropogenic activities consequently generate environmentally harmful industrial and agricultural waste in huge amounts, contributing significantly

toward several environmental issues, such as global warming, contamination of soil, air and natural aqueous matrices, *etc.*[1–3] Additionally, the rapid depletion of fossil fuels because of the enormous global energy demand constitutes a genuine threat to the development and survival of mankind.[4,5] To this end, development and exploration of novel materials for task-specific applications are of fundamental importance for sustainable socio-economic progress and advancement toward a clean environment.[6] The emergence and promising growth of nanomaterials in the past few decades have highlighted the key role of porosity of a material in its performance superiority in various applications.[7–9] Hence, porous materials hold paramount importance in many emerging applications and technologies owing to their several fascinating intrinsic properties such as large surface area, diverse synthetic possibilities, tunable architecture, *etc.* Especially, the past few decades have witnessed the emergence and development of a variety of novel micro-, meso- and even macro-porous materials such as metal–organic frameworks (MOFs), covalent-organic frameworks (COFs), and porous organic polymers (POPs).[10–15] Amongst these novel materials, POPs have attracted tremendous scientific attention recently owing to their unique advantage of combining the properties of both polymers and porous materials (Scheme 1).[16–18] POPs represent the class of metal free organic materials, constructed from purely organic monomers made of mostly light elements (C, H, O, N, B, *etc.*) into macromolecular scaffolds. Typically, POPs offer several structural and physiochemical advantages over other traditional as well as contemporary porous materials which make them frontrunners as the next-generation multipurpose functional material.[19,20] For example, in comparison with the traditional inorganic materials such as activated carbon and zeolite, POPs offer several advantages like light skeletal density, high physicochemical stability, large surface area and so on. Furthermore, on demand functional moieties can also be incorporated into the POP structures *via* both pre-synthetic and post-synthetic modifications. By virtue of the liberty in monomer design and the endless variety in chemical reactions, there exist enormous possibilities to dial in any functionality in principle *via* pre-synthetic methods of POPs. On the other hand, post-synthetic modification can be utilized as a powerful tool to expand the functional versatility of the porous architecture.[21–24]

Owing to their intrinsic polymeric character, POPs offer excellent good shapeability and extendibility, rendering leverage towards molding into various macromorphologies (*e.g.*, membrane, bead, monolith, fiber, *etc.*). Such exciting features render POPs as a next-generation multifunctional platform for diverse applications and future technologies (Scheme 2).[16,25] Interestingly, porous polymers such as ion-exchange resins have a long history as a utility material toward water treatment, the pharmaceutical industry, the food industry, petrochemical engineering, synthetic chemistry, environmental protection, *etc.*[6] Recent years have witnessed a significant growth of POP-based research activity toward several burgeoning fields such as gas storage/separation, molecular recognition, electrochemical energy storage, catalysis,

Sahel Fajal

Sahel Fajal received his Bachelor's degree and Master's degree in Chemistry from Aligarh Muslim University (India). He joined Prof. Sujit K. Ghosh's group at the Indian Institute of Science Education and Research (IISER) Pune in 2017 as a PhD student. As a senior research fellow, his current research work is focused on the development of advanced functional porous materials and their hybrid composites for efficient-alternative and energy-intensive chemical separation application.

Subhajit Dutta

Dr. Subhajit Dutta obtained his BSc (Chemistry) from the University of Calcutta in 2014 and MSc (Chemistry) from the University of Calcutta in 2016. Thereafter, he joined the Indian Institute of Science Education and Research (IISER), Pune, as a PhD student under the supervision of Prof. Sujit K. Ghosh and completed his PhD in 2022. Subsequently, Subhajit joined BCMaterials (Basque Center for Materials, Applications and Nanostructures; Spain) to pursue his post-doctoral research work under Prof. Stefan Wuttke. His current research interests embrace the development of next-generation functional porous materials that foster environmental sustainability.

Sujit K. Ghosh

Sujit K. Ghosh is Professor of Department of Chemistry at Indian Institute of Science Education and Research, Pune, India. His current research interest is primarily focused upon the development of advanced functional porous materials (such as metal–organic frameworks (MOFs), porous organic polymers (POPs), metal–organic polyhedra (MOPs), porous hybrid composites, etc.) for clean energy and safe drinking water.

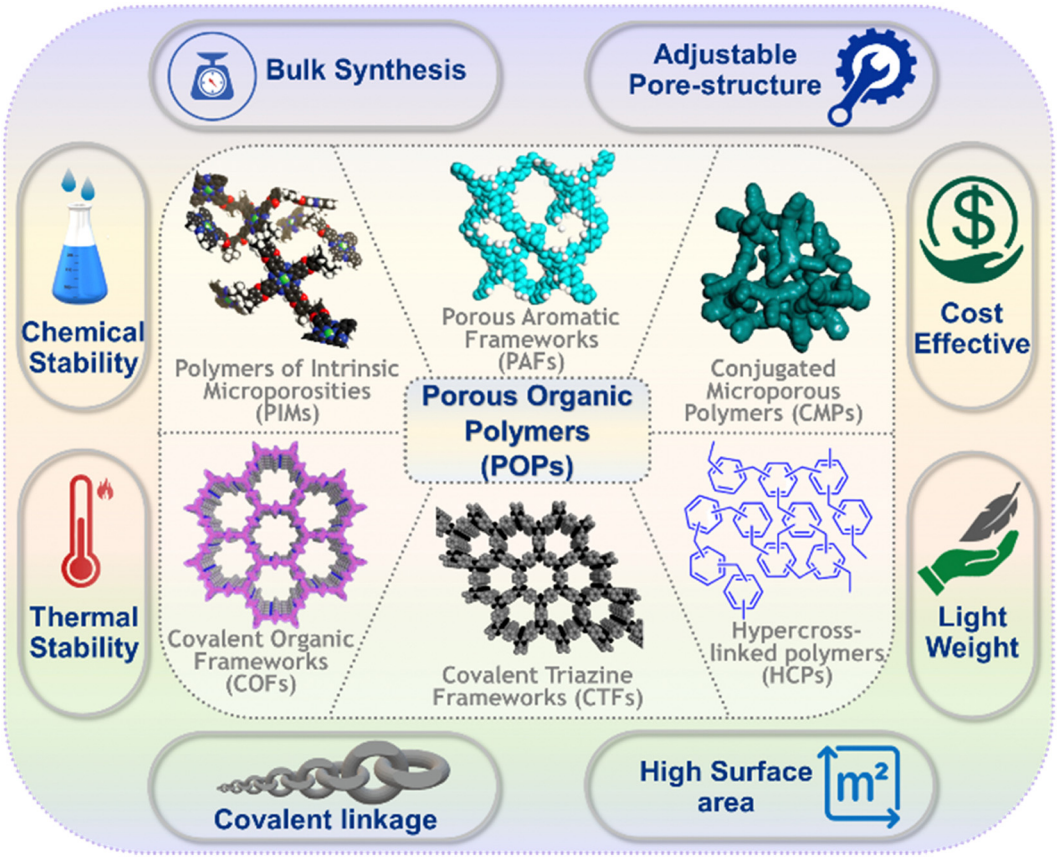

Scheme 1 Representation of examples of different types of POPs such as PIMs,[55] PAFs,[38] CMPs,[58] HCPs,[41] CTFs,[36] and COFs[35] and their potential properties including strong covalent linkage, adjustable pore-structure, high surface area, chemical and thermal stability, light weight/low density, scalable synthesis, and cost effective production. Reproduced with permission from ref. 55. Copyright 2007, The Royal Society of Chemistry; reproduced with permission from ref. 38. Copyright 2009, Wiley-VCH; reproduced with permission from ref. 58. Copyright 2008, American Chemical Society; reproduced with permission from ref. 41. Copyright 2014, American Chemical Society; reproduced with permission from ref. 36. Copyright 2008, Wiley-VCH; reproduced with permission from ref. 35. Copyright 2016, Nature Publishing Group.

photo-energy conversion in solar cells, drug delivery, proton conduction, and so on.[26–30] In order to explore the potential of POPs, several research groups have delved into different subclasses of POP materials, including covalent triazine frameworks (CTFs), porous aromatic frameworks (PAFs), covalent organic frameworks (COFs), hypercrosslinked polymers (HCPs), polymers of intrinsic microporosity (PIMs), and conjugated microporous polymers (CMPs) (Scheme 1).[31–38] The chronological development of diverse POP materials and the increasing number of scientific publications relevant to these materials are summarized in Schemes 3 and 4. POPs can be divided into two subclasses mainly depending upon the degree of long-range order: amorphous POPs and crystalline POPs.[18] Amorphous POPs mainly include porous aromatic frameworks (PAFs), hyper-crosslinked polymers (HCPs), conjugated microporous polymers (CMPs) and polymers of intrinsic microporosity (PIMs), while crystalline POPs are represented by covalent organic frameworks (COFs). It is noteworthy to mention that the prime objective of this review article is to summarize and highlight the design principles of amorphous POPs and their applications in environmental remediation. Hence, all the crystalline POPs, such as COFs, are excluded from this specific review. In addition to the structural diversity, POPs can be divided into two classes depending upon the charge neutrality of the network: ionic porous organic polymers (iPOPs) and neutral POPs.[39] iPOPs can be further divided into two, cationic POPs and anionic POPs. iPOPs are organic porous networks with abundant ionic sites inside the network. iPOPs provide unique windows of opportunities for fine-tuning the ionic functionality and the electrostatic interactions of the host network material, which plays a crucial role in improving host–guest interactions and efficiency as a sorbent material.

Considering the rapid growth in scientific research (Scheme 4) and future potential of these emerging materials, herein we present a comprehensive review to highlight the current status and recent advances of various types of POPs towards diverse environmental applications. In the subsequent sections, we give an overview of various subclasses of POPs and their unique structural properties. Further, their different synthetic strategies and functionalization methods are highlighted. Afterwards, a detailed discussion is provided regarding the applicability of POPs toward environmental remediation, including toxic gas adsorption and separation, pollutant sensing, pollutant removal, and heterogeneous catalysis (Scheme 2). Finally, we also highlight the current challenges, windows of opportunities and future

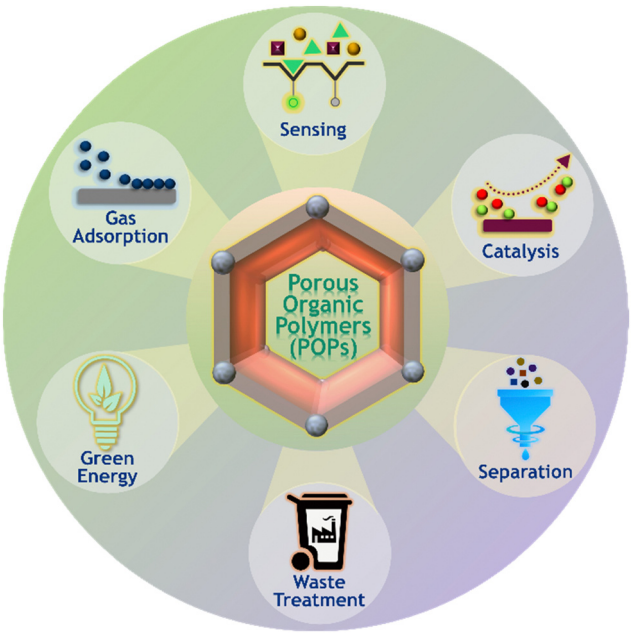

Scheme 2 Representative examples of applications of POPs towards waste treatment, chemical sensing, gas adsorption, heterogeneous catalysis, molecular separation, green energy, biomedicine, *etc.*

perspective of these promising materials for environmental remediation.

2. Basic design principle and different types of POPs

The POP-based research activities in the past years have evolved with significant synergistic contribution from the ever-developing modern organic synthesis, emerging nanotechnologies and advanced polymerization techniques. Typically, synthetic methods of POPs involve various physical methods including interface polymerization, emulsion polymerization, suspension polymerization, polycondensation, hyper-crosslinking, phase separation, templating, phase inversion, drying, stretching, *etc.*[6] In addition, POP synthesis is also associated with different modern bond-forming methodologies such as metal-catalyzed coupling, boronic acid condensation, Friedel–Crafts alkylation, imine formation and so on.[17] Numerous synthetic strategies based on the pre-synthetic approach (bottom-up) and post-synthetic modification have been developed. In the case of pre-synthetic design, the desired functional building blocks are chosen directly for POP fabrication. However, to address the few existing limitations associated with the pre-synthetic methods, such as structural defects, economic factors and other considerations, post-synthetic modification-based methods have emerged as an important alternative tool, providing a convenient solution to the above-mentioned problems.[21–23] Nonetheless, by virtue of the diverse organic reaction choices and rational design of monomers, the fabrication of POPs leads to diverse structural topologies, dimensionalities and physiochemical porosities. To this end, design of POP materials involves three main aspects, *i.e.*, geometrical aspects, topological aspects and diverse functionality aspects.

Geometrical aspects: The prime prerequisite for the formation of a POP network is to have building blocks with at least two functional reactive groups. There are two main approaches to fabricate POPs: (1) homo-coupling of the building units *via* self-condensation reactions and (2) cross-coupling of building units with distinct geometrical properties to create a 3D polymeric architecture. In both cases, formation of covalent bonds results in 3D networks with fixed nanopores and permanent porosity of the POP.[40]

Topological aspects: The topological consideration of POPs is crucial from both design and control over the structural connectivity aspects of the materials. Understanding the topological characteristics of porous materials can be beneficial for strategic design and manifestation of such materials. The topology of amorphous porous organic materials can be explained *via* two topological models: (1) continuous random network (CRN) model and (2) ideal amorphous solid (IAS) model.[17] Goodwin *et al.* have comprehended the topology of amorphous POPs by the CRN model. According to this model, the building units of a particular material are connected to each other in an extended three-dimensional network structure which is intrinsically random as well as continuous. Glass and silica are among the most studied materials with this model. On the other hand, the IAS model is the lesser explored one for topological examination of porous organic materials. Developed by Stachurski *et al.*, this model engages with the absence of any kind of order (short, medium, long) and exquisite random packing of the building units.

Diverse functional groups: Different chemical systems such as diverse aromatic systems, arenes, various heterocyclic units, porphyrin units, different imidazolium units, phenylethynylene derivatives, macrocyclic systems, *etc.* have been explored as the building blocks for POP synthesis. Reactive groups, such as aromatic boronic acids, bromoarenes, iodoarenes, various arene moieties, aromatic aldehydes, aromatic amines, *etc.*, are widely used for the synthesis of POPs. The merits of diverse building blocks along with the wide range of functional groups endow POPs with unique structural and physiochemical properties.[40]

2.1 Introduction to different types of amorphous POPs

2.1.1 Hyper-cross-linked polymers (HCPs). HCPs are the oldest amorphous POP materials endued with microporosities, impressive surface areas and low densities. HCPs are mostly synthesized using Friedel–Crafts alkylation chemistry which is considerably different from the synthetic protocols for other POP materials.[23] The high degree of cross-linking of HCPs results in several unique properties such as great physiochemical stability, conspicuous swelling, *etc.* The synthesis of HCPs offers various advantages, such as inexpensive reagents, mild reaction conditions, monolithic products, *etc.*, which in combination help in their large-scale production.[41,42] Owing to their exciting structural and physiochemical properties, HCPs have shown excellent promise toward various applications including gas storage and separation, pollutant sensing and removal, catalysis, *etc.*[23] Synthesis of HCPs involves three main techniques, namely, direct one-step polycondensation, post-cross-linking of polymers, and

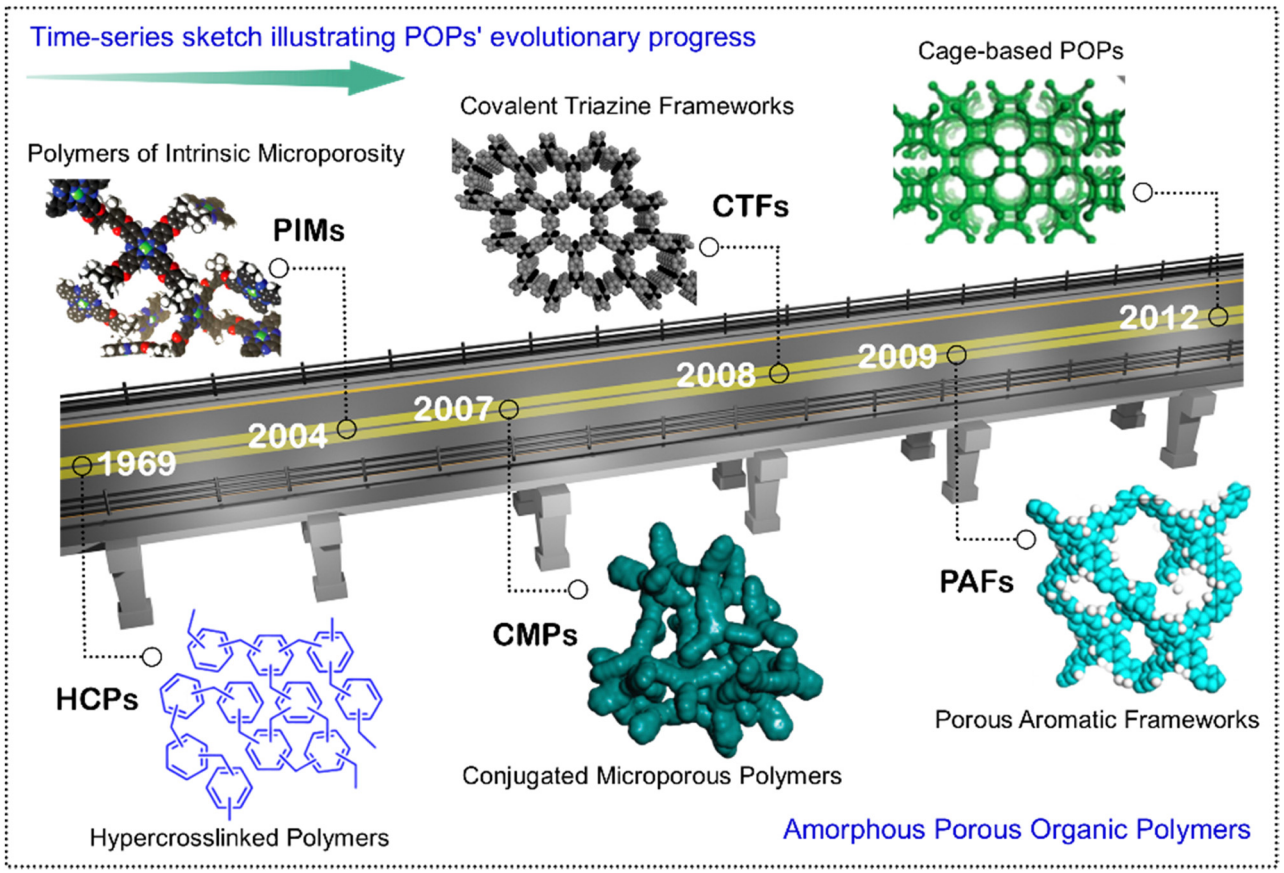

Scheme 3 An overview of the development of amorphous porous organic polymers over time, covering key advancements in the synthesis of novel POPs. From the left, 1969, first reported HCP,[41] 2004, discovery of PIMs,[55] 2007, first development of CMP (CMP-1),[58] 2008, discovery of CTF,[36] 2009, first reported PAF (PAF-1),[38] 2012, first development of cage-based POPs172. Reproduced with permission from ref. 41. Copyright 2014, American Chemical Society. Reproduced with permission from ref. 55. Copyright 2007, The Royal Society of Chemistry. Reproduced with permission from ref. 58. Copyright 2008, American Chemical Society. Reproduced with permission from ref. 36. Copyright 2008, Wiley-VCH. Reproduced with permission from ref. 38. Copyright 2009, Wiley-VCH; Copyright 2005, American Association for the Advancement of Science. Reproduced with permission from ref. 172. Copyright 2018, Wiley-VCH Verlag GmbH & Co. KGaA, Weinheim.

utilization of external cross-linkers. In the 1960s, Davankov *et al.* reported the first example of hyper-crosslinked polystyrene.[43] They further continued to synthesize HCPs with polystyrene as a precursor while exploring different cross-linkers such as chloromethyl methyl ether, *p*-xylylenedichloride, *etc.* for which they achieved the maximum BET surface area of 1106 $m^2\ g^{-1}$.[44–46]

Thereafter, they also explored vinylbenzyl chloride-divinyl benzene as a precursor with which they achieved a BET surface area of 2090 $m^2\ g^{-1}$.[47] The customization of the pore size of HCPs by changing the divinylbenzene precursor concentration and the hyper-cross-linking conditions was established by Tan *et al.*[48] Such a strategy is useful for the controlled manipulation of the porous character of HCPs. On the other hand, utilization of external cross-linkers for the synthesis of HCPs was first reported by Tan and co-workers in 2011.[49] This strategy offers an easy pathway to connect aromatic units through external cross-linker knitting. Moreover, this strategy opened a new avenue in the design and fabrication of HCPs as it allows the utilization of a wide range of functional monomers without any modification.

2.1.2 Polymers of intrinsic microporosity (PIMs). PIMs are amorphous microporous POPs fabricated from mostly rigid polymeric chains. They feature a series of interconnected aromatic rings chained together with contorted/disfigured sites, depriving them of the ability to pack efficiently. PIMs were first introduced by McKeown *et al.* in 2002.[50,51] They synthesized a phthalocyanine-based POP network *via* adopting a phthalocyanine-generation reaction of a bis(phthalonitrile) monomer. The phthalocyanine-based POPs exhibited BET surface areas in the range of 450–950 $m^2\ g^{-1}$.[52] The same group subsequently reported the fabrication of porphyrin-based POPs by utilizing the dibenzodioxane-generation reaction between the bis-(catechol) monomer and *meso*-tetrakis(pentafluorophenyl)porphyrin. These porphyrin-based POPs exhibited BET surface areas in the range of 900–1000 $m^2\ g^{-1}$.[53] In 2003, the same group reported another series of PIMs, namely, PIM 1–6, among which PIM 1–3 are the classic examples of tuning the porous properties of PIMs *via* altering the comonomer.[54] The solution-processability of PIMs and their thin-film formation abilities are also explored in this report. In 2007, triptycene-based PIMs were reported which

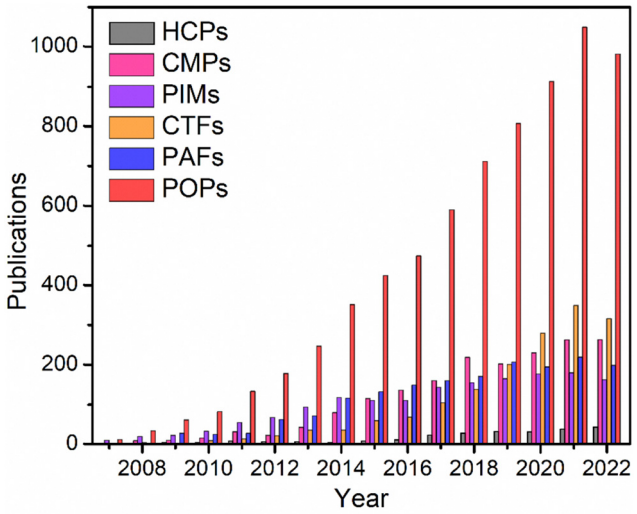

Scheme 4 Comparison of the increasing number of publications on POPs and related materials with the key words "hyper crosslinked polymers" (HCPs), "conjugated microporous polymers" (CMPs), "polymers of intrinsic microporosity" (PIMs), "covalent triazine frameworks" (CTFs), and "porous aromatic frameworks" (PAFs). The result for porous organic polymers (POPs) in each year in the profile is the sum of total publications related to individual categories (source: Web of Science).

exhibited BET surface areas of 1065 $m^2 g^{-1}$.[55] Further it was observed that the BET surface area of triptycene-based PIMs can be improved to 1760 $m^2 g^{-1}$ *via* tuning functionalization. Recent years have witnessed breakthroughs in the mechanochemical approach for strategic synthesis of PIMs which enables green solvent-free reaction and rapid synthesis. Overall, structurally PIMs differ significantly from the other POPs as the inherent flexibility of the polymer chains results in the generation of the porosity of these materials.[56,57] PIMs offer several key advantages such as high surface areas and solubility; the soluble nature of some PIMs makes them promising for the development of POP-based membranes for real-time applications.

2.1.3 Conjugated microporous polymers (CMPs). CMPs are one of the most unique classes of POP materials which offer an extended π-conjugation along with permanent network microporosity.[58–60] Fabrication of CMPs involves linking of rigid aromatic groups, either directly or through double bonds or triple bonds, resulting in π-conjugated microporous structures. Conjugation originates from the alternation of single and double/triple bonds all through the network, which subsequently result in excellent electronic properties. CPMs are intrinsically amorphous in nature because of freedom of rotation about the single bonds between building units.[17] A broad range of network-forming reactions and synthetic building blocks culminate in enormous possibilities of CMPs with diverse properties and structures. In 2007, a series of CMPs, namely, CMP-1, CMP-2, CMP-3 and CMP-4, were synthesized *via* the Sonogashira–Hagihara cross-coupling reaction by Cooper and co-workers.[32] In 2010, the same research group reported the synthesis of another series of CMPs exhibiting high surface areas from tetrahedral monomers.[61] Exploration of tetrakis(4-bromophenyl)-1,3,5,7-adamantane and tetrakis(4-iodophenyl)methane monomers as the precursor was demonstrated to fabricate CMPs *via* the Yamamoto coupling reaction yielding BET surface areas as high as 3180 and 3160 $m^2 g^{-1}$ respectively, which are regarded as the highest surface area of CMP materials. Apart from Yamamoto coupling reactions, several other reactions such as Suzuki–Miyaura cross-coupling, Sonogashira–Hagihara cross-coupling, and phenazine ring fusion reactions are also found to yield very high surface areas of CMPs.[62–65]

2.1.4 Covalent triazine frameworks (CTFs). CTFs started their scientific journey in 2008 from the work of Thomas and co-workers. This exciting genre of POPs was mainly established from the cyclotrimerization of the nitrile functional groups of the nitrile compounds resulting in triazine rings.[66,67] The most classical CTF, namely, CTF-1, was rationalized by the cyclotrimerization reaction of 1,4-dicyanobenzene under iono-thermal conditions.[36] The reaction conditions as well as the concentration of the monomers, reagents and the solvent play crucial roles in the structure and properties of CTFs. In another report, Thomas *et al.* also reported the synthesis of CTF-0 polymers *via* the cyclotrimerization of 1,3,5-tricyanobenzene with $ZnCl_2$ as a catalyst, which exhibited a BET surface area of 232–687 $m^2 g^{-1}$.[67] Although the CTFs synthesized from these ionothermal reactions exhibit good surface area, they also involve a few limitations such as complex reaction conditions, elevated temperature, and problems in complete separation of $ZnCl_2$ at the end of the reaction. To address these issues, Cooper and co-workers came up with a unique strategy wherein trifluoromethanesulfonic acid is used as a catalyst and they reported a series of CTFs fabricated from aromatic nitriles as monomers under microwave heating conditions at room temperature.[37] These CTFs were found to be semi-amorphous in nature, but the level of orderliness could be controlled *via* tuning the microwave heating conditions.

2.1.5 Porous aromatic frameworks (PAFs). PAFs are another classical example of open framework POP materials offering excellent stability and surface area. The presence of rigid phenyl units along with the formation of covalent bonds results in excellent physio-chemically stable PAF materials.[68] The prime difference between PAFs and CMPs is that the level of conjugation gets decreased in the case of PAFs upon breaking the conjugation by the central atom of the tetrahedral monomers, but in the case of CMPs, as the conjugation originates from the monomers, they can maintain the conjugation.[69] The first PAF was reported in 2009, namely, PAF-1, exhibiting an excellent BET surface area of 5600 $m^2 g^{-1}$.[38] PAF-1 was synthesized *via* the Yamamoto coupling reaction which enables direct homo-coupling of the monomers. Along the same line, two other PAFs were synthesized, namely, PAF-3 and PAF-4.[61,70,71] Both PAF-3 and PAF-4 showed excellent BET surface areas of 2932 $m^2 g^{-1}$ and 2246 $m^2 g^{-1}$. In 2011, another very promising class of PAFs, JUC-Zs, was reported ("JUC" stands for Jilin University, China and "Z" for zeolites). The first example of JUC-Zs, namely, JUC-Z1, is a porous network fabricated from *p*-iodooctaphenylsilsesquioxane building units connected together *via* covalent bonds.[72] Recently, Zhu and co-workers established the synthesis of fullerene-based PAF materials, which are structurally different from the other PAF materials.[73] Another class of POPs is cage-based POPs with a 3D

molecular framework, constructed by covalent linking of different aromatic moieties, first reported by Zhang *et al.* in 2011.[212] Apart from this class of POPs, recently, from 2015 onward, a few other new types of amorphous POPs have been developed by employing various functional groups, including triazine,[372] cyclodextrin,[258] pillar[5]arene,[373] calix[4]arene,[374] resorcin[4]arene,[156] C-phenylresorcin[4]arene,[375] *etc.*, which have demonstrated significant advancement in the field of environmental remediation.

3. Synthetic methods of POPs

As discussed in the introduction section, POPs are made up of pure organic building blocks connected through covalent bonds. The formation of covalent bonds between the small organic linkers to synthesise the porous polymers can be done with the help of various chemical reactions using several systematic synthetic strategies. The widely used synthetic methods for the preparation of POPs are categorized as discussed below. In addition, the fabrication of POP-based thin films or mixed matrix membranes (MMMs) for the demonstration of many prospective applications directly related to environmental remediation has also recently attracted the attention of the entire scientific community. These synthetic techniques have also been discussed below in detail.

3.1 Solvothermal method

The method which has been most widely used for the synthesis of POPs is solvothermal synthesis. A large number of POPs have been constructed by utilizing this method and further used in different applications. In this synthetic technique, POPs are synthesized by reacting two or more different monomers or sometimes by reacting a single monomer in a homocoupling way in an appropriate solvent combination under high temperature (typically 90–150 °C) for a certain time period (1–3 days). In this synthetic condition, various organic monomers are coupled with each other to form stable covalent bonds, which are further propagated in either two or three dimensions to create a kinetically controlled extended network, *i.e.*, POPs. In this method, the choice of reactants, solvents, reactant solubility and temperature of the reaction play a crucial role in various properties of POPs, such as morphology, surface area, degree of polymerization, stability, *etc.* A few representative examples of successful development of POPs by the solvothermal method are also discussed here. For the first time, a 2D sandwich graphene-CMP was created by Zhuang *et al.* using a solvothermal technique.[74] After thermal carbonization, this POP was employed as a 2D porous carbon material for supercapacitor application. Wan *et al.* utilized the solvothermal approach to create a triazine-based CMP, which was then used as a coating material for solid-phase extraction.[75] Recently, our group developed an imidazolium-based cationic polymeric network (iPOP-5) by solvothermal reaction.[76] In this work, two monomers, 2,4,6-tris(4-bromomethyl)phenyl-1,3,5-triazine (precursor-1) and 1,4-di(1*H*-imidazol-1-yl)benzene (precursor-2), were reacted by refluxing in a solvent combination of acetonitrile and tetrahydrofuran (THF) to create iPOP-5 (Fig. 1a). Furthermore, by fine-tuning the reaction conditions in terms of varying the reaction time, various morphologies of iPOP-5 were fabricated. Upon reacting the reactants for ~8 hours the POP exhibited spherical morphology. On further increasing the time of the reaction, the spherical morphology was found to convert into flake morphology (Fig. 1a). In another report, our group synthesized a porous covalent framework (PCF-1) by applying solvothermal reaction between two different monomers using dimethylacetamide (DMAc) solvent under a nitrogen atmosphere.[77] As a result, an off-white colored fibrous solid product was obtained upon cooling down the reaction, which was then modified to PCF-1-SO_3H by further reacting with chlorosulfonic acid at high temperature. This material was further used for proton conduction application. Despite the fact that the solvothermal approach has been widely employed in the synthesis of POPs because it allows for relatively simple and straightforward reaction process management, it nevertheless has certain drawbacks, including a lengthy reaction time and difficult reaction situation monitoring.[78]

3.2 Ionothermal method

An ionothermal reaction is a type of solid-state reaction, which has been shown to be used to synthesise various classes of POPs. In a typical ionothermal synthesis method, no reaction solvent has been used, rather the monomers are mixed with a molten salt (such as $ZnCl_2$), which acts as a catalyst as well as a reaction solvent. The whole mixture is heated at high temperature (>400 °C) in a sealed Pyrex tube for a long time. In this prolonged time of reaction, trimerization occurs at high temperature to give the desired POPs. One of the commonly used POPs *i.e.*, CTFs, have been frequently found to be constructed by the ionothermal method owing to the exceptional compatibility with cyano-containing monomers. By applying the ionothermal technique, at high temperature, taking advantage of nonplanar or distorted monomers one can easily synthesize CTF-based POPs. However, it should be mentioned that planar monomers are useful for the construction of crystalline CTFs as at high temperature kinetically controlled products are dominant due to the feasibility of reversible reaction. Therefore, although limited, the first crystalline CTFs were made with this method.[79] Coskun *et al.* synthesized a charged CTF using a cyanophenyl substituted viologen dication monomer by utilizing ionothermal reaction in the presence of $ZnCl_2$ salt.[80] By varying the temperature of the reaction (~400, 450 and 500 °C) the authors developed variable porosity and surface area based CTF analogues. These CTFs were further used for carbon dioxide capture and conversion into cyclic carbonates. Apart from cyano substituted monomers, using molten $ZnCl_2$ as the reaction solvent and methyl ketone as the reaction monomer, Kim and co-workers created a POP through C–C bond formation (Fig. 1b).[81] This POP was used for supercapacitor application. Although the ionothermal method has a few advantages such as no use of solvents, low catalyst cost, large-scale synthesis, *etc.*, it also suffers from several limitations. Among them, difficulties associated with the removal of trace amounts of spent $ZnCl_2$ and the need for monomers that are resilient to difficult reaction conditions are the major ones.

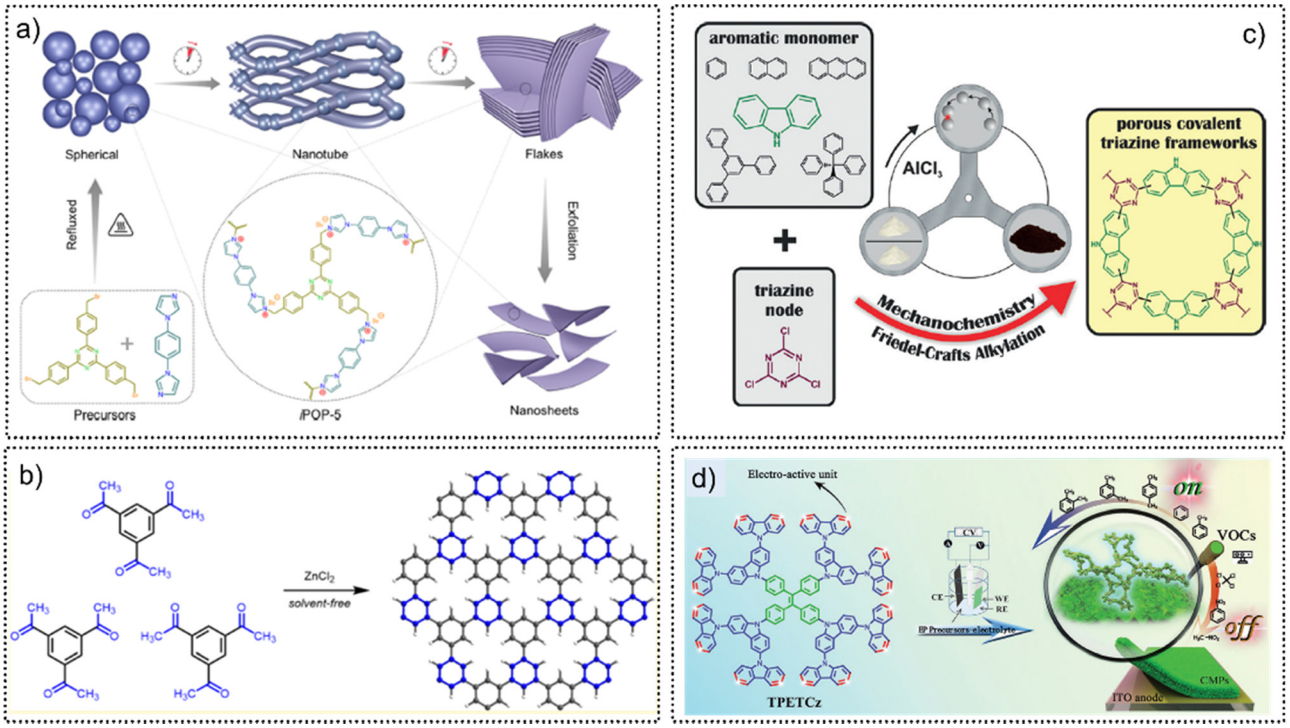

Fig. 1 (a) Solvothermal synthesis of imidazolium-based ionic porous organic polymers *via* refluxing of two monomers in THF/acetonitrile solvents. Adapted with permission from ref. 76. Copyright 2022, American Chemical Society. (b) Ionothermal synthesis of a CMP *via* solvent free cyclotrimerization of methyl ketones with $ZnCl_2$ as a catalyst. Reproduced with permission from ref. 81. Copyright 2021, American Chemical Society. (c) Mechanochemical synthesis of porous covalent triazine frameworks *via* the Friedel–Crafts reaction. Reproduced with permission from ref. 82. Copyright 2008, Wiley-VCH Verlag GmbH & Co. KGaA, Weinheim. (d) Electropolymerization fabrication of CMP-based films from a novel dendrimer. Adapted with permission from ref. 88. Copyright 2020, Wiley-VCH Verlag GmbH & Co. KGaA, Weinheim.

3.3 Mechanochemical grinding method

The mechanochemical synthesis method is considered as a green technique for POP synthesis. This technique produces POPs with relatively good yield by grinding the organic monomers or linkers in a mortar and pestle for several minutes. The driving force for the formation of POPs by this method is generated by the mechanical energy produced during the grinding process. Most of the mechanochemical reactions have been carried out without solvent; however, liquid-assisted grinding (LAG), which entails the addition of a tiny amount of catalytic solvent to the reaction mixture, is used to speed up the reaction rate. This helps to achieve a high degree of polymerization by preserving the reaction's homogeneity and thoroughly mixing the reactants to ensure the presence of monomers. By applying the mechanochemical method, Troschke *et al.* synthesized porous CTFs through the Friedel–Crafts alkylation reaction.[82] This is the first example of application of the Friedel–Crafts alkylation reaction in a mechanochemical way to react carbazole moieties with electrophilic cyanuric acid to produce amorphous triazine-based POPs (Fig. 1c). Although the mechanochemical grinding method offers the benefits of being environmentally friendly, using no solvents, and taking less time, it has a few limitations also. The limited scope of monomers, production of a large amount of oligomers, in a few cases the presence of catalyst as impurity, *etc.* are viewed as drawbacks for the mechanochemical grinding technique.

3.4 Microwave-assisted method

The microwave-assisted solvothermal approach can increase the synthesis efficiency and reduce the reaction time due to the enhancement in the rate of the reaction when compared to the solvothermal method. In this procedure, the reactants are sonicated into solution or dispersion in an appropriate solvent mixture before being sealed in a microwave compatible Pyrex tube under vacuum. Thereafter, the sealed tube is heated briefly while also being exposed to microwave radiation for a short period of time (~10–60 min). In a report, Trabolsi *et al.* synthesized viologen-based cationic covalent organic amorphous networks through the Zincke reaction by utilizing the microwave solvothermal method.[83] In this synthesis protocol a triamine-based reactant was reacted with the viologen monomer in an EtOH–water (4 : 1) solvent mixture under microwave irradiation of 2.45 GHz at 100 °C for 2 h in a microwave reaction vessel (25 mL). This reaction yielded a hollow-sphere morphology based solid powder polymer. However, upon changing the solvent to dioxane, the reaction produced a hollow tube shaped POP. The POPs formed in these reactions were further used for efficient iodine capture in the cyclohexane phase. By reacting 1,3,5-triformyl-resorcinol and *m*-phenylenediamine reactants at 150 °C for two hours, a novel β-ketoenamine-linked CMP was created by Wei *et al.* by applying the microwave technique.[84] Post-synthetic modification of POPs can also be done with the

help of the microwave method. Recently, Cui and co-workers incorporated three different functional moieties into a copper porphyrin-based CMP polymer by applying the microwave technique and further used these modified POPs for photocatalytic dye degradation application.[85] The microwave solvothermal approach is more effective in terms of less time consumption and environmentally friendliness, owing to the use of microwave heating, but it is challenging to carry out a large-scale preparation of POPs.

3.5 Room temperature synthesis method

The synthesis of POPs in the bulk powder form has also been reported based on the room temperature synthesis method. In this method, the reactants are mixed with each other in a particular single solvent or a combination of solvents in the presence of a catalyst (sometimes without the catalyst) and the whole mixture is stirred at room temperature for certain time to complete the reaction. By adopting this simple synthesis strategy, several POPs have been synthesized. Using Schiff-base chemistry, Li *et al.* synthesized three-component based hybrid covalent organic polymers through a facile room temperature synthesis method.[86] These POPs were used to sequestrate sulfonamide antibiotics such as sulfadiazine (SDZ) from water with a high adsorption capacity and rapid kinetics. This approach saves energy because it does not require excess heat, but it can only be used in a small number of reactions.

3.6 Electropolymerization method

One of the recent techniques that have been adopted to synthesize POPs is the electropolymerization process. Especially, apart from the bulk powder, POP-based thin films are fabricated with this technique. Among them CMP based films were found to be fabricated by the *in situ* electropolymerization process. In this method, by applying voltage, POPs are constructed onto an anode (such as ITO) plate inside a typical three electrode cell chamber, taking the electroactive functional moieties. Using the electropolymerization method, Ma *et al.* created a CMP film with a zinc porphyrin core and dimer carbazole linkers, and it was used for an energy storage application (as a supercapacitor).[87] In another report, applying the electropolymerization technique, with dendritic macromolecules as the precursor, Liu and co-workers created dendrimer (TPETCz) CMP films having extensive micro-porosity, which have excellent adsorption capabilities for several volatile organic chemicals (Fig. 1d).[88] Zhou *et al.* synthesized a polybenzazole CMP membrane and used it for ion filtration application.[89] Although the simple *in situ* electropolymerization approach provides a quick and simple means to create POPs, its limited monomer scope and expensive nature restrict its wide-scale use. Apart from these synthetic methods, few other synthetic procedures were reported for the development of POPs. The catalytic vapor-assisted solvent-free method for the preparation of POPs is one among them.[90]

4. Reactions involved in the synthesis of POPs

In order to enhance the performance of porous polymers in various applications, the fundamental challenge for synthetic chemists continues to be the invention of a straightforward and highly productive synthetic route that enables control over the specified structure and surface area in POPs. This entails refined control over the architectural aspect of designing the network's topology as well as the molecular dimension. As mentioned before, to construct porous organic polymers, the small organic molecules or monomers must be covalently linked with each other in the applied desired synthetic reactions. A wide range of synthetic approaches for creating POPs have been established up to this point. The polycondensation reaction is a frequently utilized technique. The chemical processes that are widely used to create POPs can be broadly categorized into metal catalyzed and non-metal catalyzed reactions. Among the metal catalyzed reactions, Sonogashira–Hagihara cross-coupling, Suzuki–Miyaura coupling, Friedel–Crafts alkylation, Yamamoto coupling (oxidative polymerization), Glaser-coupling, metal-free Friedel–Crafts polycondensation, and Lewis acid assisted cyclotrimerization are widely used reactions. On the other hand, among the non-metal catalyzed reactions, benzodioxane formation, boronate ester formation, amidation, boroxine formation, nitrile cyclization, imidization, Schiff-base reaction, *etc.* are well established for the synthesis of POPs.[91] These synthetic reactions are discussed in the sections that follow.

4.1 Suzuki–Miyaura coupling reactions

Two monomers, tris(4-bromo-2,6-dimethylphenyl)borane and tris(4-dihydroxyboroylphenyl)amine, were combined by a Suzuki–Miyaura coupling reaction to create a triarylboron-linked POP, which was further used for capture of fluoride ions from water.[92] In another report, Xu *et al.* created a CMP with ethylphosphate ligands (CMP-EP) by applying Suzuki–Miyaura coupling reactions between 1,3,5-tris(4,4,5,5-tetramethyl-1,3,2-dioxaborolan-2-yl)benzene and 2,7-dibromo-9,9-bis(diethyl propylphosphonate)fluorine monomers (Fig. 2a).[93] The polymer (CMP-EP) was found to extract uranium metal cations from nuclear waste. Cooper *et al.* used a method based on the two-step Suzuki cross-coupling reaction to create a soluble POP (SCMP1) by adding bulky organic units, such as *tert*-butyl, to the exterior of CMPs.[94] The final product of the reaction, the pyrene-based SCMP1, was found to be microporous in nature with moderate surface area (505 $m^2 g^{-1}$).

4.2 Sonogashira–Hagihara coupling reactions

The Sonogashira–Hagihara coupling reaction refers to the copolymerization of terminal alkynes with aryl halides in the presence of a palladium catalyst along with copper species.[95] Among the polycondensation reactions, these coupling reactions have largely been used to synthesize carbon–carbon bonded POPs since the discovery of poly(aryleneethynylene) CMPs.[96] Cooper *et al.* synthesized fully π-conjugated poly(aryleneethynylene)-based microporous polymers (CMPs) based on the palladium-catalyzed Sonogashira–Hagihara coupling reaction. The resultant POP exhibited high surface areas up to 834 $m^2 g^{-1}$. Liu *et al.* reported the synthesis of metallo (Zn)-porphyrin-based CMP microspheres with outer diameters of 320–740 nm by using silica nanoparticles as a template.[97] In another report, efficient extraction of uranium cations has been demonstrated by developing a fluorescent POP

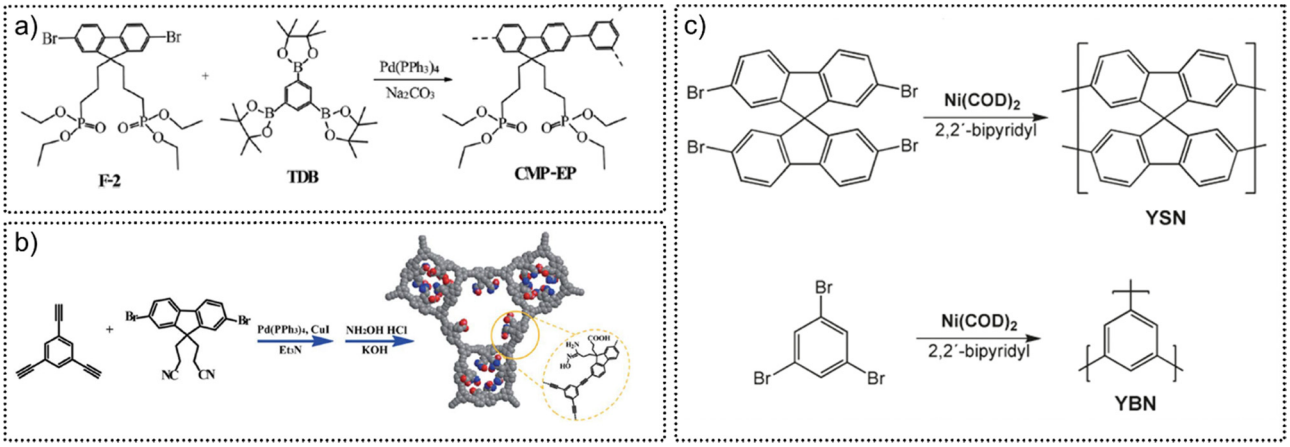

Fig. 2 (a) Synthetic route to CMP-EP by the Suzuki coupling polymerization. Reproduced with permission from ref. 93. Copyright 2018, the Royal Society of Chemistry. (b) Synthesis of the amidoxime functionalized polymer (CMPAO) by the Sonogashira–Hagihara coupling reaction. Reproduced with permission from ref. 98. Copyright 2019, the Royal Society of Chemistry. (c) Polymerization of tetrabromo and tribromo substituted monomers *via* the Yamamoto reaction. Reproduced with permission from ref. 101. Copyright 2009, American Chemical Society.

(CMPAO), which was synthesized using Sonogashira–Hagihara coupling reactions between 1,3,5-triethynylbenzene and amidoxime/carboxylate-substituted fluorene moieties (Fig. 2b).[98] Moreover, a hydroxyl functionalized porous aromatic framework (PAF-18-OH) was synthesized from its precursors *via* Sonogashira copolymerization.[99]

4.3 Yamamoto coupling reactions

Cooper's group developed a series of CMPs with variable surface areas *via* homocoupling of 1,3,5-triethynylbenzene and 1,4-diethynylbenzene monomers.[100] Thomas *et al.* synthesized a series of spirobifluorene-based CMPs using Yamamoto coupling reactions, with various brominated monomer ratios, which exhibited a large BET surface area (>1000 m^2 g^{-1}) and pore volume (Fig. 2c).[101] In order to create nanofiber-based POP thin films for electrospinning technology, the Yamamoto coupling reaction was also applied. These films were successfully used as chemosensors and supercapacitors.[102]

4.4 Scholl coupling reactions

The Scholl coupling reaction, which involves the coupling of phenyl rings of aromatic compounds, uses $AlCl_3$ as a catalyst (Fig. 3a). A set of four PAFs were fabricated *via* the $AlCl_3$ catalyzed low-cost and straightforward synthetic Scholl coupling reaction, taking 3D monomers, such as triphenylamine, tetraphenylmethane, tetraphenylsilane, and tetraphenylgermane.[103,104] All these synthesized PAFs exhibited a high sorption capacity of CH_4 and CO_2 gases. Li and co-workers used the Scholl coupling process to create a number of conjugated POPs by utilizing a simple precursor system along with $AlCl_3$ catalysis. The created CMPs show effective gas adsorption for CH_4 and CO_2.[103] Another conjugated POP having carbazole units (CZ-CMP) was synthesized by Guo *et al.* by applying Scholl coupling reactions.[105]

4.5 Ullmann coupling reactions

Dehalogenation and polycondensation of aryl halides are steps in Ullmann coupling processes, which are catalysed by the nickel(0) complex. The Ullmann coupling reaction has been exclusively applied for the synthesis of PAFs with large BET surface area (>4000 m^2 g^{-1}).[106,107] Moreover, electron donor groups like pyrene and electron acceptor moieties such as phenanthrene, benzene, and pyrazine were coupled with each other using the Ullmann coupling reaction to synthesize donor–acceptor-based conjugated POPs.[108] The resultant CMPs have further been effectively used as a photocatalyst for hydrogen production under visible light owing to their outstanding photocatalytic activity and stability.

4.6 Heck coupling reactions

In the Heck coupling reaction, an unsaturated halide is coupled with a primary alkene in the presence of a Pd catalyst and base, forming a C=C bond between the two units. Utilization of the Heck coupling reaction for the development of conjugated POPs was demonstrated by Sun *et al.*[109] A highly luminescent CMP was synthesized by the coupling of aromatic halides with vinyl aromatic compounds, using $Pd(Ph_3)_4$ as the catalyst, K_2CO_3 as the base and DMF as the solvent under anaerobic conditions. Owing to the strong fluorescence properties the developed CMP was applied for the turn-off detection of explosives such as picric acid.

4.7 Glaser coupling reactions

In a report by Chen *et al.* a 2D conjugated polymer (2D-PTNS) was synthesized from the triethynyltriptycene monomer by employing the Glaser coupling reaction.[110] As a result of the reaction, a bottom-up layered structure of a gelatinous mixture was formed at the gas–liquid interface. Furthermore, the synthesized POP exhibited gas adsorption properties. Zade *et al.* synthesized a thiophene and triazine functionalized conjugated porous polymer (TT-CPP3) by the Glaser coupling reaction and used it for CO_2 capture.[111] The cost-effective Glaser coupling process was used to create a variety of butenyl

CMPs from arylene monomers with various configurations, which exhibited high CO_2 adsorption capacity.[112]

4.8 Oxidative coupling reactions

Oxidative coupling reactions, which liberate two electrons from the reactants and trap them by an oxidant, have arisen as a versatile alternative to cross-coupling in the synthesis of POPs. Nitrogen-rich conjugated polymers (NCMPs) have also been created using oxidative coupling processes. Through this coupling procedure, the intermediates produced when various brominated monomers react with aniline are employed to synthesise NCMPs.[113] Further, these POPs have been used for gas storage and heterogeneous catalysis application. By utilising oxidative Scholl reactions of electron-rich aromatics with a Lewis acid catalyst, most frequently $FeCl_3$ or $AlCl_3$ in a $CHCl_3$ solvent, POPs can be created.[114]

4.9 Friedel–Crafts reactions

Friedel–Crafts reactions have been widely used to prepare several POPs, including CMPs, HCPs, PAFs, *etc.* Owing to some clear benefits such as being quick and easy, requiring no metal catalyst and being inexpensive, the Friedel–Crafts reaction is the preferred choice for many POP synthetic chemists. Geng *et al.* utilized Friedel–Crafts reactions to synthesise a series of three triazine-based polymers (TTPPA, TTDAB and Tm-MTDAB) by the reaction of 2,4,6-trichloro-1,3,5-triazine (TCT) with three triphenylamine derivatives (Fig. 3b).[115] These polymers exhibited a high surface area and pore volume and excellent uptake of iodine in the gas phase as well as in solution. In another report, the same group again synthesized three nitrogen core containing POPs *via* the Friedel–Crafts reaction catalysed by methanesulfonic acid.[116] These high BET surface area based CMPs were used for efficient and reversible uptake of iodine vapour. The Friedel–Crafts alkylation process was also found to connect the aromatic motifs *via* methylene linkage, catalyzed by a Lewis acid under mild conditions, which further creates PAFs. A series of PAFs (PAF-32, PAF-32-NH_2 and PAF-32-OH) were produced by reacting the monomer tetraphenylmethane and its amino and hydroxyl derivatives.[117]

4.10 Buchwald–Hartwig reactions

The Buchwald–Hartwig reaction is a widely used reaction in organic synthesis for the formation of polar C–N bonds *via* coupling of amines and aryl bromides, catalyzed by palladium. This reaction is also known as an amination reaction. Thomas *et al.* synthesized a library of 3D polyaminoanthraquinone-based POPs by applying Buchwald–Hartwig reactions between 2,6-diaminoanthraquinone and a diverse number of bromine substituted aryl monomers (Fig. 3c).[118] All these CMPs were tested for supercapacitor application. It was noticed that the Buchwald–Hartwig reaction often resulted in POPs with a relatively low surface area. Therefore, inorganic salts such as $LiNO_3$, NaCl, and NaF were also used along with the Buchwald–Hartwig reaction to enhance of specific surface area of the synthesized POPs. As a result, the addition of inorganic salts greatly improved the specific surface area of the resultant CMPs without changing their structural properties.[118] A novel N-rich POP was synthesized through the Buchwald–Hartwig reaction

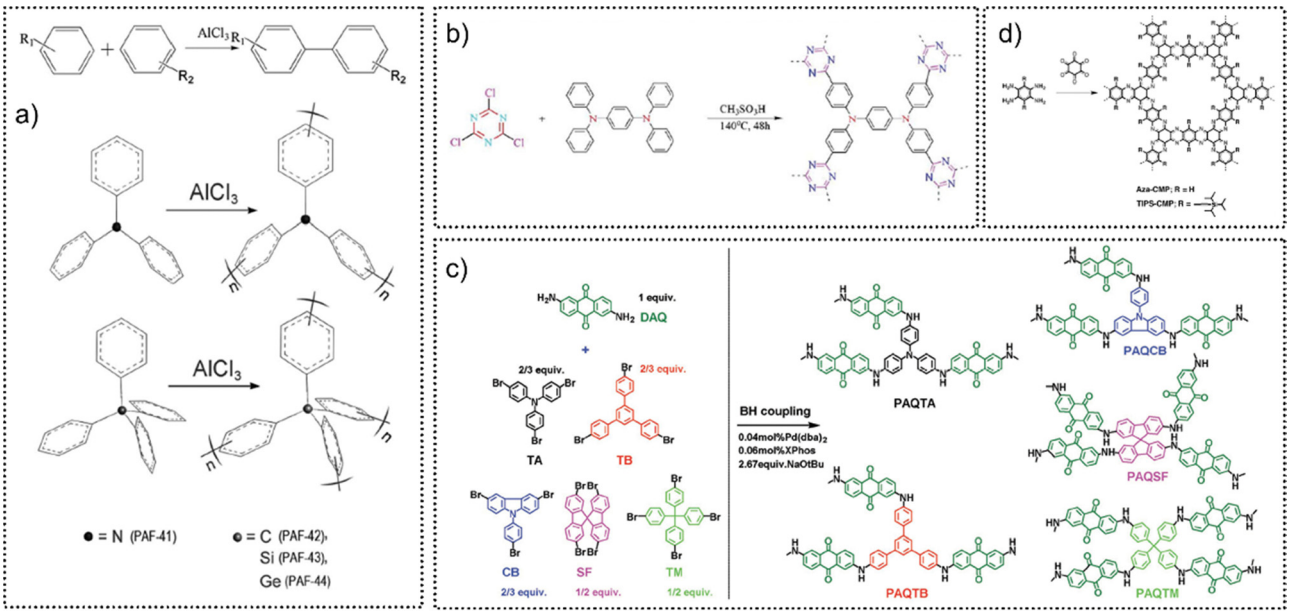

Fig. 3 (a) Development of extended frameworks *via* Scholl coupling reactions with $AlCl_3$ as the catalyst. Reproduced with permission from ref. 103. Copyright 2014, the Royal Society of Chemistry. (b) Synthesis of triazine-based CMPs by the Friedel–Crafts reaction catalyzed by methanesulfonic acid. Reproduced with permission from ref. 115. Copyright 2018, the Royal Society of Chemistry. (c) Synthesis of the polyaminoanthraquinone (PAQ) network by the Buchwald–Hartwig reaction of monomers, TA: triphenylamine, TB: triphenylbenzene, CB: carbazole, SF: spirobifluorene, TM: tetraphenylmethane. Reproduced with permission from ref. 118. Copyright 2018, Wiley-VCH Verlag GmbH & Co. KGaA, Weinheim. (d) Creation of the pyrazine-fused CMP (Aza-CMP) and the triisopropylsilyl CMP (TIPS-CMP) by the Friedel–Crafts reaction. Reproduced with permission from ref. 133. Copyright 2017, Wiley-VCH Verlag GmbH & Co. KGaA, Weinheim.

by using 1,3,5-tris(4-bromophenyl) benzene and *p*-phenylenediamine/benzidine monomers as building blocks. Owing to the presence of electron-rich heterocyclic moieties and mesoporous structure, this POP was applied for volatile iodine capture.[119]

4.11 Cyclotrimerization reactions

Cyclotrimerization reaction was applied for the creation of highly porous organic frameworks, taking bifunctional acetyl moieties as monomers. Moreover, different morphology of the POP was found upon changing the medium of the reaction. Highly dispersed powders were produced during solution-based silicon tetrachloride synthesis, whereas polymeric monoliths were produced during molten 4-toluene sulfonic acid synthesis.[120] Bohra *et al.* synthesized a POP having triazine moieties in its structure with the help of direct arylation of a polybrominated monomer and 2,4,6-tri(2-thiophene)-1,3,5-triazine using cyclotrimerization reaction.[121] In this cyclotrimerization reaction, triazine monomers are introduced into the structure of POPs without the need of C–H bond preactivation in aromatic monomers. Further, the photooxidation of benzylamine was carried out using the produced CMPs as photocatalysts. Milner *et al.* explored solvent-free synthesis of CMPs and PAFs *via* ionothermal cyclotrimerization of methyl ketones.[81] Highly porous POPs were synthesized by the polymerization of 1,3,5-triacetylbenzene and tetrakis(4-acetylphenyl)methane, catalyzed by molten zinc chloride. Thus the prepared POP was used for charge storage or capacitor purpose. Zade, Mandal, and co-workers synthesized a triazine-based conjugated porous polymer (TT-CPP1) using the alkyne cyclotrimerization reaction taking the tris(thienyl)triazine unit.[111] The POP exhibited excellent adsorption of the Lewis acidic CO_2 at 263 K under 100 kPa pressure. Moreover, it has been demonstrated that amide groups can trimerize in the presence of P_2O_5 as a catalyst.[122]

4.12 Schiff-base condensation reactions

In POP synthetic reactions, one of the most important classes of reactions is Schiff-base condensation. This polymerization reaction has been extensively used to develop a large number of POPs. Aiming at functionalizing monomers with amine and aldehyde, the process creates an imine link.[123] By reacting 9,10-bis-(4,6-diamino-*S*-triazin-2-yl)anthracene with 2-furaldehyde in a metal-free Schiff base polycondensation process, a triazene-anthracene-based fluorescent aminal linked POP (TALPOP) was created by Sabri's group.[124] The prepared highly stable POP exhibited exceptional iodine uptake in both vapour and solution phase. By utilizing Schiff-base condensation reactions a novel nitrogen-rich triaminopyrimidine (TAP) core-based POP (TAP-POP) was synthesized and used for heterogeneous base catalysts.[125] Metallic phthalocyanine-based porous polymers (MPc-CMPs) were developed *via* Schiff-base condensation reactions.[126] In this report, Ding *et al.* used their POP as a photosensitizer to produce singlet oxygen ($^1O_2$).

4.13 Aldol condensation reactions

The aldol triple condensation technique was employed for the scalable synthesis of conjugated porous polymers with inexpensive monomers. This bottom-up synthetic strategy produced POPs which demonstrated rapid and selective adsorption of small organic molecules from water.[127] Han and colleagues created microporous organic polymers using thionyl chloride-catalyzed aldol self-condensation of building blocks including di- and multiacetyls.[128] A porous polymeric compound with an olefin link was created by Lyu *et al. via* the aldol condensation procedure.[129] The olefin-linked material exhibited high stability in harsh acid and alkaline environments and possessed a significant specific surface area (1715 $m^2\ g^{-1}$). Further, it was used as a catalyst support for the benchmark Diels–Alder reaction.

4.14 Knoevenagel condensation reactions

Ma *et al.* prepared a olefin-linked conjugated POP (COP-CN) *via* the Knoevenagel condensation reaction, which showed good stability and excellent fluorescence property. Additionally, because of the high N atom content, it exhibited good uranium adsorption and separation capability.[130] Utilization of the Knoevenagel polycondensation reaction to create the first olefin-linked porous polymer was demonstrated by Zhuang *et al.* by using 1,4-phenylene diacetonitrile and a C3-based aromatic aldehyde.[131] The synthesized olefin-linked CMP exhibited sheet-like morphology along with a fully sp2-bonded C–C conjugated structure with pendant cyanide groups. This compound was employed as an electrode for supercapacitors and as an electrocatalyst for the oxygen reduction reaction. Gong *et al.* reported a pyrylium-containing POP (TMP-P) *via* the Knoevenagel condensation reaction between 2,4,6-trimethylpyrylium salt (TMP) and 1,4-phthalaldehyde monomers.[132] The synthesized POP exhibited efficient visible-light-driven heterogeneous degradation of Rhodamine B dye.

4.15 Other reactions

Other types of reactions, in addition to the coupling and condensation reactions indicated above, have also been investigated for the synthesis of POPs. Phenazine ring fusion links aryl diamines and aryl diketones at high temperature. Phenazine ring fusion reaction was employed for the successful construction of twisted 2D conjugated polymers (Aza-CMPs) with molten aromatic rings (Fig. 3d).[133] Triisopropyl silicon (TIPs) groups and acetylene groups were added to the skeleton of the POP during the solvothermal creation of a highly deformed aromatic structure (TIPs-CMPs) in a dioxane/acetic acid solvent mixture. The distinctive structure of the polymer improved its dispersion in solvents, making it simple to create uniform and optically transparent films. Heterocycle linkages of monomers, such as the reaction of aldehydes with ortho diamines, can be used to form benzimidazole linkages. POPs with benzimidazole bonds were also established in the literature by Rabbani, El-Kaderi and co-workers.[134] Cationic cyclization polymerization has been utilized to develop POPs. By using monomers with multiple acetylenes, three olefin polymers were produced. These POPs were then employed to adsorb iodine and carbon dioxide gases.[135] Moreover, alkyne metathesis reaction was also used for the synthesis of porous polymers, catalyzed by Mo(VI) in chloroform solvent.[136] Our group synthesized a charged viologen-based organic network (compound-**1**) *via* the Zincke reaction between two precursors by refluxing in a dioxane/ethanol/chlorobenzene

solvent combination.[137] This POP was used for the detoxification of wastewater by removing selective metal-oxoanions. Li *et al.* used the quaternization reaction between tetrakis(4-pyridylphenyl)-ethylene (TPPE) and 1,4-bis(bromomethyl)benzene (BBMB) to develop a cationic POP (CON-LDU2) for chemosensing and removal application of Cr(VI)-oxoanions from water.[138] The Gilch reaction was used by Dawson *et al.* to create a conjugated porous polystyrene polymer *via* the self-condensation of 1,2,4,5-tetrabromomethylbenzene in an anhydrous tetrahydrofuran solvent.[139] The polymer was used for hydrogen storage application. Hypercrosslinking was also used to create linear conjugated polymers. Further, cross-linking of linear polypyrrole and polyaniline generates a porous polymer with a high BET surface area.[140,141] Moreover, the Chichibabin reaction was also applied to synthesise porous polymers. The reaction between aryl aldehyde and ketone is called the Chichibabin reaction. He and co-workers reported the synthesis of pyridine core based CMPs by the Chichibabin reaction.[142]

It should be mentioned that because of the rapid advancement of the study area, processes for the synthesis of POPs are today not just restricted to those that result in the formation of carbon–carbon bonds, but also include those that result in the covalent connection of heteroatoms like N, O, and S. Among them, azo-linkage formation,[143,144] imidazolium linkage formation,[145,146] polyimide formation[147,148] and others[149,150] were found in the literature for the development of various POPs. However, the presently employed reactions are frequently catalysed by expensive, air-sensitive organometallic compounds. Thus, the use of these catalysts raises the cost of the polymers and reduces the amount that can be produced on a large scale. Therefore, one needs to focus on cost reduction and increased production of POPs for their practical application.

5. Characterization techniques for POPs

From the discussion above, it is clear that POPs differ from discrete molecules (such as small organic molecules, organic cages, *etc.*) or linear polymers in that they are indefinitely expanded polymeric materials that are insoluble in common solvents. Therefore, structural as well as morphological characterization of POPs in the solution state is not compatible. However, with the aid of various solid-state start-of-the-art characterization techniques, structural analysis of POPs can be done to gain insight into the textural and chemical composition of POPs. These characterization tools are discussed in the following sections.

5.1 Fourier transform infrared (FT-IR) spectroscopy

For reaction monitoring as well as structural analysis of POPs, FT-IR is one of the most significant and basic characterization tools in order to understand the covalent bond construction, and thus formation of the POP structure. Owing to its easy and facile operation and analysis, this technique is widely used to characterize POPs, which provides crucial information about the solid polymeric backbone and functional groups present on it. The inclusion of various functional moieties into the POP skeleton, whether as part of a pre- or post-synthetic strategy, is also understood *via* FT-IR spectroscopy. FT-IR spectroscopy has largely been used to characterize almost all of the known POPs. Hupp *et al.* reported the synthesis and CO_2/CH_4 gas sorption properties of a highly stable diimide-functionalized microporous organic polymer (Fig. 4a).[147] In this report, they synthesized a POP by the coupling reaction of dianhydride with tetraamine-based monomers in DMF solvent. The formation of polyimide linkage and the presence of both monomers' functionality in the synthesized POP were characterized by solid-state FT-IR spectroscopy. In the FT-IR spectra it was found that when compared to the dianhydride monomer, the carbonyl stretching frequency in the FT-IR spectra was observed to be pushed toward lower energy by about 100 cm^{-1}, indicating the establishment of amide bonds. Additionally, N–H stretches are reduced to undetectable amounts, indicating that the initial amines were effectively converted into imide linkages (Fig. 4a). This technique has also been utilized to explore the structure formation of triazine-based POPs. In a report, the Thomas group showed the lowering of the C–N stretching vibration at 2228 cm^{-1} and the appearance of a triazine ring at 1507 and 1352 cm^{-1} which both are obvious signs that the triazine production reaction is complete.[36] Ma *et al.* established the effective incorporation of nitro groups onto the POP (PAF-1) structure by the two asymmetric and symmetric stretching vibrations of the nitro group at 1528 and 1344 cm^{-1} in the FT-IR spectra of PAF-1-NO_2. The conversion of the nitro group to the

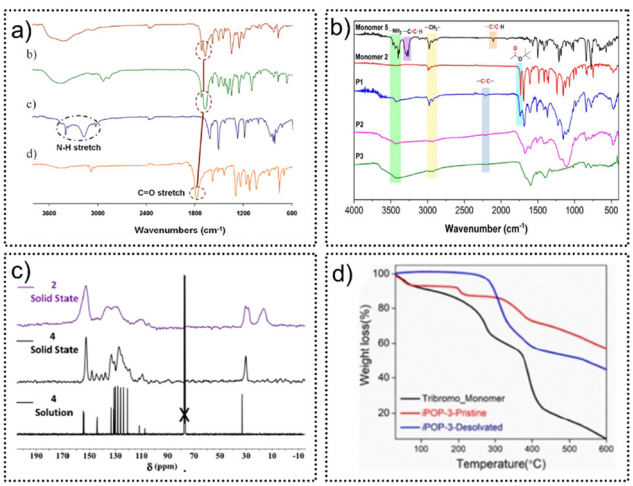

Fig. 4 (a) FT-IR spectroscopy data for the formation of a diimide-based microporous organic polymer. Reproduced with permission from ref. 147. Copyright 2009, American Chemical Society. (B) FT-IR spectra indicating the formation of calix[4]pyrrole-based POPs. Reproduced with permission from ref. 152. Copyright 2021, Wiley-VCH Verlag GmbH & Co. KGaA, Weinheim. (c) ^{13}C CP/MAS NMR spectroscopy data indicating the formation of the structure of resorcinarene cavitand polymers. Reproduced with permission from ref. 156. Copyright 2019, American Chemical Society. (d) TGA profile displaying the thermal stability of pristine and desolvated iPOP-3 along with its monomers. Reproduced with permission from ref. 39. Copyright 2021, Wiley-VCH Verlag GmbH & Co. KGaA, Weinheim.

amino group was also observed in the FT-IR spectra of PAF-1-NH_2. The occurrence of absorption peaks at 1229 and 1033 cm^{-1}, the typical bands of the -SO_3H group, provides evidence for the presence of sulfonic groups in the final POP structure.[151] Formation of calix[4]pyrrole-based porous polymeric networks was confirmed by FT-IR analysis, as no terminal alkyne stretching frequencies (2108 cm^{-1} for –C≡C– and 3285 cm^{-1} for terminal alkyne –C–H) were present in the spectra of the synthesized POPs (Fig. 4b).[152] In addition to this, the retention of desired functional groups in PAFs during synthesis and modification can also be revealed by FTIR. For instance, the FT-IR spectra of both the starting reactants and the as-synthesized PAF show the C–O stretching vibration at 1728 cm^{-1} and the O–H stretching vibration at 3431 cm^{-1} during the synthesis of carboxyl-decorated PAF-26-COOH. These data show the presence or retention of the carboxylic acid group in the POP structure.[153]

5.2 Nuclear magnetic resonance (NMR) spectroscopy

NMR spectroscopy is a widely used technique to describe the local chemical surroundings of specific nuclei. The restricted spatial arrangements of the detectable nuclei produce considerably widened spectra for materials like POPs, which are insoluble in common solvents. In detail, when the NMR sample is rotating at an angle of 54.74° with regard to the direction of the external magnetic field, the dipolar–dipolar coupling in the solid phase can be averaged. In this context, the technique that can offer short-range ordering information about the POPs in the solid state is the magic angle spinning nuclear magnetic resonance (MAS NMR).[107,154] Both ^1H and ^{13}C solid-state MAS NMR spectroscopy techniques were employed to characterize the chemical configuration of the POPs. For example, Tan *et al.* developed a novel strategy to synthesize a series of microporous polymers by utilizing knitting rigid aromatic monomers as an external cross-linker. The structural backbone of all these POPs was analysed by ^{13}C cross-polarization magic-angle spinning (CP/MAS) NMR. As a result of Friedel–Crafts synthesis, NMR resonance peaks, which are caused by substituted aromatic carbon and non-substituted aromatic carbon, respectively, were near 137 and 130 ppm. Also, the carbon in the methylene linker shows resonance peaks at about 36 ppm. Resonance peaks of 22 ppm were visible in the network based on methylbenzene, and they can be attributed to the methyl carbon linked to the benzene ring. Moreover, the resonance peaks in the phenol-based network at 150 ppm were caused by aromatic carbons connected to the phenolic hydroxyl group.[155] In another work, along with FT-IR, solid-state cross-polarization magic angle spinning (CP-MAS) ^{13}C NMR spectroscopy was employed to understand the structure of resorcinarene cavitand polymers, along with the spectra of soluble model compounds. The spectra indicated noticeable resonances in the case of both polymers near 153 ppm, which are suggestive of the generation of aryl C–O bonds, as well as resonances between 136 and 129 ppm, which correspond to aryl carbons on polymer-1. In addition, the presence of nitrile, methylene carbon, and the methyl group, respectively, is indicated by resonances at a chemical shift of 110, 30, and 17 ppm, respectively (Fig. 4c).[156] Molecular level characterization of CMP-1 has also been done with the help of ^1H and ^{13}C CP/MAS NMR spectrsocopy.[32] Moreover, this technique was employed to explore the structural formation of a series of calix[4]pyrrole-based crosslinked polymer networks. The solid-state CP/MAS ^{13}C NMR spectra of the POPs exhibited broad peaks in the spectral range of 150–120 ppm and 110–100 ppm. These characteristic peaks were attributed to the sp^2-hybridized carbons of the aromatic phenyl and pyrrole moieties in the polymeric structure, respectively. Additionally, peaks in the range of 90–100 ppm were attributed to the sp-hybridized acetylene (–C/C–) groups of the POPs.[157]

5.3 Thermogravimetric analysis (TGA)

One of the important characteristic features of extended polymeric materials (POPs) is the thermal robustness. The development of strong, durable materials capable of withstanding extreme heat conditions is one of the main challenges in POP synthesis chemistry.[158] TGA is a technique used to weigh samples before and after burning in order to determine how thermally stable POPs are. The weight change at different temperatures in the TGA profile of POPs can be due to multiple reasons. Among them, the removal of the guest molecules (such as solvents) from the framework, the breakdown of the organic polymeric structure, and the oxidation of the leftover metals from catalysts in the coupling reactions are only a few of the factors. A common analytical technique begins by performing TGA on POPs that have just been produced in order to determine how many solvent molecules are present in their pores. The temperature at which the POPs should be activated or heated for a period of time to archive the desolvated phase may therefore be inferred from this TGA profile. In a typical procedure, the TGA of POPs can be done in the temperature range of 30 to 800 °C under a N_2 atmosphere. In a POP-based literature example, two cationic imidazolium POPs have been synthesized for the metal-based oxoanion capture application. These two POPs have been characterized by TGA.[39] In the pristine phase of iPOP-3, TGA analysis revealed an initial weight loss of about 8%, which may have been caused by retained solvent molecules. Also, the TGA curve for the desolvated phase of iPOP-3 exhibited negligible weight loss until 300 °C, and the profile for iPOP-4 confirms the guest free nature by showing negligible weight loss until 350 °C (Fig. 4d).

5.4 X-Ray photoelectron spectroscopy (XPS)

POPs are majorly composed of light elements including C, N, O, S, and P. Qualitative determination of the composition of these elements of POPs provides insightful information. XPS is a technique which is used to ascertain the elemental composition, which aids in describing the general makeup of POPs. A typical XPS spectrum discloses the electron counts with respect to the binding energy for a specific or all relevant elements present in the composition of POPs. Along with the identity and concentration of an element present in the POP backbone, it also directly indicates the subshell of the expelled electron (such as 1s, 2s, 2p, or 3d). Furthermore, this spectroscopic method can also be used to determine the bonding pattern between two monomer units.[159] Characterization of POPs with

the help of XPS analysis has attracted special attention in the recent past.[160] A few of the POPs that have been characterized by XPS analysis are described here as an exemplary example. Among the pristine POPs, CTFs are majorly characterized by XPS analysis. In a report, Coskun *et al.* explained the charged structure of a CTF made up of viologen-based monomers.[80] They carried out XPS to recognize the nature of chemical bonding in cCTFs. The cCTF-500 XPS survey spectrum showed the peaks of C 1s, N 1s, O 1s, and Cl 2p, proving the materials' purity. Furthermore, the C 1s core-level deconvoluted spectra indicated the presence of three components with binding energies corresponding to C–C, C═N, and C═O of 284.8, 286.8, and 289.02 eV, respectively (Fig. 5a). Moreover, the N 1s spectra of cCTF-500 exhibited three different peaks with binding energies of 398.5, 400.5, and 402.5 eV. Among them, the peaks at 398.5 and 400.5 eV were assigned to the nitrogen atoms of triazine linkages, and the peak located at 402.5 eV was assigned to the nitrogen atoms of viologen units (Fig. 5b).

5.5 Porosity measurement

The porosity of POPs, especially at the microporous scale (below 2 nm), is their primary structural characteristic.[161] POPs exhibit large surface areas with various hierarchical (micro/meso/macro) porosities. As already discussed, the porosity of POPs generally originates from the covalent binding of repeating units in a three-dimensional way. It is well known that the most popular method for determining their surface area, pore volume, and pore size distribution is gas adsorption–desorption measurement, with the help of the multi-layered Brunauer–Emmett–Teller (BET) adsorption isotherm. Typically, N_2 and Ar are inert, non-polar gases that physically adsorb in the material's pores to create these isotherms. However, due to its nonspherical shape and low critical temperature (77 K), N_2 has difficulty in diffusing into the pores of POPs of size smaller than 0.7 nm, and it takes a relatively long time to equilibrate. Therefore, in some cases, to measure the pores of POPs that are less than 0.7 nm, carbon dioxide (CO_2) sorption study at 195 or 273 or 298 K is carried out. According to the IUPAC classification, there are six different types of adsorption isotherms, which are categorized as type I to type VI and provide details about the nature of sorption, the type of pores based on their size, gas adsorption capacity, *etc.* A typical isotherm depicts the equilibrium adsorption quantity of an adsorptive in terms of its volume at standard temperature and pressure (STP) as a function of relative pressure (P/P_0). The shape of the isotherms shows how POPs are structured. Micropore filling is the cause of the quick gas uptake seen at relatively low P/P_0 (< 0.1). The resulting isotherm begins as convex with respect to the gas uptake axis and progresses to an adsorption plateau as the relative pressure rises. This curve's form is categorized as type I adsorption, which is considered to be proof that the microporous nature is present in the polymer. On the other hand, mesopore containing POPs exhibit capillary condensation at medium relative pressure with a hysteresis loop (type IV or V). Herein, a few representative examples of the structure of POPs with their gas uptake properties, surface areas, pore volume, and pore size are discussed. By utilizing the Sonogashira–Hagihara coupling reaction, Cooper *et al.* reported the fabrication of a number of microporous poly(aryleneethynylene) (PAE) networks with high BET surface areas.[58] By using nitrogen adsorption and desorption at 77.3 K, the surface areas and pore size distributions of various POPs were calculated. All these POPs exhibited type I N_2 gas sorption isotherms with BET surface areas of 512 $m^2\ g^{-1}$ for CMP-5 and 1018 $m^2\ g^{-1}$ for CMP-0 (Fig. 5c). Notably, in the case of CMP-2 and CMP-5, the authors found a small increase in the N_2 uptake profile at high relative pressures ($P/P_0 > 0.8$), which may be attributed to the interparticle porosity responsible for the meso- and macrostructures of the samples. Also, the pore size distribution of these polymers was calculated using NL-DFT

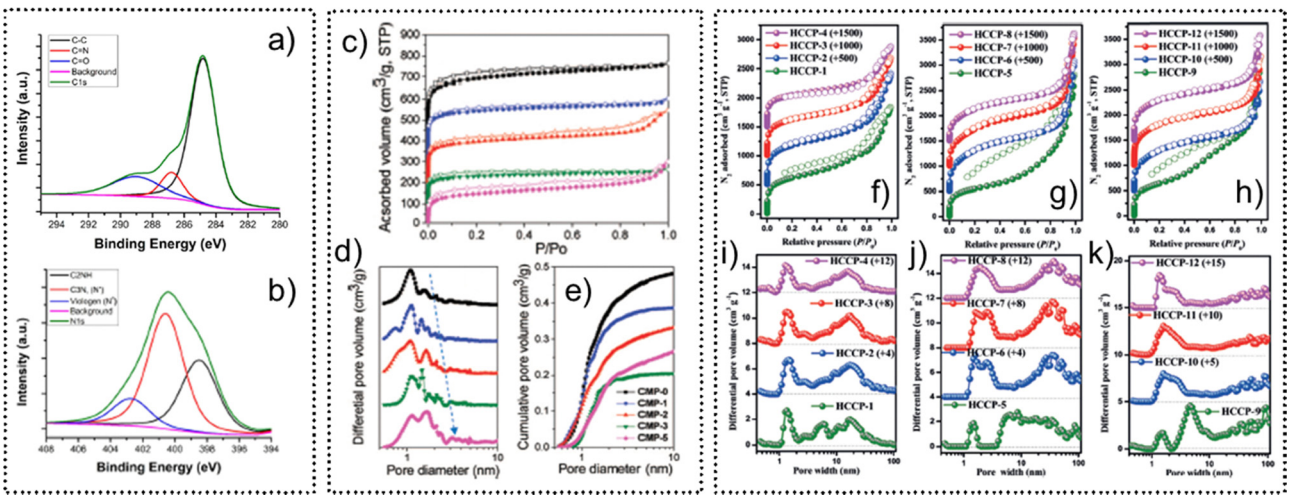

Fig. 5 Core-level deconvoluted XPS spectra of (a) C 1s and (b) N 1s of cCTF-500. Reproduced with permission from ref. 80. Copyright 2017, American Chemical Society. (c) N_2 gas sorption isotherms, (d) NL-DFT pore size distribution profile, and (e) NL-DFT cumulative pore volume plots for CMP-0 to CMP-5. Reproduced with permission from ref. 58. Copyright 2008, American Chemical Society. (f–h) N_2 gas sorption data for HCCP-1 to HCCP-12 showing type-IVa isotherms, (i–k) NL-DFT pore size distribution profile for HCCP-1 to HCCP-12. Reproduced with permission from ref. 163. Copyright 2021, Wiley-VCH Verlag GmbH & Co. KGaA, Weinheim.

(Fig. 5d). The NL-DFT cumulative pore volume plots indicated that the micropore volume of these POPs falls in the range of 0.38 to 0.16 $cm^3\ g^{-1}$ (Fig. 5e). In another report, by employing nitrogen as the sorbate molecule in a sorption assay, the porosity properties of CPOP-1 were examined.[162] The results of N_2 sorption indicated the permanent microporous nature with a fully reversible isotherm and quick absorption at low pressure (0–0.1 bar). A close inspection of the N_2 sorption data at a high relative pressure (>0.9) indicated a significant rise in the gas uptake. This might be because of the combined effect of interparticle porosity associated with the meso- and macrostructures of the polymers and interparticle void. Moreover, the BET surface area of CPOP-1 was found to be as high as 2220 $m^2\ g^{-1}$, and the corresponding pore size distribution (PSD) was calculated with the help of the NLDFT method as 0.62 nm. Liang and Zhao *et al.* reported a strategy to develop a series of hyper-crosslinked conjugated polymers (HCCPs) with exceptional porosity and high surface areas.[163] The N_2 sorption study was applied in order to investigate the porous properties of these POPs. These HCCPs displayed type IVa isotherms with hysteresis for mesopores larger than 4 nm. The steep uptake at higher relative pressures ($P/P_0 > 0.9$) may have been brought on by the existence of macropores with molecular clustering of N_2 (Fig. 5f–h). Among the POPs, HCCP-2, HCCP-6 and HCCP-11 exhibit the highest surface areas of 2515, 3083 and 3010 $m^2\ g^{-1}$, respectively, and excellent total pore volumes up to 3.98 $cm^3\ g^{-1}$ (Fig. 5i–k). Apart from this, the porous properties of highly porous polymers such as PAF (*i.e.*, PAF-100, PAF-101, *etc.*) materials have also been explored with N_2 sorption data.[164]

5.6 Field emission scanning electron microscopy (FESEM)

FESEM is a microscopic technique which provides the surface morphology of materials by scanning the surface with a negatively charged electron beam. Besides morphology, qualitative elemental analysis with their respective colour mapping can also be performed with this technique. Apart from these, bulk phase purity and reproducibility of POP-like materials can be verified by FESEM images. It is important to note that the morphology of POPs is a significant factor that influences a number of POP attributes, including surface area and others. Therefore, it is important to have a thorough understanding of the morphology of POPs. Most of the POP-based studies have explored the distinct and attractive morphologies based on FESEM images. In the literature, various surface morphologies of POPs have been reported including spherical, flakes, sheets, nanorods, nanotubes, *etc.* A few representative examples of utility of FESEM for microscopic analysis of POP structure are discussed here. Bhaumik *et al.* characterized their synthesized series of POPs with the help of FESEM analysis.

The morphological features of TrzPOP-1, TrzPOP-2, and TrzPOP-3 polymers exhibited a spherical shape with an average particle diameter of 17 to 25 nm.[165] Tan *et al.* reported construction of hollow microporous carbon spheres (HCSs) from hollow microporous organic capsules (HMOCs) with a good control over the pore morphology, hollow cavity, and the shell thickness. This study has been finely monitored with the help of FESEM analysis of each synthesized HCS, which were synthesized by using different HMOCs as precursors (Fig. 6a–f).[166] Furthermore, the functionality and possible applications of POPs are influenced by morphology. To explore this, a cationic organic network has been synthesized using the Zincke reaction under either solvothermal or microwave conditions. Depending upon the use of solvents along with the reaction conditions, the material revealed hollow sphere (HS), hollow tube (HT) and nanosheet morphologies. All these morphologies have been characterized by SEM images (Fig. 6g–k).[83] Additionally, the mechanism (Ostwald ripening) of formation of hollow spheres under solvothermal conditions was evaluated by SEM images (Fig. 6l). Monitoring of the progress of the reaction and morphological evolution with the help of FESEM analysis was also performed by our group. Evolution of flake morphology of an ionic POP from spherical through nanotubes and nanoribbons has been shown systematically by respective FESEM images.[76] The nature (amorphous or crystalline) of the POPs can also be uncovered by analyzing the FESEM images. FESEM images of solution-processable hypercrosslinked polymers showed an amorphous bulk structure, while the surface was dense and compact.[167] In addition to this, SEM-energy dispersive X-ray spectroscopy (EDS) was used to assess the elemental composition and color mapping of elements present in POPs.[168]

5.7 Transmission electron microscopy (TEM)

Another sophisticated microscopic technique is TEM, which provides nanometer scale surface morphologies of POPs. Unlike SEM/FESEM, TEM offers much more additional information about the surface morphology of POPs, even at very close to atomic level. The primary distinction between FESEM and TEM techniques is that FESEM scans images by detecting the electrons reflected from the sample surface, while in the case of TEM, it makes use of transmitted electrons that pass through the sample to produce a highly enlarged image. Apart from TEM images, high-resolution TEM (HR-TEM) images also provide crucial and meaningful information regarding the details of the POP surface. Moreover, similar to FESEM, EDS and elemental mapping analysis can also be performed by this technique. However, TEM-EDS offers qualitative elemental composition information of POPs close to the atomic level ($\sim$5 to 20 nm). However the majority of the surface morphology examination conducted on POPs using TEM is identical to that using FESEM. A few other examples are described here. Trabolshi *et al.* showed the development of two distinct morphology based cationic POPs by using two different amine monomers in a solvothermal reaction. One of the POPs exhibited nanosheet morphology, whereas the other showed nanotube morphology, as revealed by the HRTEM images (Fig. 6m and n). Also, the *d*-spacing of the nanosheets was evaluated by the low magnification HRTEM images (Fig. 6o).[169] Our group used the TEM/HRTEM technique for morphological characterization and morphological evolution of an ionic POP, which displayed spherical and flake morphology.[76] Similarly, in another interesting report, Patra *et al.* demonstrated the use of TEM/HRTEM to investigate the various morphologies of POPs as well as their morphological evolution. In this work, the authors developed a

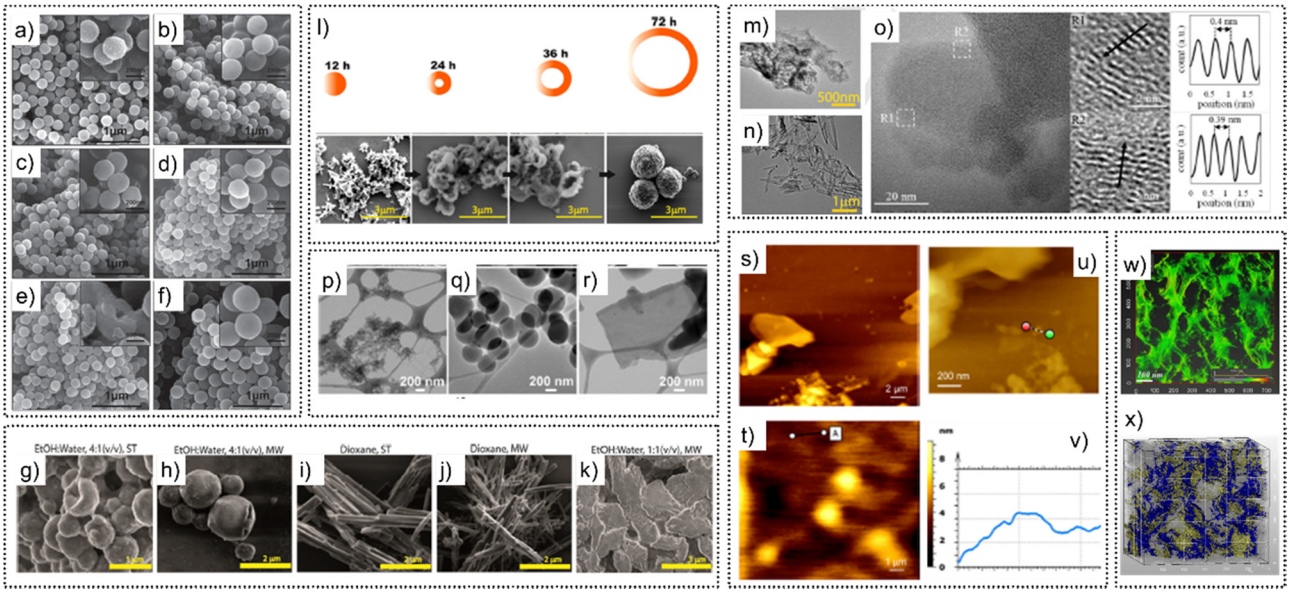

Fig. 6 (a)–(f) FESEM images of hollow microporous carbon spheres (HCSs). Reproduced with permission from ref. 166. Copyright 2016, Wiley-VCH Verlag GmbH & Co. KGaA, Weinheim. (g)–(k) SEM images of cationic viologen organic networks with hollow sphere (HS), hollow tube (HT) and nanosheet morphologies. (l) Schematic diagram and the corresponding SEM images of formation of hollow spheres. Reproduced with permission from ref. 83. Copyright 2017, American Chemical Society. (m)–(o) TEM and HRTEM images indicating the formation of nanosheets and nanotubes. The magnified HRTEM images show the *d*-spacing of the nanosheets. Reproduced with permission from ref. 169. Copyright 2017, Wiley-VCH Verlag GmbH & Co. KGaA, Weinheim. (p)–(r) HRTEM images of three different morphologies of HCPs. (s)–(v) AFM images of iPOP-5 revealing flake-like, spherical particle and nanosheet morphology with its height profile, respectively. Reproduced with permission from ref. 76. Copyright 2022, American Chemical Society. (w) and (x) 3D electron-tomography images of iVOFm showing the distribution of ordered macropores. Reproduced with permission from ref. 171. Copyright 2022, Wiley-VCH Verlag GmbH & Co. KGaA, Weinheim.

series of three different morphology (such as irregular, rigid sphere and sheet-like) based HCPs (FCTP, SCTP and SKTP) depending on three different fabrication routes. The surface morphology characterization of all these POPs was done by TEM or HRTEM. As a result, irregular aggregate-like morphology for FCTP, rigid spherical particles for SCTP and stacked nanosheets for SKTP were observed from the HRTEM images (Fig. 6p–r). Further, they performed the time-dependent morphological analysis of one POP (SKTP) using HRTEM, along with FESEM. They found that upon changing the reaction time and conditions, the initial nanospheres were fused to form nanoribbons, which further converted into 2D-nanosheets.[170] In addition to this, they also showed the TEM-elemental mapping images, which exhibited the presence of all relevant elements throughout the surface of the POP.

5.8 Atomic force microscopy (AFM)

AFM is another microscopic technique that is used to characterize the POP surface. AFM provides more informative 2D or 3D images of POP surfaces to understand the height and surface roughness. This technique creates images by scanning the micrometre square area surface of a sample with a tiny cantilever with a depth of field of ~10–60 μm. AFM is particularly important to characterize POPs when the materials exhibited sheet/layer like morphology or other shapes such as spherical. The height profile images from AFM provide important information regarding the rough surface of layers of POPs. An example of utilization of AFM to understand the morphology of the POP structure has been described here. Our group demonstrated morphological investigation of an ionic POP (iPOP-5) with the help of AFM images and its height profile. In this study, an ionic polymer was synthesized, which exhibited two different morphologies (flakes and spherical) depending upon the reaction time. The AFM images of this POP revealed clear flake-like and spherical particle morphology (Fig. 6s and t). Moreover, upon analyte mediated exfoliation, these flakes were converted into nanosheets, which were again visualized in the respective AFM images and the corresponding height profile images(Fig. 6u and v).[76] This technique has also been used to understand the complete polymerization of monomers on the surface of graphene, in the case of synthesis of POPs with graphene. The AFM images and thickness analyses revealed free-standing sheets with morphology similar to that of graphene and with sizes ranging from 200 nm to several micrometers.[74]

5.9 Electron tomography

The state-of-the-art characterization of POPs has skyrocketed in the recent past with outstanding development. The electron tomography technique is also used to visualize the presence of large pores in the polymeric network. Moreover, the volume rendered 3D electron tomographic images, which are reconstructed by probing a segment of the targeted materials, provided crucial information about the hierarchical porous nature of POPs. In a recent report, we demonstrated the utility of the electron tomography technique as an effective tool for

better understanding of the hierarchical porous nature of a charged macro–microporous organic polymer (iVOFm). In this work, a viologen unit grafted cationic polymeric network with macro–micro hierarchical porous nature has been constructed and used for efficient removal of anions from water.[171] A 3D electron-tomography experiment was carried out to gain more understanding of the hierarchical porosity structure of the iVOFm. This showed the color-coded picture of a widespread dispersion of macropores with enormous nanometer sizes connected across the iVOFm volume (Fig. 6w and x).

6. Functional exploration and state-of-the-art of POPs towards environmental remediation

Owing to the unique characteristic features, POPs were highly explored as promising materials in the field of various leading applications. Advanced functions of POPs have been flourishing in recent years by controlled engineering at the molecular level. The diversity of POPs with customizable structure, porosity, and function is influenced by the abundance of designable building components. From the application view point, in-depth fundamental understanding of POPs with clear structure–property correlation is typical but highly challenging. Precise control over the structure and composition of POPs, *e.g.* pore size, framework functionalities, *etc.*, can render better hold over the structure–property relationship for a specific application which can result in optimized performances. Typically, the pore size and surface area are the most important aspects for the applications of POPs. For example, the nanoporous (micro/meso) nature with high surface area of POPs aids in the exploration of a micro environment for gas storage and separation application. However, the pore size of POPs also governs the overall adsorption capacity toward a specific gas molecule as for an efficient sorption process the kinetic diameter of the incoming gas molecules should match the pore size of the POP framework. In addition, by utilizing facile diverse synthetic strategies, the introduction of functional recognition sites into the nanospace of POPs helps in achieving selective binding affinity to specific gas molecules. Moreover, the functional group decorated pi-conjugated porous surface with confined pores of POPs offers recognition space for different guest molecules, which enables functional exploration towards catalysis and chemical separation or extraction application. In particular, in applications associated with size or shape selectivity, *e.g.* molecular sieving, catalysis, *etc.*, the pore size of the POPs should be adequately big to accommodate the substrates and allow the reaction for high size selectivity and conversion. For such applications, trade-off between kinetics and selectivity is also an important factor toward overall performance. For example, POPs and POP-based membranes often encounter such trade-off between selectivity-kinetics and selectivity-permeability, which limits their separation performance. To this end, POPs with hierarchical porosity enabled with small and large interlinked pores are proven to be more suitable. In addition, the presence of appropriate pore functionalities also plays a crucial role in targeted applications. Pre-synthetic modification of the monomers and post-synthetic modification of the organic skeletons are the main pathway to incorporate targeted functionalities inside POP structures. Installation of appropriate functionalities can improve the chemical affinity between the POP framework and the incoming guest molecules. Moreover, the heterogeneous nature of POPs renders superior recyclability for various potential applications. Additionally, the presence of pure organic components without any metal ions in the pristine POPs offers no generation of secondary pollutants during application. Furthermore, the excellent stability of POPs in various complex environments ensures their use as a potential platform across a variety of contexts. Taking into account the structural integrity of this review and the specialization of environmental remediation, here, we provide a brief overview of several types of POPs that have been used for the challenging environmental issues such as gas storage and separation, heterogeneous catalysis, removal of contaminants and chemical sensing application with the relevant synthetic approaches, and the associated mechanisms.

6.1 Environmentally related pollutant sensing

From the view point of environmental safety, human health, chemical and food industries, defense, *etc.*, detection of various toxic species has piqued the interest and attention of scientists to an increasing degree. In the past few years, considering the importance of the detrimental effect of various harmful toxic substances on living beings along with the national security standards, development of potential sensors and further analysis of their sensing mechanism have become a topical research interest. Among the various sensing techniques, the luminescence based detection method is regarded as more productive over others, owing to the relatively easy technical operation, low cost, rapid detection response, and high sensitivity.[172,173] In this context, because of the characteristic features described above along with the unique properties such as electronically rich pi-conjugated structural moieties, facile incorporation of functional recognition sites and the pre-concentration effect of POPs, which trigger signal transition in highly sensitive sensing of analytes, POPs have been widely investigated as potential luminescence sensors for detection application.[159,174–177] In addition, POPs are unique when compared to other porous materials owing to the fine control over both electronic and photo-physical properties at the molecular level.[178] In the case of POP-based sensing, among others, fluorescence-based detection mechanisms including photo-induced electron transfer (PET), resonance energy transfer (RET), inner filter effects and adsorption competition quenching along with the nature of fluorescence quenching (such as static and dynamic) have been widely studied in the literature.[174–176] Apart from these quenching or ''turn-off'' mechanisms, the luminescence-enhancement or ''turn-on'' mechanism has also been reported for POP-based sensing application. With the help of these insight mechanisms, POPs were explored towards selective and sensitive detection of multiple analytes such as heavy metal ions, explosives, small organic molecules, gases, biological samples and many

more. Moreover, POPs have also been used to develop various devices for the on-site detection of different environmentally relevant toxic chemicals. In the following section, a brief description of the recent advancement in the field of POP based sensing studies has been systematically organized depending upon the nature of the analytes.

6.1.1 Explosive sensing. One of the important classes of species that are to be detected is explosives. From the perspective of personal, environmental, and national security, selective, sensitive and fast detection of these explosives has become a significant research topic. Among the most potential explosives, trinitrotoluene (TNT), trinitrophenol (TNP, also known as picric acid (PA)), 2,4-dinitrotoluene (2,4-DNT), nitro-benzene (NB), *etc.* have been majorly detected by POP materials, owing to their detrimental effect on the environment, especially towards human beings.[179] As mentioned earlier, the high porosity with large surface area, conjugated electron rich surface, and robustness in synergy with heterogeneous nature make POPs some of the best compatible materials for highly sensitive and selective identification of explosives under various conditions.

The study of sensitive detection of explosives (TNT and PA) by developing novel luminescent POPs was first led by Cao *et al.* in 2012. In this study the group synthesized three carbon-carbon conjugated covalent organic polymers (COPs) by rationally changing the central cores of the polymers from nitrogen (COP-2) to benzene (COP-3) to triazine (COP-4) by utilizing the Ni-metal catalyzed Yamamoto reaction.[180] After synthesis and thorough characterization, all these COPs were employed to detect explosives. Interestingly, these COPs were found to sense trace concentrations (<1 ppm) of PA and TNT explosives selectively and sensitively. In this line, in another work, to demonstrate the role of the central core and other pendent functional groups of polymers in the sensitive detection of PA, two new luminescent COPs were synthesized by utilizing the Ni-catalyzed Yamamoto coupling reaction and applied for PA recognition.[181] The two COPs, COP-301 and COP-401, were constructed by the coupling reaction of 1,4-dibromobenzene with 1,3,5-tris(4-bromophenyl)-benzene and 2,4,6-tris-(4-bromophenyl)-[1,3,5]-triazine, respectively. Both the benzene core containing COP-301 and triazine core containing COP-401 exhibited high fluorescence intensity in methanol, which was quenched rapidly upon incremental addition of PA with high quenching constant values. Along with the high sensitivity (low concentration of $\sim$1 ppm), the COPs were observed to detect PA selectively even in the presence of other explosive analytes including DNT, TNT, NB, and mDNB. Moreover, the authors found electron transfer between the probe and analytes as a major mechanism behind such quenching phenomena. Furthermore, interestingly, the quenching constant value (K_{sv}) of the benzene core-based polymer (COP-301) was found to be significantly higher than that of the triazine core-based COP-401. The authors concluded that the relatively high LUMO energy of COP-301 promoting the easy electron transfer from the electron rich benzene core polymeric network to electron deficient PA in the PET process might be the cause of such difference in sensitivity. Thereafter, in another report, in order to explore the role of the length of monomers of porous organic polymers in the detection of explosives, Cao *et al.* synthesized a series of porous nanotubes (PNTs) by the coupling reaction of 1,3,5-tris(4-bromophenyl)-benzene with three different sized monomers such as 1,4-dibromobenzene, 4,4′-dibromo-1,1′-biphenyl and 4,4″-dibromo-1,1′:4′,1″-terphenyl to produce PNT-4, PNT-5, and PNT-6, respectively (Fig. 7a).[182] Both the porosity or surface area and the fluorescence nature of these polymers were found to decrease with increasing length of the monomers of the PNTs. Further, these polymers were applied for fluorescence based detection of PA with high quenching constant values (2.4–6.2 $\times$ 10^5 M^{-1}) and a low limit of detection value ($<2.36 \times 10^{-9}$ M), which indicated the high sensitivity of these polymers for real-time detection of PA (Fig. 7b–g). Moreover, the mechanism of selective identification of PA in the presence of other explosives was explained with the help of resonance energy transfer (RET) and adsorption competition quenching.

Our group demonstrated the aqueous phase detection of 2,4,6-trinitrophenol (TNP), a highly explosive nitro aromatic species, by developing a rationally functionalized porous CTF.[183] Owing to the presence of electron-rich aromatic moieties the POP (CTF-IP10) exhibits strong fluorescence in water (Fig. 7h). Notably, this fluorescence was found to be quenched dramatically upon introducing TNP solution in the aqueous ethanolic phase. Almost complete quenching of emission intensity was observed with the addition of only 80 μL of 1 mmol TNP solution (Fig. 7i). The quenching constant (K_{sv}) was calculated as 8 $\times$ 10^5 L mol^{-1}, which is one of the high values in the domain of POP based explosive sensing. Moreover, this fluorometric detection was highly selective towards TNP, as no other NAC exhibits any response to CTF-IP10 (Fig. 7j). The mechanism of detection was reported as electron transfer from the conduction band of the POP to the LUMO of the analyte (TNP) upon absorbing light. Furthermore, because of the electron-rich and electron-deficient surface dual functionality of the CTF, it was further applied for separation of benzene from its cyclic saturated congener, *i.e.*, cyclohexane.

Triazine group containing polymers are a promising class of POPs that have been used for the detection of explosives. By utilizing the Friedel–Crafts reaction, Geng *et al.* developed a covalently bonded triazine framework (TTPT) by reacting 2,4,6-trichloro-1,3,5-triazine with tetraphenylthiophene.[184] TTPT was found to sensitively and selectively detect o-NP with a K_{sv} value of 6.20 $\times$ 10^3 M^{-1} in the presence of PA, NT, NB and DNT. The authors explored the underlying mechanism of selective detection of o-NP, which suggested the contribution of donor–acceptor electron transfer in synergy with strong H-bonding interactions in the quenching of fluorescence intensity.

However, the selectivity of TTPT towards o-NP over PA was explained by the attenuation of H-bonding between the polymeric backbone and the hydroxyl group of PA, owing to the strong polarity of PA. As discussed above, another class of POPs that exhibited excellent detection ability is PAFs because of their high luminescence nature as well as superior chemical stability. Through the Suzuki coupling reaction, Zhu *et al.* created a

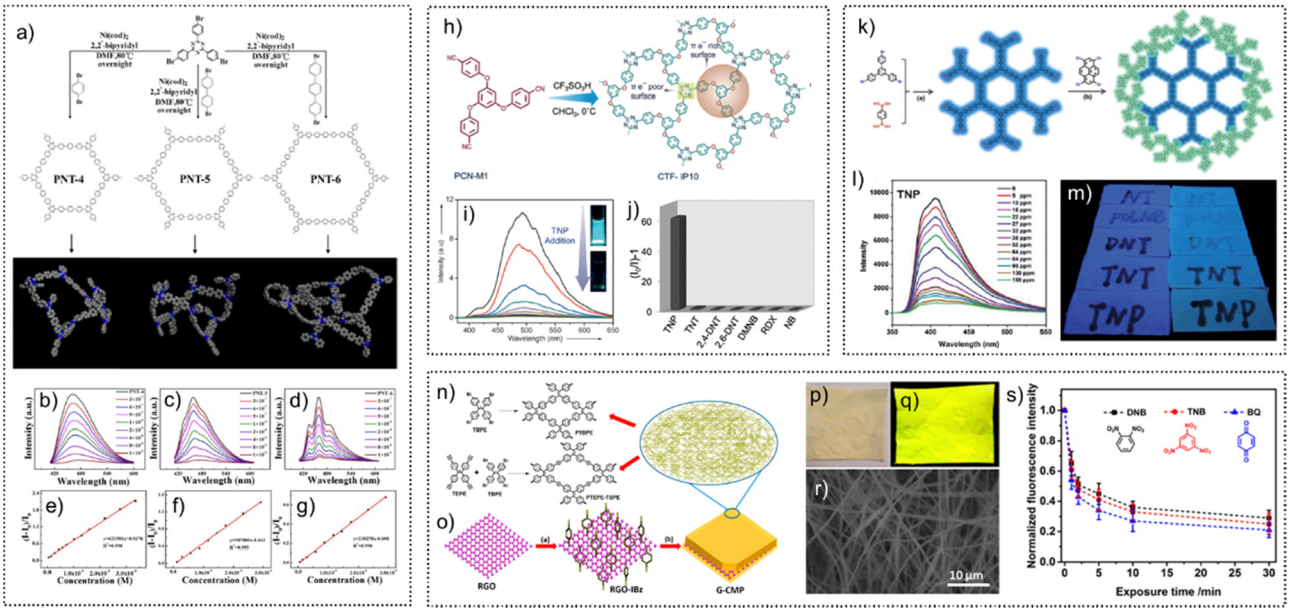

Fig. 7 (a) Synthetic routes for preparation of PNTs by the Ni-catalyzed Yamamoto-type Ullmann cross-coupling reaction. (b–d) PL emission spectra of PNT-4, PNT-5 and PNT-6, respectively, dispersed in solvents after adding different concentrations of PA. (e–g) Stern–Volmer plots of PNT-4, PNT-5 and PNT-6 for sensing PA, respectively. Reproduced with permission from ref. 182. Copyright 2018, Elsevier. (h) Illustration of the preparation of CTF-IP10. (i) PL emission spectra of CTF-IP10, dispersed in H_2O/EtOH after incremental addition of TNP. (j) Selective fluorescence response of CTF-IP10 towards TNP in the presence of various nitroaromatics. Reproduced with permission from ref. 183. Copyright 2016, Wiley-VCH Verlag GmbH & Co. KGaA, Weinheim. (k) Schematic illustration of the synthesis of core–shell PAFs. (l) PL emission spectra of PP-PAF dispersed in ethanol upon incremental addition of TNP. (m) Photographs of the PP-PAF and PPC-PPyS-PAF-2 test strips under UV light after writing with 100 ppm solutions of NT, Cl-NB, DNT, TNT and TNP. Reproduced with permission from ref. 185. Copyright 2015, the Royal Society of Chemistry. (n) Synthetic route for preparation of CMPs: PTBPE and PTEPE-TBPE. (o) Illustration of the process of fabricating graphene-templated CMPs. (p–r) Digital photographs of electrospun PTBPE/PLA nanofibrous films excited by sunlight and a 365 nm UV lamp, respectively. (r) SEM image. (s) Normalized fluorescence intensity of the electrospun PTBPE/PLA nanofibrous films upon exposure to vapors of 1,2-dinitrobenzene (DNB), 1,3,5-trinitrobenzene (TNB), and 1,4-benzoquinone (BQ) for different time periods. Reproduced with permission from ref. 102. Copyright 2015, American Chemical Society.

number of conjugated core–shell PAFs (PPC-PPyS-PAFs), with the polypyrene PAF (PPy-PAF) serving as the shell and the blue-emitting polyphenylene PAF (PP-PAF) serving as the core (Fig. 7k).[185] Due to the probe–analyte electron transfer between the electronically enriched PAFs and the electron-deficient nitro aromatics, these core–shell PAFs exhibit enhanced sensing responsiveness toward TNP in ethanol solution with a high quenching constant value (Fig. 7l). That being said, apart from the solution phase, explosive detection from the vapour phase is critically important for real-time sensing application. Considering this fact, in the above work the authors fabricated a highly emissive thin layer of the polymer and applied it for the detection of nitro aromatic vapours. It was observed that the strong emission intensity of the PAF-based thin layer was quenched when treated with nitro aromatic vapour for 2 min (Fig. 7m). Moreover, upon vapour exposure the emission wavelength was found to be significantly shifted. This result suggests the rapid recognition of nitro aromatics by the developed thin-layer PAFs and also indicates that the adopted core–shell method is a viable protocol to create luminous POPs with unheard-of potential uses.

It is important to note that sometimes the practical conditions for using a POP-based sensor in powder form cannot be fully accomplished. Therefore, POPs' capacity to be processed into many more cohesive usable forms, such as thin films and mixed-matrix-membranes (MMMs), is greatly valued for applications involving extensive real-time sensing. Notably, there are several protocols for fabricating POP-based films or MMMs, including crosslinking, layer-by-layer assembly, surface-initiated growth, *etc.*[174–177] The development of a technique for making self-standing, crack-free, robust thin films or MMMs that can maintain their porosity and polymeric framework is greatly desired. Additionally, POP films or MMMs can advance fluorescence sensing technology and broaden the scope of POP materials for sensing.

In this line, the development of POP-based microporous films is made possible by the use of a few effective techniques such as electron-spinning, electrochemical oxidative polymerization, *etc.*, which are prospective methods for growing high-quality POP thin films with regulated thickness and surface roughness suited for device construction.[174] This is particularly important for vapour phase toxic analyte sensing. With this aim, Scherf *et al.* successfully fabricated composite based POP films by utilizing the electro-spinning method for the detection of nitro aromatic vapors. Based on 4-iodophenyl substituted graphene (RGO-IBz), the group at first created the graphene templated CMP hybrids (G-CMPs) (called G-PTBPE) using the Yamamoto cross-coupling process and further constructed the PTBPE-based light-emitting nanofibrous films with the help of poly(lactic acid) (PLA) (Fig. 7n and o).[102] This hybrid PTBPE and PLA film was found to be highly luminescent in nature with

enough porosity, self-standing and flexible (Fig. 7p–r). Inspired by these unique properties, the thus fabricated films were employed for the vapour phase detection of nitro aromatics, vapours of benzoquinone and metal ion oxidation (Fig. 7s). Interestingly, the films were found to sense nitro explosives rapidly with a significant quenching efficiency.

In another report, utilization of the electrochemical polymerization technique for the fabrication of POP-based films and their further use for fluorescence-on and fluorescence-off based explosive recognition was demonstrated by Jiang *et al.* In this study, inspired by the remarkable π-conjugation and photoluminescence properties, a conjugated microporous polymer (TCB-CMP) with a large surface area and blue luminescence was created *via* condensation of the carbazole derivative TCB.[186] Thereafter, when exposed to arene vapours, TCB-CMP demonstrated improved detection sensitivity and enabled quick identification of arenes. Moreover, the polymer was found to exhibit 'turn-on' fluorescence response in the presence of electron rich arene vapours and 'turn-off' or fluorescence quenching when exposed to electron-deficient arene vapours. The TCB-CMP polymer could be reused for sensing. The authors explored the underlying mechanism and found the rapid absorbance followed by broad interface interaction of arene molecules with the polymeric network behind such drastic change in the fluorescence properties of the CMP. In another study, by taking the benefit of low oxidative potential and strong electroactivity, N-substituted carbazole was employed to create conjugated microporous polymer (CMP) films (TPBCz-CMP) using multicycle cyclic voltammetry.[187] These films were then applied for the label-free chemo- and biosensing of nitro arenes, and were found to exhibit fluorescence enhancement and quenching (turn-on and turn-off) response towards electronically saturated and deficient explosives, respectively, with a rapid response time, excellent selectivity and reusability. As a result, when exposed for 20 seconds to 1,2-dinitrobenzene (DNB), the CMP films showed an improved response, with 75% of the fluorescence intensity. Also, after 20 minutes of exposure to hexafluorobenzene (HFB), 87% of the fluorescence intensity was found to be quenched. Motivated by this work, the same group again applied the electrochemical polymerization method to develop POP films taking N-substituted carbazole units along with an AIE core and a twisted linker.[188] This time, a high-throughput and simple approach was optimized for making the porous films (polyTPECz) that are extremely emissive in nature (Fig. 8a–c). The thickness of the films could be adjusted by varying the number of CV cycles and created directly on the electrode (Fig. 8d and e). The polyTPECz films were found to exhibit high fluorescence quantum yield owing to the presence of AIE moieties in the polymeric π-network. Moreover, the films were found to be capable of detecting TNP at low concentrations in a selective and sensitive manner based on the decrease in the strong fluorescence intensity (Fig. 8f and g).

There are several other reports in which luminescent POPs have been used as a potential sensory material for the detection of various explosives by developing thin films with the help of the electrochemical polymerization method. The Scherf group demonstrated the use of different AIE core-based polymers for the detection of TNT by developing films using chemical and electrochemical oxidative coupling.[189] TPE-core containing multifunctional carbazole and thiophene AIE moieties have been chosen for synthesizing a series of microporous polymer networks (MPNs). Owing to the presence of AIE cores, these

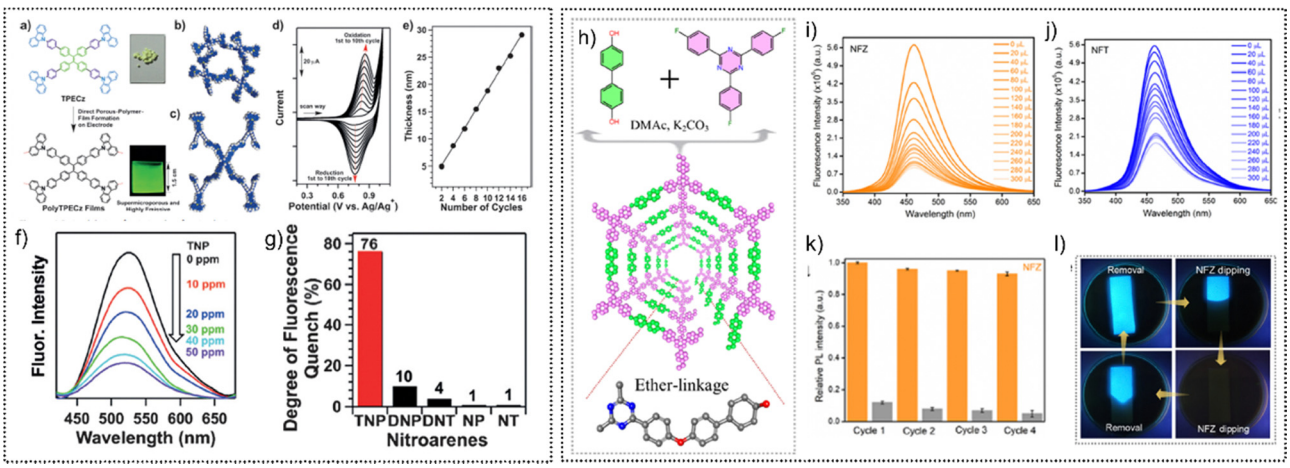

Fig. 8 (a) Illustration of the formation of emissive photofunctional microporous polymer-based films by electropolymerization (top: photograph of TPECz powder, bottom: image of an emissive microporous polyTPECz film). DFT simulated (b) closed and (c) open optimal structure of the TPECz-based segments of the polymer. (d) CV profiles of a solution of TPECz in acetonitrile/CH_2Cl_2. (e) Plot of the film thickness *versus* the number of CV cycles. (f) PL emission spectral change and (g) degree of fluorescence quenching of a 10 nm thick polyTPECz film upon immersion in solutions of TNP and various nitroarenes (50 ppm) in acetonitrile for 1 min, respectively. Reproduced with permission from ref. 188. Copyright 2015, Wiley-VCH. (h) Schematic illustration of synthetic preparation of IP_{POP}-1. (i) and (j) Fluorescence emission spectra of IP_{POP}-1 in acetonitrile/H_2O solvent upon incremental addition of NFZ and NFT aqueous solutions, respectively. (k) Result of the recyclability test of the NFZ antibiotic detection by IP_{POP}-1. (l) Digital images of the application of IP_{POP}-1@PVDF films for the detection of NFZ under UV light. Reproduced with permission from ref. 194. Copyright 2022, American Chemical Society.

MPNs exhibit strong fluorescence and the high degree of cross-linking provides a large surface area. These MPN films were further applied for the detection of nitro aromatics, wherein the sharp fluorescence intensity was found to be quenched gradually with high sensitivity (LOD = 1 ppm) upon incremental addition of acetonitrile solution of 50 ppm TNT. Riedl *et al.* reported electro-production of POP-based thin films of a blue fluorescent spiro-carbazole functionalized polymer (PSpCz-MPNs) and further used them for the sensitive detection of trace-level TNT vapour.[190] Apart from this study, a few other excellent works explored the potential of POPs and POP-based films towards explosive sensing (Table S1, ESI†).

6.1.2 Biologically relevant toxic organic pollutant sensing. The selective and sensitive identification of various biologically relevant molecules such as different drug molecules including antibiotics, pesticides, herbicides, *etc.* is considered to be highly important owing to their significant importance in terms of the environment, public safety and human health.[191] Therefore, development of efficient stable sensory materials for the detection of trace amounts of these molecules from water or different chemical environments in a selective manner is desirable. From this viewpoint, POPs could serve as promising materials for sensing various biological molecules.

Tetracycline is a well known and widely used antibiotic. Fluorescence based selective detection of tetracycline by POPs was investigated by Liang *et al.*[192] In this study, two different CMPs (CMP-LS7 and CMP-LS8) were synthesized through the Suzuki coupling reaction of 2,4,6-tris(4-bromophenyl)pyridine with di and tri borate substituted aromatic moieties, respectively. Both the polymers were found to exhibit excellent porosity with large surface areas as well as high luminescence nature due to the presence of an expanded π-conjugated network. After understanding the properties of the polymers, both CMP-LS7 and CMP-LS8 were applied for sensing and adsorption of tetracycline (TC). Notably, these two polymers were observed to demonstrate sensitive detection ability towards the tetracycline antibiotic with superior quenching constant values of K_{sv} = 1.92 × 10^4 and 8.86 × 10^4 M^{-1} for CMP-LS7 and CMP-LS8, respectively. Also, the corresponding LOD values were calculated as 0.94 and 0.22 μM, respectively. Moreover, the polymers were found to selectively detect tetracycline even in the presence of other relevant antibiotics. In another work by the Bhattacharya group, by using the Pd(0) catalyzed Suzuki–Miyaura coupling reaction, a nickel-porphyrin core containing donor–acceptor-based CMP (PER@NiP-CMOP-1) was successfully synthesized and further employed for sensing antibiotics.[193] For this study, neomycin was chosen as the aminoglycoside antibiotic, which is an important species exclusively used in the pharmaceutical industry as a preventive medicine. After synthesis and characterization, the polymer was found to exhibit turn-on blue fluorescence response with a significant enhancement (~62-fold) of emission intensity when exposed to neomycin. The LOD value for highly sensitive stereospecific biosensing of neomycin was calculated as 137 ppb. Further, the insight mechanism of fluorescence-on behaviour of the polymer was carefully explained by the authors. The restriction of the electron transfer process from the electron rich perylene core to the Ni-porphyrin units owing to the formation of a coordination complex between the amino groups of neomycin and metal Ni^{2+} along with the generated new O–H–π interaction causes the enhancement of fluorescence intensity. Furthermore, the authors found the reduction of non-radiative energy loss due to rotational freezing of the polymeric network by analyte inclusion as another probable mechanism behind such turn-on response of neomycin sensing. The sensing study was observed to be highly selective towards neomycin in the presence of other antibiotics. Motivated by these results, and to demonstrate paper strip-based application, PER@NiP-CMOP-1 was further applied to detect neomycin in commercial milk samples and commercially available antibiotic tablets. The high sensitivity of this polymer for neomycin in these systems indicated the practical application of the POP.

Based on their electrical characteristics, such as whether they are electron-rich or electron-deficient, antibiotics and pesticides can be categorized. Therefore, the creation of materials with electronically polarised moieties could be useful for quickly discriminating these species. With this aim, in a recent report, our group explored the potential of POPs towards detection of antibiotics and pesticides, which are emerging toxic pollutants in water.[194] The polymer (IPpop-1) was synthesized by reacting TFPT and BPDO monomers at high temperature in DMAc solvent catalyzed by K_2CO_3 (Fig. 8h). The synthesized chemically stable IPpop-1 exhibited a highly luminescent sky-blue colour in acetonitrile/water medium. Inspired by this unique characteristic, IPpop-1 was employed for the selective and sensitive identification of antibiotics and pesticides in water. In the presence of electron-deficient antibiotics like nitrofurantoin (NFT) and nitrofurazone (NFZ), and pesticides like chloropyriphos (CHPS) and nitrofen, IPpop-1 had a selective strong quenching response (Fig. 8i and j). IP_{POP}-1 was reported to have detection limits of 0.046 and 0.045 mM, respectively, and to be very sensitive to NFT and NFZ at trace levels. Contrarily, the detection limits for the insecticides CHPS and nitrofen were 0.470 and 0.471 mM, respectively. The turn-off sensing behaviour was found to be reversible (Fig. 8k) and detectable for NFZ in simulated hospital water. In the mechanism study, both FRET and PET were found to be responsible for the selective emission quenching. Furthermore, mixed-matrix membranes (MMMs) based on IP_{POP}-1 were created and used to simulate real-time antibiotic detection in water (Fig. 8l).

As mentioned before, apart from antibiotics, another important class of biological species is pesticides. The detection of toxic pesticides with hyper-cross-linked polymers was demonstrated by Wang *et al.* The group synthesized microporous (PAN-L) and mesoporous (PAN-L-Br) poly-aminal networks (PAN) by applying a condensation reaction between pendant triphenylamine and dibromotriphenylamine chromophore groups and melamine.[195] Both the polymers were found to exhibit high fluorescence nature with an intense turquoise colour under the excitation of UV light. Interestingly, the strong emission intensity of these POPs was observed to be quenched when treated with highly toxic pesticides such as fenitrothion (an insecticide) and trifluralin and glyphosate (herbicides). The investigation of the underlying

sensing mechanism revealed that the energy transfer from the electron-rich triphenylamine moiety of the polymer to the electron deficient analytes (pesticides) causes the fluorescence quenching response. In a more detailed study the authors found that although the LUMO energy of PAN-L-Br is lower than that of PAN-L, the bromo substituted polymer was more sensitive with higher quenching constant values towards pesticides. The authors addressed this interesting observation by means of triggered mass transfer by the mesoporous cavity of PAN-L-Br, which is much higher than that due to the microporous nature of PAN-L. Motivated by the result, PAN-L-Br ethanolic solution@ test-paper based recyclable chemo-sensing of the toxic pesticides was demonstrated in order to explore the practical application of the probe towards potable sensing of biological molecules. Along with these, there are several other representative examples, which exhibit the potential of POPs for biological molecule or biomarker sensing, and bioimaging application.[196–198]

6.1.3 Cationic pollutant sensing from water. Detection of cations, especially metal ions, is highly important owing to their application in biology, energy and environment. Two main factors have prompted significant interest in the development of POPs for the selective and sensitive detection of metal ions in water. The first is the biochemical perspective, as metal ions are essential for many physiological processes, and their disruption can have serious biological health consequences. The second consideration is the environment, as greater concentrations of metal ions in water streams create severe environmental damage when they exceed the permissible level.[199] On the other hand, radioactive metal cations such as uranium ions (UO_2^{2+}) are extremely problematic due to their high level of radiotoxicity. Therefore, preferential identification of metal cations is highly important and desirable. In this context, owing to the high chemical and thermal stability along with luminescence properties, POPs are ideal candidates for sensing metal cations, especially Fe^{3+}, Cu^{2+}, Hg^{2+}, UO_2^{2+}, *etc.* It should be mentioned that an extensive number of studies have been reported on cation sensing by POP materials, and in this review a few systemically described works have been included which are organized in Table S2 (ESI†).

Among the heavy metal cations, the mercury ion (Hg^{2+}) is well known for its toxicity and therefore its detection by POPs is of interest. Sulfur containing moieties have widely been used in a probe for selective detection of Hg^{2+} ions. Thioether functional groups exhibit selective affinity towards Hg^{2+} ions due to their facile soft–soft interaction. Inspired by this concept, Cao *et al.* synthesized a thioether functionalized POP (COP-108-S) by the coupling reaction between 1,4-dibromo-2,5-bis((ethylthio)-methyl)benzene (DB-S) and 1,3,5-tris-(4-bromophenyl)benzene (TBB) using the Ni-catalyzed Yamamoto reaction.[200] The synthesized POP exhibited high fluorescence emission in the solid state as well as in ethanolic dispersion owing to the presence of extended π-conjugation and the effect of aggregation caused quenching (ACQ) of the polymeric network. Further, COP-108-S was applied for the detection of metal cations. Interestingly, it was found that the PL intensity was quenched upon treatment with Hg^{2+} and Fe^{3+} metal cations. As an insight mechanism of Hg^{2+} sensing, contribution of both electron transfer and static quenching was reported. Moreover, in a detailed sensing study, after the addition of 1.0 mM Hg^{2+}, COP-108-S showed 83% quenching efficiency. Also, the POP exhibited excellent recyclability after Na_2S treatment for regeneration.

It should be pointed out that the thioether alkyl chains embellished on the polymeric structure of POPs may obstruct the pore channels and decrease the exposure of S atoms for coordination with Hg^{2+}, which would affect the sensing effectiveness and further the sensitivity. Therefore, as an alternative way, it would be more effective to directly introduce thioether functionality into the backbone of POPs. This strategy motivated the Yan and Yu group for demonstrating Hg^{2+} sensing with framework integrated thioether functional POPs. For this, by using a simple one-pot Friedel–Crafts reaction, they were able to create porous sulfide-bridged polytriazine nanospheres (NOP-28) (Fig. 9a).[201] The thus synthesized sulfur rich thioether functionalized POP was employed for Hg^{2+} sensing in ethanol medium. NOP-28 was found to exhibit selective binding affinity to Hg^{2+} metal cations and therefore the fluorescence emission wasquenched (Fig. 9b). The turn-off sensing response was quite selective towards Hg^{2+} even in the presence of other metal cations. The quenching constant (K_{sv}) and LOD values for the detection of Hg^{2+} were calculated as 3.7×10^4 M^{-1} and 12 ppb, respectively.

The fact that most reported POPs are frequently insoluble and cannot be effectively dispersed in solvents is a disadvantage. This restricts their use in liquid systems, particularly in aqueous solutions, and may hinder the processing required to incorporate them into flexible sensing devices like films and test papers. Creating nanometer-sized POPs (nanoPOPs) in mini-emulsion environments, which considerably increases these materials' solution processability without affecting their porosity, could be an effective strategy for enhanced sensing ability. With this aim, in a recent report, Li *et al.* explored the rapid, highly sensitive and selective detection of Hg^{2+} ions in water with a nano size-based solution processable POP (TPA-POP-CHO) (Fig. 9c).[202] The authors designed the POP in such a way that it exhibits high fluorescence, target-specific binding sites as well as high water dispersity. The thiosemicarbazide group was incorporated in the triphenylamine (TPA)-fluorophore containing POP as a receptor for Hg^{2+}. Also, the nanometer size powder form of the POP makes it highly solution processable. The nanoPOP was found to exhibit remarkable selectivity for Hg^{2+} over other ions (Fig. 9d and e) with outstanding sensitivity ($K_{sv} = 1.01 \times 10^6$ M^{-1}) and quick reaction times. In addition, the sensing study was completely recyclable in nature. Moreover, TPA-POP-CHO coated paper strips were fabricated to demonstrate naked eye Hg^{2+} detection. This result highlighted the portable, affordable, quick, extremely sensitive, and reusable nature of POP sensors for sensing metal ions.

Another environmentally relevant cation is the copper (Cu^{2+}) metal ion. Intramolecular hydrogen bond interaction within the structure of polymeric materials is reported as a key strategy for selective binding of Cu^{2+} ions.[209] McGrier *et al.* utilized this strategy for detection of Cu^{2+} ions by synthesizing a series of Schiff-base POPs based on the tris(N-salicylideneaniline) (TSA)

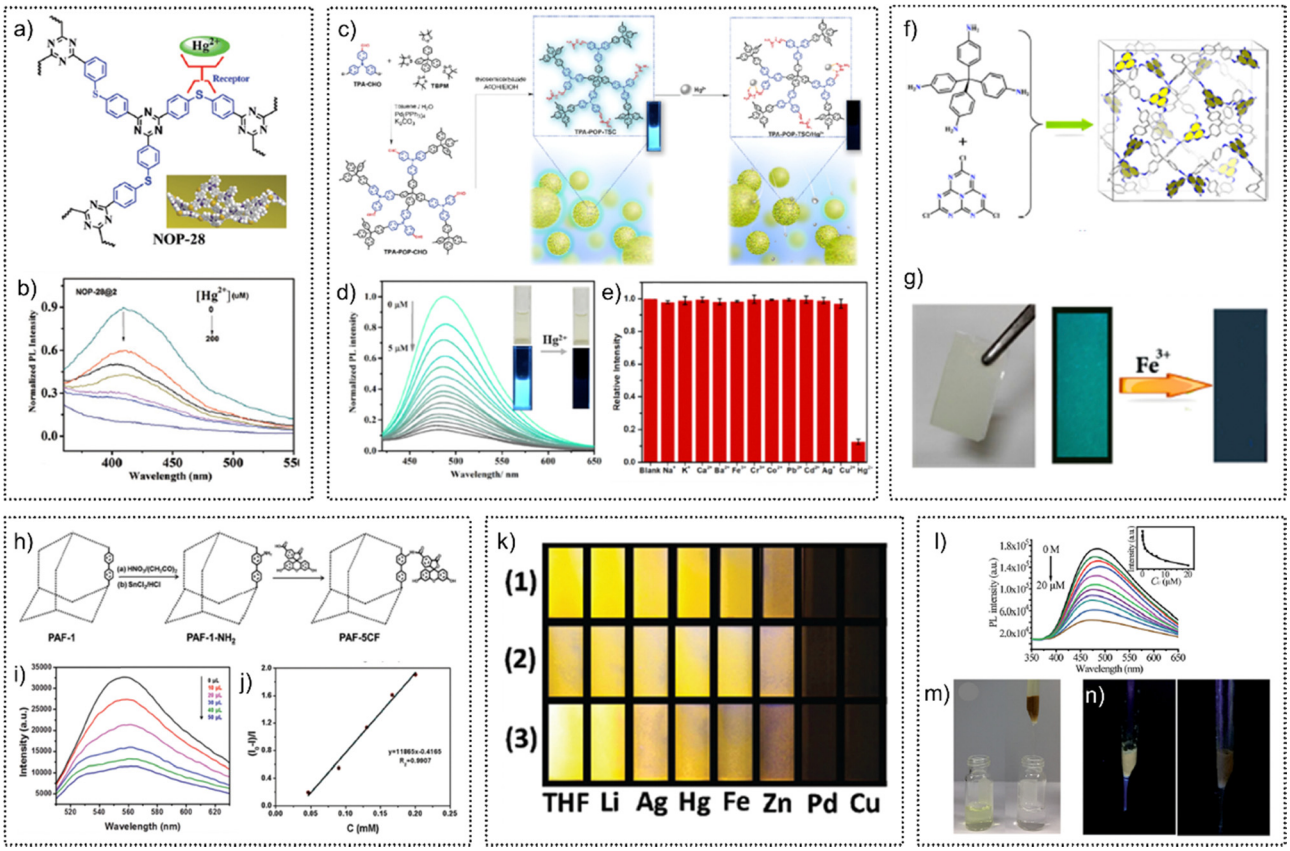

Fig. 9 (a) Chemical structure and 3D illustration of NOP-28 showing the receptor for Hg^{2+}. (b) PL emission spectra of NOP-28@2/ethanol with incremental addition of Hg^{2+}. Reproduced with permission from ref. 201. Copyright 2018, the Royal Society of Chemistry. (c) Synthetic route to TPA-POP-CHO and subsequent postpolymerization modification to afford TPA-POP-TSC, which shows specific binding with Hg^{2+} ions. (d) Fluorescence spectra of TPA-POP-TSC nanoPOP in THF/H_2O solution upon addition of various concentrations of Hg^{2+} (inset: corresponding photos under ambient light and UV light, before and after the addition of 10 μM Hg^{2+}). (e) Results of selective Hg^{2+} ion sensing by TPA-POP-TSC nanoPOP. Reproduced with permission from ref. 202. Copyright 2019, American Chemical Society. (f) Synthesis scheme of POP-HT. (g) Digital images of the POP-HT test film under natural light and UV light before/after Fe^{3+} addition. Reproduced with permission from ref. 204. Copyright 2016, American Chemical Society. (h) Synthetic route to PAF-5CF from post-synthetic modification of PAF-1-NH_2. (i) PL emission spectra of PAF-5CF after the addition of different concentrations of Fe^{3+}. (j) Corresponding Stern–Volmer plot of PAF-5CF. Reproduced with permission from ref. 205. Copyright 2019, the Royal Society of Chemistry. (k) Images of TSA–POP 1 (1), TSA-POP 2 (2), and TSA-POP 3 (3) under a 365 nm UV-lamp suspended in THF before and after the addition of metal ions. Reproduced with permission from ref. 218. Copyright 2017, the Royal Society of Chemistry. (l) PL emission spectra of CMPAO-4 in uranyl solution (inset: the correlation between the PL intensity and uranyl concentration). (m) Column adsorption of uranyl ions using CMPAO-4 as the adsorbent. The left bottle contains uranyl solution, which was subjected to column separation as shown on the right. (n) The images of CMPAO-4 in the column exposed to UV light before and after uranyl adsorption. Reproduced with permission from ref. 98. Copyright 2019, the Royal Society of Chemistry.

core.[210] The presence of hydroxy (–OH) groups close to the imine bonds of the POP facilitates photoinduced enol–keto tautomerization. As a result, the materials displayed excited-state intramolecular proton transfer (ESIPT) and demonstrated significant fluorescence emission in both solid and solution states. Notably, due to the metal–ligand charge transfer process, it was found that Cu^{2+} ions could effectively quench the emission of the POP (Fig. 9k). In another report, Liu *et al.* showed dynamic quenching of Cu^{2+} ions by developing silsesquioxane-based hybrid luminescent POPs (HLPPs).[211]

Detection of uranium (as UO_2^{2+}) metal cations is essential owing to their importance in nuclear energy along with environmental significance. In the literature the selective strong interaction of the amidoxime group with UO_2^{2+} ions *via* coordination with the N and O center has been widely studied.[212] Taking advantage of this selective interaction, Hua and coworkers reported a UO_2^{2+} sensing study by synthesizing a CMP (CMPAO).[98] The fluorescent polymer was fabricated by Sonogashira coupling reactions taking 1,3,5-triethynylbenzene as a core. Further, the POP was modified by decorating with amidoxime (–NH_2C═N–OH) and carboxylate (–COOH) groups through the reaction of hydroxylamine hydrochloride (NH_2OH·HCl) and base KOH. The presence of the pi-conjugation network makes the polymer highly fluorescent in nature. Also, the functional groups create high water dispersity of the POP. Thereafter, the CMPAO was used for detection of UO_2^{2+} metal ions. As anticipated, owing to the presence of the amidoxime group the POP exhibited selective and sensitive quenching of fluorescence emission with a relatively low LOD value of 1.7 nM in water when treated with UO_2^{2+} ions (Fig. 9l). Importantly, this LOD value was found to be much

lower than the permitted limit for U in drinking water (6.3×10^{-8} M) set by WHO. The adsorption and quenching response were also observed in a column setup under UV light (Fig. 9m and n).

6.1.4 Biologically important metal sensing from water. The iron metal ion, a fundamental cation, is crucial for many physiological processes in both the ecosystem and human beings. Significant effort has been made toward the creation of materials for the selective and sensitive detection of Fe^{3+}, a key metal ion in water.[199] Designing sensors with Lewis basic N-sites is considered as an effective strategy for recognition of Fe^{3+} ions.[203] Guided by this, Li and Shi *et al.* developed a N-enriched polymer (POP-HT) through the polycondensation of tetra(*p*-aminophenyl)methane and chromophoric 2,5,8-trichloro-*s*-heptazine to demonstrate selective sensing of Fe^{3+} ions (Fig. 9f).[204] The N-atoms which decorate the porous surface of the highly luminescent POP-HT act as free Lewis base sites to interact with Lewis acidic Fe^{3+} metal ions. As a sensing result, in acidic aqueous or DMF solution, Fe^{3+} was found to reduce the emission intensity of the POP continuously upon increasing the concentration of Fe^{3+}. The LOD value of this quenching action was calculated as 5 ppm. The authors explained the mechanism of quenching as due to the strong interaction between the N-atoms of heptazine moieties of the POP and Fe^{3+} ions. Furthermore, a portable, easy-to-use fluorescent test film was fabricated for the detection of Fe^{3+}. Under 365 nm UV light, the test film appeared bright aquamarine; nevertheless, it became black when submerged in an aqueous solution of $FeCl_3$ (Fig. 9g).

As discussed above, PAFs are a promising class of porous organic polymers exhibiting potential for various leading applications including chemical sensing, owing to their high chemical stability, high degree of polymerization, abundant aromatic rings induced high fluorescence, *etc.* Zhu and coworkers reported PAF-based Fe^{3+} sensing by a post synthetically modified PAF with fluorescein (PAF-5CF) (Fig. 9h).[205] The presence of fluorescein along with aromatic moieties makes PAF-5CF highly fluorescent in both solid and solution state. When PAF-5CF was employed for metal ion sensing in ethanolic solution, only Fe^{3+} was found to quench the emission intensity with an obvious colour change from yellow to dark under UV light. Interestingly, other metal ions (Na^+, K^+, Ca^{2+}, Zn^{2+}, Ni^{2+}, Al^{3+}) had negligible impact on the emission of PAF-5CF. In addition, a similar observation was noticed in the solid-state. This result clearly indicated the highly selective detection ability of the PAF towards sensing Fe^{3+} ions (Fig. 9i and j). In addition to this, a few more Fe^{3+} sensing studies have been reported with POP materials. Yavuz *et al.* used stable C–C conjugated COP-100 for dynamic fluorogenic detection of Fe^{3+} ions selectively with a quenching efficiency of 70.3% in water.[206] Liu and coworker reported selective and sensitive detection of Fe^{3+} cations with AIE core containing silsesquioxane-based hybrid porous polymers (HPPs).[207] Cao *et al.* reported selective detection of Fe^{3+} ions with various luminescent core containing POPs (COP-6, 7, 9).[208]

In addition to these studies, POPs are found to demonstrate highly efficient detection ability towards other metal cations such as Al^{3+},[213] Co^{3+},[187] and Fe^{2+},[206] with significant quenching constant and LOD values, which proves the potential of POPs for cation sensing.

6.1.5 Anionic pollutant sensing from water. Anions play a crucial role in the environment. Several specific anions such as cyanide (CN^-), halides (*i.e.* fluoride (F^-), iodide (I^-)), and metal-based oxoanions (*i.e.* chromate (CrO_4^{2-}), dichromate ($Cr_2O_7^{2-}$), *etc.*) have significant importance in the field of both biology and environment.[214] Among them, CN^- is one of the most dangerous and possibly lethal anionic species, posing a major hazard to the environment and primarily to living things by ingestion or inhalation and fast distribution throughout the body. Therefore, the maximum permitted level of CN^- in drinking water by WHO is 1.9 mM.[215] Another important anion with the highest permitted level in drinking water of <1.5 ppm is F^-. An excess amount of fluoride in water is highly hazardous, and can result in fatal poisoning.[216] In addition to these, EPA's priority pollutants' list includes heavy metal-based oxoanions, which are also regarded as possible harmful pollutants. Therefore, considering both the biological significance and detrimental consequences of overuse of these anionic species, selective and sensitive identification is critically needed and substantial. In this context, POPs have been widely used as an excellent sensory material for the regular monitoring of these anions.

Sensing of heavy metal-based oxoanions by POPs is a topical research interest. Among oxoanions, dichromate ($Cr_2O_7^{2-}$) is particularly important, which is the stable Cr(VI) species extensively used in pigment, electroplating and printing industries.[138] Cr(VI) is one of the harmful contaminants in wastewater, and can affect humans severely even at low concentration. Successful demonstration of Cr(VI) sensing by a POP material has been done by Wang *et al.* Through the Yamamoto coupling reaction of 1,3-bis(4-bromophenyl)-imidazolium bromide and tetrakis(4-bromophenyl)-ethylene, the group created a series of TPE and imidazolium-based cationic POPs, POPIms (Fig. 10a).[146] Due to the presence of TPE cores, the polymers exhibited strong fluorescence. Also, the cationic nature of the imidazolium POP offers facile exchange of $Cr_2O_7^{2-}$ ions with its integrated Br^- ions. Among the synthesized POPs, POP-Im1 exhibits a broad emission peak centered at $\sim$595 nm with a yellow color in the solid state (excitation at 365 nm). The emission intensity of the luminescence was significantly reduced after $Cr_2O_7^{2-}$ adsorption, which was attributed to the electron-transfer of $Cr_2O_7^{2-}$ lowering the energy of the π–π^* transition in the polymeric network of POP-Im1 (Fig. 10b). In addition to this, the authors also explored the capture study of $Cr_2O_7^{2-}$ ions by these POPs in water. In an interesting work, Wang *et al.* reported radioactive $^{99}TcO_4^-$ detection by a rationally modified PAF (Ir-PAF) with a luminescent iridium(III) organometallic complex (Fig. 10c).[217] This was the first example of a POP-based efficient sensor for facile and selective detection of trace ReO_4^-/TcO_4^- in aqueous solutions. Ir-PAF exhibited turn-on recognition ability towards ReO_4^-/TcO_4^- with a low LOD value of 556.9 μg L^{-1} (Fig. 10d and e). Moreover, the sensing of ReO_4^- was found to be selective in the presence of other anions as well as recyclable up to three cycles (Fig. 10f and g).

As mentioned before, cyanide is a highly toxic anionic species causing serious problems to living beings. Due to their

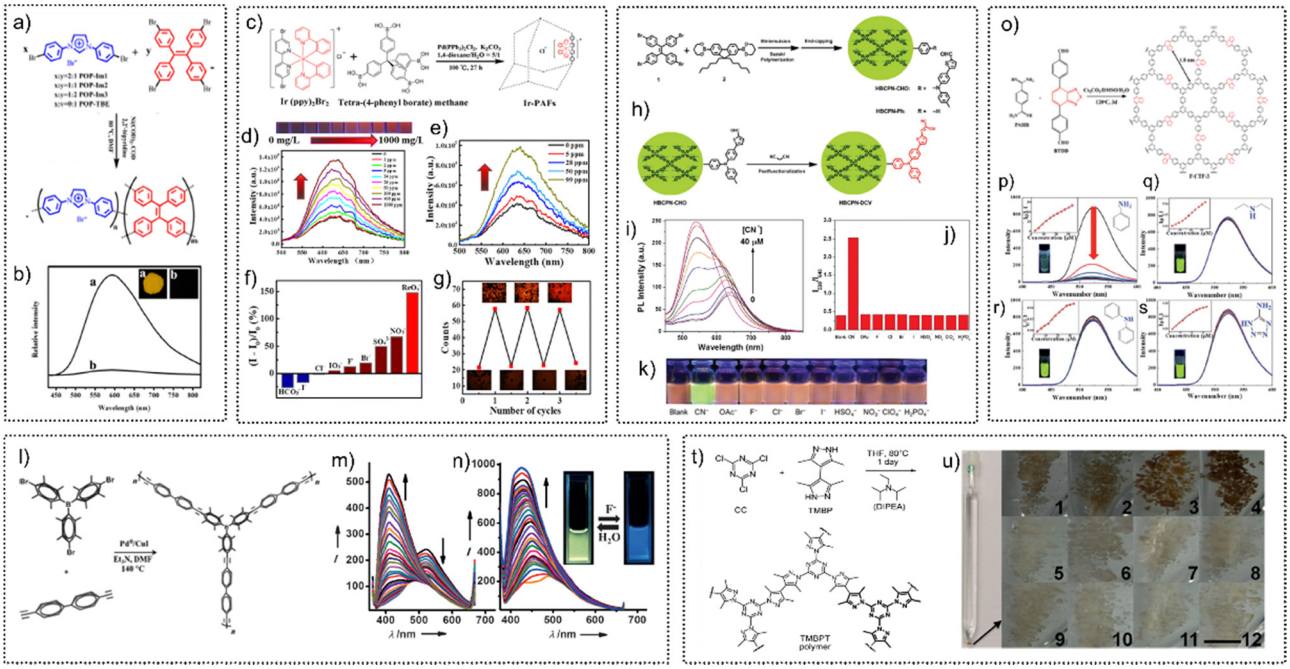

Fig. 10 (a) Schematic representation of the synthesis of POP-Ims and POP-TBE. (b) Room-temperature solid-state emission spectra upon excitation at 365 nm for (curve a) POP-Im1 and (curve b) POP-Im1-Cr (inset: corresponding fluorescent images under UV irradiation). Reproduced with permission from ref. 146. Copyright 2016, American Chemical Society. (c) Synthetic route to Ir-PAF. (d) and (e) PL emission spectra of Ir-PAF in $NaReO_4$ and $^{99}TcO_4^-$ solutions of various concentrations, respectively. (f) Relative PL emission increasing rate of Ir-PAF in different anions. (g) Solid-state PL counts and luminescence brightness changes during three detection cycles. Reproduced with permission from ref. 217. Copyright 2020, American Chemical Society. (h) Synthetic preparation of HBCPN-Ph and HBCPN-DCV, and the model compound M-DCV. (i) PL spectra of HBCPN-DCV in the presence of different concentrations of the cyanide anion in THF dispersions. (j) Ratiometric fluorescence response profiles. (k) Photos of visible fluorescence responses of HBCPN-DCV in the THF/H_2O dispersion in the presence of 100 μM concentration of various anions. Reproduced with permission from ref. 218. Copyright 2014, the Royal Society of Chemistry. (l) Synthesis route to BMOP. (m, n) Changes in the fluorescence spectra of BMOP upon incremental addition of F^- ions in DMSO/H_2O (8 : 2) and THF/H_2O (9 : 1) solvent combination, respectively (inset: images of BMOP dispersed in THF/H_2O under UV light before and after F^- addition and reversibility of the colour change). Reproduced with permission from ref. 220. Copyright 2015, Wiley-VCH. (o) Synthesis route to F-CTF-3. (p)–(s) The emission spectra of F-CTF-3 dispersed in water upon incremental addition of four representative amines: PA, DEA, DPA and ATZ, respectively (inset: corresponding Stern–Volmer plots and images of the amine treated F-CTF-3). Reproduced with permission from ref. 226. Copyright 2020, the Royal Society of Chemistry. (t) Synthetic route to the TMBPT polymer. (u) Images of the setup for the detection of H_2S (left) and the $AgNO_3$-loaded TMBPT powder after being stirred for 4 h at 50 °C in (1) 5 μM H_2S; (2) 10 μM H_2S; (3) 50 μM H_2S; (4) 100 μM H_2S; (5) 5 mM glutathione; (6) 5 mM cysteine; (7) 5 mM NaSCN; (8) 5 mM Na_2SO_3; (9) 5 mM $Na_2S_2O_3$; (10) Kpi buffer; (11) DI water; and (12) 5 mM H_2O_2 solution. Reproduced with permission from ref. 231. Copyright 2014, American Chemical Society.

restricted specific functionality and the weak CN^- ion binding affinity with the POP skeleton, POPs have not been extensively studied for the selective detection of CN^- ions. In a report, the Tong and Wang group explored the selective CN^- ion detection ability of POPs by developing a hyperbranched conjugated polymer (HBCPN-DCV) *via* the Suzuki coupling polymerization reaction.[218] The synthesized HBCPN-DCV nanoparticles exhibited fluorescence emission under UV light. Furthermore, the polymer was subjected to post-synthetic modification by a cyanide-responsive dicyanovinyl fluorophore by reacting with the terminal functional aldehyde groups present on the surface of the polymer (Fig. 10h). This target specific functional nanoprobe was then applied for the detection of CN^- ions in THF medium. Aqueous solution of tetrabutylammonium salt was chosen as a source of CN^- ions for the sensing study. In a sensing titration experiment, the emission peaks at 538 nm increased as aqueous CN^- ions were incrementally added to the THF dispersion of HBCPN-DCV, while a second peak at 640 nm increased slowly at first and eventually disappeared at higher CN^- concentrations. A greater than 10-fold increase in emission enhancement (at 538 nm) was noticed following the addition of 40 μM CN^- (Fig. 10i). In addition, after adding various CN^- concentrations, the emission color likewise shifted from red to yellow to green, which was also visible with the naked eye when seen under a UV lamp (365 nm) (Fig. 10k). The polymer was found to be highly sensitive toward CN^- ions with a LOD value of 0.2 μM. More interestingly, the probe exhibited selective detection of CN^- ions as no other anions were found to change the emission of HBCPN-DCV (Fig. 10j). In the mechanism study, the enhanced energy transfer from the HBCPN core of the polymer to the cyanide-responsive DCV fluorophore was found to play a significant role in the fluorescence change.

Fluoride is another environmentally relevant anionic species, which needs to be monitored. Typically, F^- ions are electronically rich; therefore materials containing electron deficient cores are beneficial for selective detection of F^- ions. From this viewpoint, electron deficient boron (B) atom containing materials/POPs are considered as one of the effective strategies for

sensing F^- ions. Fluorescent off may result from electron transfer from F^- ions to the vacant p orbital of the B atom in B-containing luminescent POPs. Taking this concept into consideration, Feng and colleagues used the Suzuki and Sonogashira reactions to create two novel boron-π-nitrogen-based donor–acceptor type POPs, namely, BN-ph and BN-ph-ae, respectively.[219] Due to their high fluorescence characteristics, these two POPs were chosen for the F^- sensing study. An aqueous solution of tetrabutylammonium fluoride (*n*-Bu_4NF) was used as a source of F^- ions. It was observed that the strong emission intensity of THF dispersion of BN-ph gradually diminished as the molar ratio of fluoride was increased. This is due to the fact that F^- ions slowly fill in the remaining vacant orbital of the B atoms in the polymeric structure and prevent the charge transfer from N to the B centre. This was explained as the probable mechanism behind the sensing of F^- ions. In another work, using a similar concept, Maji and coworkers developed a boron-containing microporous POP (BMOP) using methyl-protected triarylborane as a node and diethynylbiphenyl as a linker for sensing F^- ions (Fig. 10l).[220] It was discovered that BMOP exhibits an increased fluorescence signal when F^- ions are introduced in an aqueous/HF mixture, as well as a clear colour change from green to blue. The POP was found to show highly sensitive (low LOD value) and selective (in the presence of Cl^-, Br^-, I^-, NO_3^- and SO_4^{2-} ions) detection of F^- ions (Fig. 10m). Moreover, BMOP also demonstrated exceptional recyclability from aqueous solution, in which the green emission could be totally regenerated after adding an excessive amount of water to F^-@BMOP due to the enormous hydration enthalpy of the F^- ion (Fig. 10n). In the same line, Liu *et al.* also explored both the colorimetric and fluorescence-based F^- ion sensing ability of another boron-containing POP (BCMP-3) in THF medium.[92]

A few other anions which were detected by POPs are I^-, S^{2-}, MnO_4^-, *etc.* Iodide (I^-) is a vital component of the human body and plays a crucial role in biological processes. Zhang and coworkers created a carbazolic POP (Cz-TPM) for the colorimetric detection of the I^- anion.[221] After adding I^- to the THF dispersion of the POP, the colour changed noticeably, going from practically colourless to yellow in day-light. On the other hand, detection of S^{2-} ions has been demonstrated by Cao *et al.* by developing a luminescent POP nanotube (PNT-1).[222]

According to the explanation above, creating cationic frameworks followed by anion exchange or including electron-deficient atoms in the primary skeletons may be effective design methods for POP-based anion sensors. More work is still required because the POP examples that have been documented so far are so infrequent for anion sensing.

6.1.6 Environmentally relevant small molecule sensing. Small molecules such as volatile organic compounds (VOCs) and other organic–inorganic molecules including amines, molecular iodine (I_2), gases like ammonia (NH_3), hydrochloric acid (HCl) vapour, *etc.* have been found to be sensed by POPs in the last few years. Among them, POPs exhibited promising results for the detection of VOCs such as benzene and its derivatives, hydrocarbons and halo-benzenes. Most of these molecules are carcinogenic in nature owing to their high level of toxicity and cause harmful effects in human beings. Therefore, detection of these species by POPs is of paramount interest to a broad scientific community. In the following section a few representative examples of small molecule sensing by POP materials have been discussed. In a work, through the Ni-catalyzed Yamamoto reaction, Cao *et al.* created three COPs with various central cores of N (COP-2), benzene (COP-3), and triazine (COP-4) and further explored their sensing ability towards VOCs along with nitro explosives.[180] Among the COPs, COP-2 exhibited turn-on luminescence response upon exposure to diethyl ether; however, no significant changes were observed when treated with other small molecules/solvents like DMF and THF. On the other hand, COP-3 and COP-4 could be selectively quenched by chloroform, while other solvents had no effect on their emission intensity. The difference in the recognition ability between COP-2 and COP-3/4 was explained by the alteration of HOMO–LUMO electron density and their corresponding band gaps. In this way the authors explored the role of central atoms of monomers of POPs in the tunable sensing of small molecules. Furthermore, apart from the role of central cores, the same group also showed in a different study the importance of several pendent functional groups of POPs for the adaptive sensing of VOCs.[180] In this study, a series of POPs (COP-401-R) with different functional groups including carboxylic (–COOH), nitro ($-NO_2$), hydroxy (–OH), amine ($-NH_2$), aldehyde (–CHO) and $-SO_2Cl$ were synthesized. Among them, the emission intensity of COP-401-COOH was found to be quenched when exposed to methanol, whereas COP-104-SO_2Cl exhibited yellow luminescence under UV light. Moreover, COP-104-SO_2Cl, in other typical solvents including DMF, THF, MeOH, and acetone, displayed blue luminescence. In another VOC sensing work, Yu *et al.* used the simultaneous Friedel–Crafts and Scholl coupling processes to create a number of spirobifluorene- and triazine-based POPs (Sbf-TMPs).[223] These POPs were found to be potential probes for the detection of electron rich VOCs such as benzene and toluene with turn-on fluorescence behaviour. Moreover, the fluorescence intensity of the thin layer of Sbf-TMP was observed to be enhanced upon exposure to the VOC, namely, ethyl ether vapor. Li, Shi and co-workers demonstrated effective sensing of 1,4-dioxane by developing nitrogen rich POP-HT.[224] Zhao and Hirao *et al.* reported size-selective fluorescence turn-on detection of electron rich VOCs by synthesizing TPE core-based POPs (NUS-20 to NUS-23).[225]

Under the category of small molecules, various aromatic and aliphatic amines are another important class of species that should be identified before their concentration increases in the environment. In this context, POPs again hold great promise for sensing amines. Exceptional selectivity and sensitivity toward primary aromatic amines have been demonstrated by Zhong *et al.* by synthesizing covalent triazine framework nanosheets called F-CTF-3 (Fig. 10o).[226] In this study, fourteen amines from nine different classes, including primary, secondary, and tertiary aliphatic and aromatic amines, heterocyclic amines, pyridine amine, and quaternary ammonium salts, have been tested for fluorogenic identification. The group found that

the primary aromatic amines including aniline, *p*-phenylenediamine (PDA), and 1-naphthylamine (NPA) could significantly reduce the fluorescence emission of F-CTF-3 in water. Notably, the quenching phenomenon was observed to be highly selective in nature (Fig. 10p–s). In another work, Zhang *et al.* synthesized two triazine-based POPs with benzothiadiazole (P1) and benzene (P2) functionalities.[227] Among the CMPs, P1 exhibited fluorescence quenching response for aniline and 1,4-phenylenediamine in water, whereas aliphatic amines do not cause any change in the emission intensity. On the other hand, the P2 POP showed turn-off and turn-on responses towards aniline/1,4-phenylenediamine and aliphatic methylamine/TEA, respectively.

As mentioned before, molecular iodine (I_2) is an example of a small molecule, which is highly significant owing to its radioactive isotopes (^{129}I and ^{131}I). These species are omnipresent in nuclear waste, making I_2 detection crucial. In the recent few years, extensive works have been reported on I_2 sensing and capture by developing various excellent POPs. In order to create POP-based sensors for I_2 detection, electron-rich moieties, particularly heteroatoms like N and S, could be incorporated into the POP structure. This is because the lone pair electrons of heteroatoms of POPs can enhance the interactions with iodine, which can further affect its fluorescence property. Considering this fact, Geng and coworkers reported chemosensing of I_2 by a CMP type POP (TTPA), having triazine and triphenylamine moieties, synthesized through triflic acid-catalyzed Friedel–Crafts polymerization reaction.[116] The TTPA CMP was found to detect I_2 in THF medium with a LOD value of 32.2 pM and a quenching constant $K_{sv}$of 2.38×10^4 M^{-1}. The mechanism of emission quenching was found to be electron transfer from the electron rich POP to electron deficient I_2 molecules. In their follow-up works, the same group explored the potential of POPs for I_2 sensing, by developing various core-based POPs. Among them, AIE effect based TPE core containing POPs (TTTAT and TTDAT), nitrogen containing CMPs, and thiophene and pyrene core-based POPs (PTThP-2 and PTThP-3) demonstrated sensitive detection ability towards molecular iodine.[228–230]

Hydrogen sulfide (H_2S) is a highly toxic gaseous species, and therefore, selective sensing of H_2S is desirable. Xu and coworkers synthesized a triazine and pyrazole core-based POP called TMBPT, which was further modified to Ag@TMBPT by post metalation of the porous polymer with $AgNO_3$ (Fig. 10t).[231] The water dispersed metal loaded POP when treated with a trace concentration (0.17 ppm) of H_2S displayed a brown color. Furthermore, at varied H_2S concentrations, Ag@TMBPT likewise displayed an amonotonic colour change. On the other hand, biologically important thiols like glutathione and cysteine, as well as other reactive sulphur species (such as thiocyanate, sulfite, and thiosulfate), barely affected the colour of the sensing probe (Fig. 10u). A few other research studies, including this one, have looked into the prospective use of POP materials for selective and sensitive detection of H_2S gas.[222] Among them, in an interesting work, Das *et al.* demonstrated sensing of H_2S gas in a dynamic flow-through electrical resistance measurement system by developing a hydrazide-based POP (THH-COP).[232] The interaction between the H_2S gas and the –CONH-group of THH-COP results in a proton conduction process. This causes a sharp enhancement in the electrical resistance of the THH-COP based sensor device when the H_2S gas is introduced which quickly reduces when the H_2S gas is removed.

6.1.7 Other environment related sensing. Another important class of sensing application of POP materials is latent fingerprint (LFP) detection. From the perspective of national security, forensic analysis, immigration screening, *etc.* fingerprinting is crucial.[174] Swift and sensitive LFP imaging on many surfaces in various environments is a fundamental problem. However, it is highly important for real-time application. Materials that are highly luminescent in the solid-state form are suitable for LFP application. From this view, POPs are potential candidates owing to their strong fluorescence properties in the solid form. In addition, easy and facile manipulation of the PL emission colour of POPs by fine-tuning and rational selection of organic building units and thus the overall polymeric structure offers advantages for LFP application. Considering the above fact, Sun *et al.* explored the LFP utility of POPs by synthesizing a series of three highly designed POPs by applying the Heck coupling reaction.[233] Strong fluorescence colour based three POPs (FPP-1, FPP-2 and FPP-3) were constructed by reacting flexible building units of tetravinylcyclotetrasiloxane with bromo-substituted pyrene, TPE and spirobifluorene moieties, respectively. Upon excitation under UV light, in the solid-state, FPP-1 to FPP-3 exhibited brick-red, yellow and green colours with strong emission intensities centered at 606, 549 and 489 nm, respectively. Inspired by these tunable colours, the POPs were coated on different substrates including paper, glass pieces, plastic bags, aluminium foil, *etc.* by a spraying method to identify the LFP images. As a result, the LFP images with respective emission colours were clearly visualized under UV light. The luminous ridge lines and nonfluorescent furrows could be recognized easily because the relatively uniform tiny particles of the polymers can generate high mechanical adherence to the moisture and oily components of the fingerprint ridges. It is noteworthy to mention that the amplified image exhibited clear visualization of whorl, bifurcation, termination, and crossing fingerprint characteristics, as well as the third-level details of sweat pores. Further research suggested that these materials could be used in a promising way for quick and efficient fluorescence imaging of both old and fresh LFPs in real-world circumstances.

Another important topic for sensing by POPs which is highly relevant to the therapeutic, biological, and environmental domains is pH. pH readings are crucial for various leading applications. Since nitrogen atoms can be protonated and deprotonated in acidic or basic environments, POP skeletons frequently have proton acceptors that are mostly nitrogen atoms. Now, because of this unique property of POPs, they have been used in the determination of pH. In a study, a polyhedral oligomeric silsesquioxane (POSS)-based hybrid POP (HPP) was created by Jiang and Liu *et al. via* the Heck coupling reaction between octavinylsilsesquioxane (OVS) and brominated distyrylpyridine (Br-DSP).[234] The synthesized POP exhibited fluorescence with the feature of pyridine cores. With these properties,

the POP was applied for pH sensing by dispersing in buffer solution of various pH values. When the pH was changed from 5.5 to 1.0, it was discovered that the fluorescence emission peaks clearly shifted from green to red, with wavelength changing from 525 to 618 nm. This observation can be explained by the protonation of the pyridine core of the POP. However, in an alkaline medium, the emission peaks remained at 524 nm and emitted green light when exposed to it. Finally, the polymer (HPP) was found to be an acid sensor owing to its high sensitivity in the pH range of 1 to 4. Apart from this, other studies also explored the potential utility of POPs in the field of pH sensing.[235]

From the above discussion it can be concluded that it may indeed be beneficial to functionalize or decorate the primary skeletons of POPs with groups containing heteroatoms for the purpose of sensing a specific analyte, since this facilitates POPs to co-ordinately bind the detected analytes. Also, the highly porous nature with large surface area of POPs offers easy inclusion of analytes and thus triggers the interaction. Moreover, POPs are useful as sensors for industrial and commercial use due to their reversibility and recyclable nature along with their high chemical and hydrolytic stability.

6.2 Pollutant sequestration from water

The escalating demand of the growing human population along with rapid industrial revolution has resulted in world-wide environmental crisis significantly affecting society's sources of potable water, leading to serious problems including water scarcity and ever-increasing water pollution. The sequestration of trace pollutants found in water has drawn a lot of scientific attention as water pollution has grown to be a serious global issue.[236,237] However, in order to satisfy this broad scientific interest, a number of sustainable sophisticated chemical separation technologies have been either applied in order to provide freshwater supplies by decontaminating various polluted water systems, including wastewater and seawater. Among them, adsorption-based purification techniques are emerging as viable energy efficient alternatives to other traditional procedures, owing to their excellent efficiencies, easy operation, and cost-effectiveness. In order to develop highly effective adsorbents for the sorption-based separation methods, significant advancement has been made in the past few years.[238–240] As mentioned before, owing to the unique characteristic features, POPs have been considered as an excellent potential sorbent material in the field of wastewater treatment for removing various contaminants, including organic contaminants, *e.g.*, dyes, solvent molecules, emerging pharmaceuticals and personal care products (PPCPs), agrochemicals, *etc.*, and inorganic contaminants, *e.g.*, toxic metal ions, radionuclides, metal or metalloid-based oxoanions, *etc.* These various contaminants' removal applications of POPs have been explored in the section that follows with illustrative examples.

6.2.1 Toxic organic pollutants sequestration. Organic pollutants such as organic dyes, pesticides, antibiotics, pharmaceuticals, personal care products and oils have been found in water resources all over the world, raising concerns about potential harmful impacts on aquatic ecosystems as well as on human health. Therefore, effective elimination of these pollutants from different water streams has become a topical research interest. In this context, POPs have been found to demonstrate efficient sequestration of these organic toxic substances from aqueous medium.[241–243]

For example, in a recent report, we explored the potential of a cationic porous organic polymer towards efficient removal of various toxic anionic organic species such as dyes and antibiotics along with inorganic contaminants.[171] In this work, we designed and developed a viologen unit grafted cationic organic network (iVOFm) with macro–micro hierarchical porous nature. iVOFm was synthesized by the solid-state acid vapour assisted synthetic strategy, using silica nanoparticles as a template to induce macroporosity into the polymeric network (Fig. 11a). The synthesized POP was characterized with the help of various state-of-the-art techniques, which explored its unique characteristic features, including the cationic backbone with highly dense free counter anions, macro–micro hierarchical porosity and high chemical stability. Interestingly, the size and number of macropores of iVOFm were found to be easily tunable with the use of a desired SiO_2 NP template. This custom-designed POP utilizes a combination of electrostatically driven ion-exchange, nanoscale sized macropores, and particular binding sites for the intended contaminants. iVOFm was tested for removal of organic dyes (methyl orange and alizarin red S) and antibiotics (sulfadimethoxine (SDM) and sulfamethazine (SMT)) from water. iVOFm showed ultrafast capture of all these organic toxic substances along with iodine and metal-based oxoanions with over 93% removal in only 30 seconds (Fig. 11b). The material demonstrated rapid removal of the antibiotic SDM with high sorption capacity from water, even when other concomitant anions like nitrates, chloride, and bromide are present. Moreover, iVOFm was found to sequestrate SDM from different pH media in a recyclable manner (Fig. 11c). In the mechanism study, the fast pollutant trapping efficiency was found to be due to rapid pollutant diffusion through the ordered, interconnected macropores that work in conjunction with the cationic backbone.

The nature of the organic contaminants can be classified based on their hydrophobic properties. Separation of organic toxic substances can also be done by developing hydrophobic/hydrophilic POPs. Now, hydrophobic POPs can be synthesized by integrating hydrophobic moieties such as fluorine in the porous surface of POPs. On the other hand, installation of hydrophilic units generates hydrophilic core-based POPs. By utilizing this strategy, Cooper *et al.* demonstrated the separation of methyl orange dye by developing a series of POPs with various hydrophobic/hydrophilic substituents.[244] These POPs were synthesized by the Sonogashira–Hagihara coupling reaction of 1,3,5-triethynylbenzene with derivatives of dibromobenzenes. When these POPs were tested for capture of methyl orange in water, an interesting result was observed. Only POPs containing the hydrophilic hydroxyl group exhibited efficient adsorption of dye molecules, whereas POPs without hydrophilic units were found to not absorb methyl orange from water.

In other report, our group explored the adsorption of cationic dyes by a postsynthetically modified anionic hyper-cross-linked polymer (HCP-91@Na).[245] At first a cost-effective

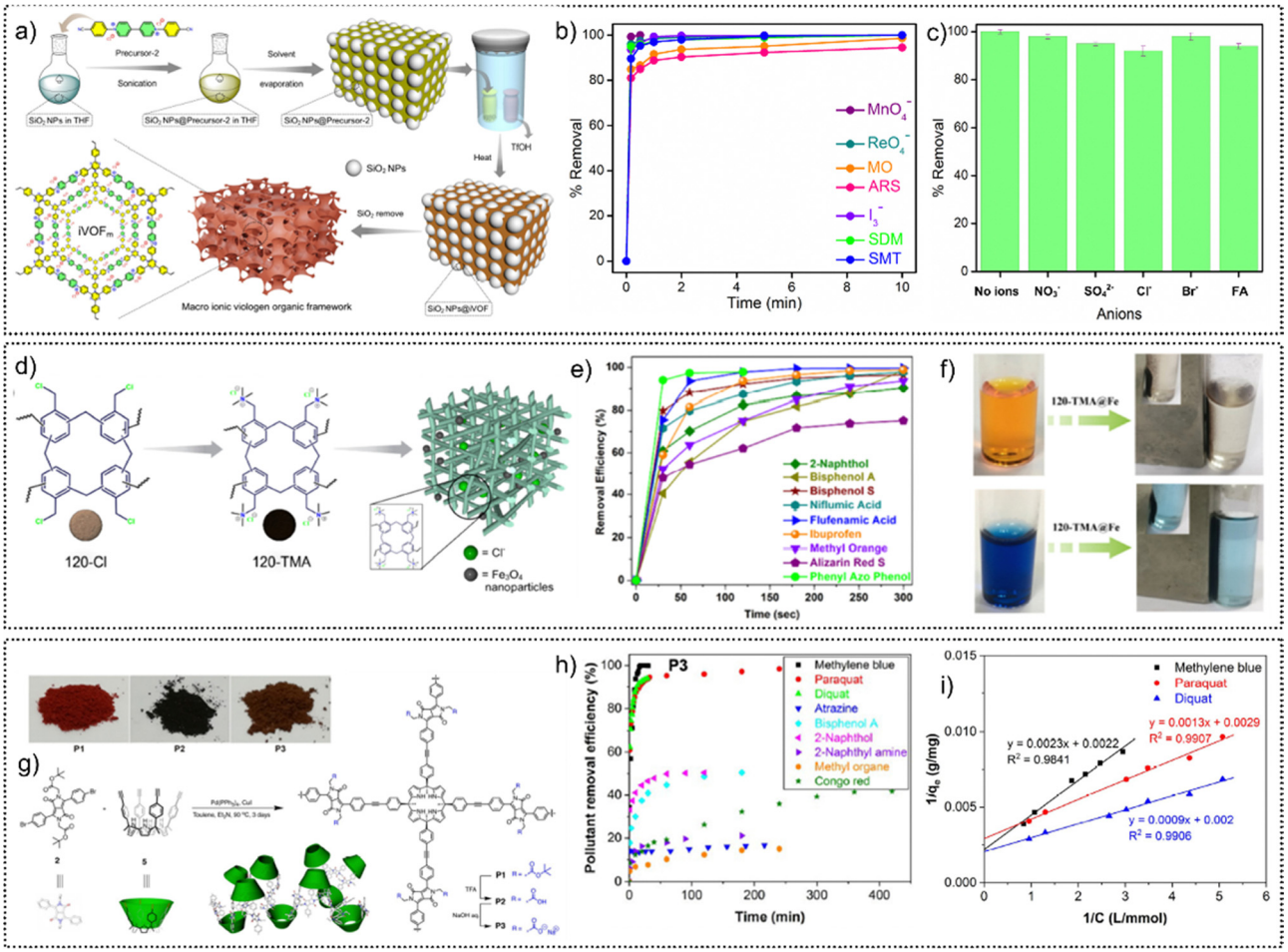

Fig. 11 (a) Schematic representation of solid-state synthesis of the ionic macroporous polymer (iVOFm). (b) Percentage removal efficiency with time of iVOFm towards various pollutants in water. (c) Selective removal efficiency of the SDM antibiotic by iVOFm in the presence of other anions. Reproduced with permission from ref. 171. Copyright 2022, Wiley-VCH. (d) Illustration of synthesis of the Fe_3O_4 embedded 120-TMA polymer. (e) Percentage removal efficiency with time of 120-TMA@Fe towards various organic pollutants. (f) Images of magnetic separation of dyes by 120-TMA@Fe. Reproduced with permission from ref. 246. Copyright 2022, American Chemical Society. (g) Synthesis scheme and the corresponding images of calix[4]pyrrole-crosslinked polymers (P1–P3). (h) Percentage removal efficiency with time of the P3 polymer towards various pollutants. (i) Langmuir adsorption isotherms for the adsorption of cationic pollutants by P3. Reproduced with permission from ref. 152. Copyright 2022, Wiley-VCH.

and chemically stable POP (HCP-91) was synthesized *via* the Lewis acid $FeCl_3$ catalyzed Friedel–Crafts reaction. Thereafter, the POP was post-synthetically modified into the anionic form (HCP-91@Na) by the treatment of a base (NaOH). Owing to its anionic nature with free exchangeable cations, it was applied for cationic dye capture such as methylene blue (MB), rhodamine B (RhB), and crystal violet (CV) from water. Although all the dyes were found to be captured by the POP, the removal kinetics of RhB was found to be faster than that of MB, owing to their size-dependent removal property. Moreover, HCP-91@Na was found to be selective toward cationic dyes only, as no anionic dyes (such as methyl orange (MO)) were removed from water, when tested with a mixture of cationic–anionic dyes (MB-MO and RhB-MO).

It is worth mentioning that following the contaminants' adsorption process, rapid extraction of adsorbent materials from the sample matrix is advantageous compared to laborious centrifugation or time-consuming filtration, which drains energy.

This problem may be easily solved by encapsulating magnetic nanoparticles within the porous matrix of an organic polymer. With this target, our group synthesized a cationic polymer accommodating magnetic Fe_3O_4 nanoparticles (120-TMA@Fe) *via* the one-pot Friedel–Crafts reaction with external cross-linking, followed by chemical modifications (Fig. 11d).[246] When tested for capture of a wide range of organic micropollutants, 120-TMA@Fe exhibited excellent adsorption capability in terms of rapid kinetics (complete removal within only 5 min) towards anionic dyes, aromatic models, plastic components, and pharmaceuticals (Fig. 11e). Moreover, the POP showed a high sorption capacity of 357 mg g^{-1} for methyl orange dye, 555 mg g^{-1} for plasticizer bisphenol A, and 285 mg g^{-1} for antibiotic ibuprofen in water. In addition, 120-TMA@Fe was found to sequestrate these pollutants repeatedly and selectively from different chemical environments as well as from complex real-world samples (Fig. 11f).

Macrocycle-based porous polymers are one of the best candidates as potential sorbent materials for the effective

removal of various toxic pollutants from water, owing to their unique features, including suitable host–guest interactions, robustness, stability, and insolubility.[247,248] Among them, calix[4]pyrrole-based moieties are promising for selective and strong interaction with specific organic micro-pollutants. In this line, efficient removal of organic micro-pollutants from water by POPs has been demonstrated by developing a unique calix[4]-pyrrole-based POP. Wang *et al.* synthesized a calix[4]pyrrole-based 3D POP (P1) by reacting the bowl-shaped a,a,a,a-tetraalkynyl calix-[4]pyrrole monomer with the diketopyrrolopyrrole monomer *via* the Sonogashira cross-coupling reaction (Fig. 11g).[152] As the developed POP (P1) was found to be highly hydrophobic in nature, it could not be used as an effective adsorbent for micro-pollutants. However, it was further modified into the neutral (P2) and anionic form (P3) with free carboxylic acid and carboxylate anion groups, respectively (Fig. 11h). A range of model organic micropollutants (such as dyes (methylene blue, congo red), pesticides (paraquat, diquat), bisphenol A, *etc.*) with varying charge, hydrophilicity, and functionality were found to be more effectively removed by the anionic POP (P3) compared to its neutral homologue (P2). Furthermore, the P3 POP exhibited high removal capacities towards these pollutants (especially for cationic pollutants) in water (Fig. 11i). In the literature most of the organic micro-pollutants reported for removal from water are either nonpolar or charged in nature. Adsorption of polar or neutral organic micro-pollutants is quite challenging; however, it has been reported by Jiang *et al.*, who developed two amide naphthotube-crosslinked polymers.[249] Through biomimetic molecular recognition, these POPs were discovered to efficiently and quickly remove a variety of polar organic micro-pollutants from water. These POPs were further found to remove a complex mixture of pollutants from water in a recyclable manner. The amide functionality in the hydrophobic cavity of the POPs exhibited hydrogen bonding sites that can interact strongly with the polar organic micro-pollutants.

Besides pyrrole-based polymers, calixarenes are another class of supramolecular moieties which show specific binding affinity towards organic micro-pollutants. Removal of organic pollutants from water by means of calix[4]arene-based POPs (CaIP2-CaIP4) has been reported by Trabolsi *et al.* in their report (Fig. 12a and b).[250] In this work, the authors synthesized a series of three hyper-cross-linked π-bond-rich POPs (CaIP2-CaIP4), and further applied them for micro-pollutant capture from water. The POPs exhibited rapid adsorption kinetics with high sorption capacities towards a wide range of water pollutants, such as bisphenol A, propranolol HCl, 1-naphthylamine, and 2-naphthol (Fig. 12c). Among the POPs, CaIP4 demonstrated superior regenerable adsorption performance, which outperformed the common commercial materials. The authors hypothesized that the presence of both calixarene and alkyne functional moieties in the POPs' structure offers a high surface area and thus further enhances the sorption capabilities. Huang and Sessler *et al.* reported the easy and facile removal of various organic and inorganic anionic pollutants from water by developing a macrocycle-based hydrogel-forming polymeric material.[251] Owing to the presence of tetracationic macrocyclic moieties, the polymer exhibited excellent adsorption performance when treated with various organic salts in water. The suitable host–guest interaction between the anions and the tetracationic macrocyclic backbone resulted in such capture performance. Moreover, the anionic pollutant removal efficiency of the polymeric hydrogel was found to be regenerable with dilute HCl solution.

Another class of highly toxic organic trace water contaminants are perfluorinated and polyfluorinated alkyl substances (PFAS), such as perfluorooctanoic acid (PFOA) and perfluorooctanesulfonic acid (PFOS), which are of significant growing concern in the recent time. Even in their very low concentration range, these pollutants are found to be highly toxic in nature towards living organisms, especially for human beings. Due to their durability, these pollutants are widely used in food packaging, firefighting foams, household products, and many industrial operations.[252] Once released into the environment, these "forever chemicals" will accumulate in living things because they cannot be biodegraded in nature. Long-term exposure to PFAS increases the risk of developing diseases like cancer, thyroid problems, kidney disease, and autoimmune disorders.[253–255] It is therefore vitally necessary to create extremely effective adsorbents for the quick capture of PFAS pollutants from water. In this context, POPs are well suited for the effective removal of these harmful pollutants due to their outstanding adsorption–desorption characteristics.[256]

The ability of β-cyclodextrin (β-CD) to encapsulate pollutants in clearly defined host–guest complexes is well established. Contrary to traditional activated carbons, crosslinked β-cyclodextrin polymers have low surface areas and poor removal efficacy. However, the creation of POPs based on β-cyclodextrin, a bioinspired substance (a sustainably produced macrocycle of glucose), may hold the key to the effective removal of microorganisms from water.[257] Considering this, for the very first time, Dichtel *et al.* demonstrated the utilization of β-cyclodextrin-based POPs for the effective removal of PFAS from water. In this work, the team strategically incorporated β-cyclodextrin moieties through crosslinking with rigid aromatic units to fabricate mesoporous POPs. The rational integration of β-CD moieties into the POP's structure (DFB-CDP) allows specific and strong binding affinity towards target-specific pollutants, *i.e.*, PFAS. Although the POP exhibited a low BET surface area (10 $m^2\ g^{-1}$), the PFOA removal efficiency of the material was found to be as high as 95% in water as it reduced the concentration from 1 $\mu g\ L^{-1}$ to 20 $ng\ L^{-1}$ with a contact time of 24 hours. The material was found to eliminate a marked proportion of these pollutants to reach concentrations below the permission limit by the U.S. Environmental Protection Agency (EPA) (70 $ng\ L^{-1}$). In another work, Dichtel *et al.* developed a highly (meso) porous (263 $m^2\ g^{-1}$) β-cyclodextrin-based crosslinked polymer (P-CDP) with rigid aromatic linkers (Fig. 12d).[258] This POP was tested for removal of a variety of micro-pollutants from water, and it was found to exhibit very fast sequestration efficiency especially towards bisphenol A (BPA). Its adsorption rate constants are 15 to 200 times higher than those of activated carbons and non-porous β-cyclodextrin adsorbent materials. Additionally, the polymer can be repeatedly regenerated utilising a simple washing process without losing any functionality. The polymer also surpassed a top-performing activated carbon for the swift elimination

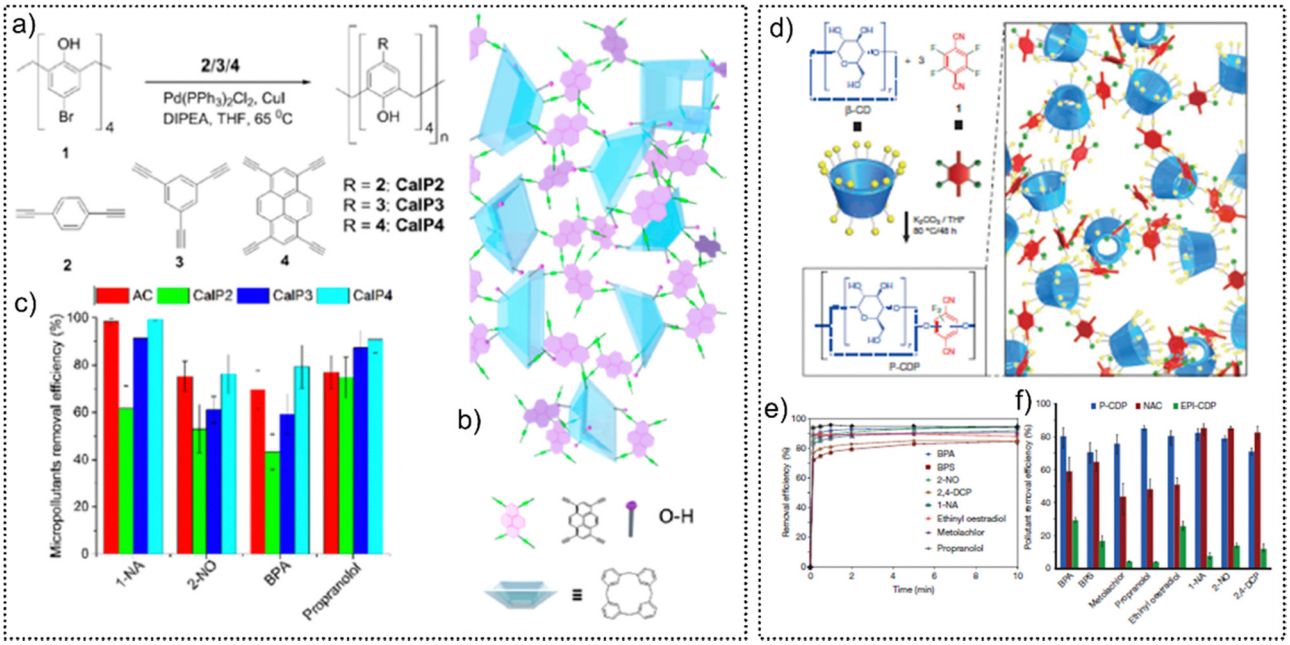

Fig. 12 (a) Synthetic procedure for porous calix[4]arene polymers CalP*n* (*n* = 2–4) by the Sonogashira–Hagihara cross-coupling reaction. (b) Representation of the network structure of CalP4 and its monomers. (c) Percentage removal efficiency of AC and CalPn polymers towards various micro-pollutants. Reproduced with permission from ref. 250. Copyright 2022, American Chemical Society. (d) Synthetic route and schematic illustration of the β-cyclodextrin-based P-CDP structure. (e) Percentage removal efficiency with time of various pollutants by P-CDP. (f) Percentage removal efficiency of pollutants by P-CDP, NAC and EPI-CDP. Reproduced with permission from ref. 257. Copyright 2016, Nature Publishing Group.

of a complex blend of organic micro-pollutants at concentrations that were meaningful to the environment (Fig. 12e and f). These results show the potential of β-cyclodextrin-based porous polymers for fast and flow-through water treatment, which is important for real-time application. Furthermore, the Dichtel group reported a number of other works based on β-cyclodextrin-based POPs as efficient adsorbents for the removal of PFAS from water.[259–261]

In another interesting work, Ma *et al.* reported a PFOA capture study with a rationally modified PAF material (Fig. 13a).[262] In this work, at first an aromatic unit containing POP was fabricated, and was further modified by integrating three different hydrophobic chains with quaternary ammonium functional groups to develop three POPs called PAF-1-NDMB, PAF-1-NDMP, and PAF-1-NDMH. Thereafter, these POPs were applied for the extraction of PFOA pollutants from water. Among the modified POPs, PAF-1-NDMB exhibited highly efficient removal of PFOA as it reduced the concentration from 1 ppm to 54 ppt with a removal percentage of 99.99% within 2 min of contact time (Fig. 13b). The maximum uptake capacity of this polymer towards PFOA was calculated as 2000 mg g^{-1} (Fig. 13c). Inspired by the unprecedented performance of this material, the group further demonstrated the breakthrough experiment for PFOA capture. The result showed that 300 mg of compound was able to sequestrate PFOA from a feed solution of 500 ppb and purified a total of 3530 mL of water by reducing the concentration below the limit in the drinking water sample (<53 ppt) (Fig. 13d). These data indicated the potential use of the material for practical water treatment application.

As mentioned above, apart from these organic dyes, micro-pollutants, plastics, pharmaceuticals and personal care products, various organic solvents and oils are other environmentally relevant organic toxic substances that should be eliminated from the contaminated water bodies. Adsorption of oils and organic solvent molecules by POPs has been explored by Deng *et al.*[263] In this study, the group developed a superhydrophobic conjugated porous polymer through homocoupling polymerization reaction, catalyzed by Pd(II) and Cu(I). Owing to the superhydrophobic nature of the POP, it efficiently separated oils and organic solvents from water with good selectivity, fast adsorption kinetics, and excellent recyclability. The adsorption capacities for 1,2-dichlorobenzene were found to be 1569 wt% and 2300 wt% for HCMP-1 and HCMP-2, respectively, which suggest their molecular sponge like behaviour. In another similar type of study, Ma *et al.* synthesized a highly hydrophobic porphyrin-based POP (PCPF-1) through the Yamamoto reaction of 5,10,15,20-tetrakis(4-bromophenyl)-porphyrin monomers.[264] The developed POP exhibited a high BET surface area (1333 m^2 g^{-1}) and the highest capacities for saturated hydrocarbons such as 14.7 g of *n*-pentane, 16.7 g of *n*-hexane, 22.5 g of n-heptane, 25.9 g of *n*-octane, 15.4 g of cyclopentane, 25.1 g of cyclohexane and 20.5 g of gasoline. Moreover, the POP was found to separate oils from the mixture of oil–water.

6.2.2 Inorganic pollutant sequestration. Among the major inorganic contaminants, metal cations, metal or metalloid-based oxoanions and radioactive species are well known. All of these species are very toxic in nature and have a negative impact on the environment, notably on human health, beyond the threshold limit set by the World Health Organization (WHO) or the United States Environmental Protection Agency

(U.S. EPA). Therefore, selective extraction of these metal species from aqueous systems is of utmost research interest. Although several effective sorbent materials have been developed, the shortcomings of current materials force the creation of new, more reliable substitutes that prevent swelling, have easily accessible chelating or ion exchange sites, high saturation/exchange capacity, and fast kinetics. In this regard, POPs are found to present excellent performance for efficient extraction of these species from the contaminated water systems, owing to their modular character, high surface areas, variable pore sizes, functional group decorated surfaces, and extraordinary chemical stability.[265–267]

6.2.2.1 Toxic metal ion sequestration from water. Among the metal cations, copper ions (Cu^{2+}) are a vital component of life. However, they also tend to hyperaccumulate in biological fluids and tissues, which is a symptom of pathologies like Wilson's and Menkes illness and other neurodegenerative disorders. In this line, currently, diseases defined by copper hyperaccumulation are difficult to diagnose due to expensive diagnostic equipment requiring significant technical workup. Therefore, it is particularly important to develop a simple yet versatile method for selective monitoring of copper ions in biological fluids.[268] With this target, Long and Chang *et al.* created a PAF material that allows for the simple and inexpensive detection of copper metal ions in biological fluid samples. The team developed a robust 3D POP (PAF-1-SMe) functionalized with highly dense thioether groups for the selective capture and detection of copper from biofluids as well as aqueous samples (Fig. 14a). When tested for capture, the synthesized POP exhibited selective extraction of Cu metal even in the presence of other co-existing metals (Fig. 14b), with a high uptake capacity of 600 mg g^{-1}. Moreover, PAF-1-SMe demonstrated selective detection of copper in biological samples with 8-hydroxyquinoline as a colorimetric indicator. This study provides a method for locating copper that has been exogenously introduced to serum and for recognizing abnormal copper levels in urine samples from mice with Wilson's disease.

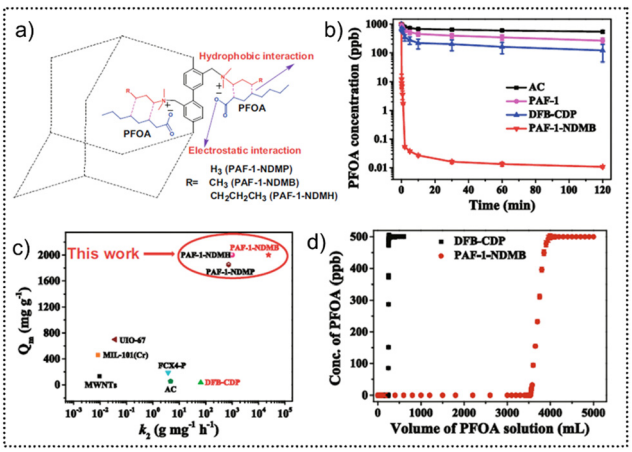

Fig. 13 (a) Representation of different interactions of functionalized PAF-1 with PFOA. (b) Result of the PFOA capture kinetics study for various compounds along with PAF-1-NDMB. (c) Comparison of the PFOA saturation capacity and adsorption rate constant (k_2) value for PAF-1-NDMB with other porous materials. (d) Result of breakthrough experiments for PAF-1-NDMB and DFB-CDP in aqueous PFOA/HA solutions. Reproduced with permission from ref. 262. Copyright 2016, Nature Publishing Group.

Another heavy metal ion which is highly toxic in nature is mercury (Hg^{2+}). Considering the public health and environmental protection, selective extraction of Hg^{2+} is highly significant. With this goal, Ma and coworkers addressed this problem by developing a POP-based adsorbent (PAF-1-SH) as an efficient nanotrap.[269] The synthesized chemically stable POP exhibited a high surface area with densely decorated Hg^{2+} chelating groups. The POP-based nanotrap showed a record high uptake capacity of >1000 mg g^{-1} for Hg^{2+} metal cations in aqueous medium. In addition, within a very short period of time, the nanotrap was found to reduce the Hg^{2+} concentration from 10 ppm to below 0.4 ppb, which is well below the acceptable limits (2 ppb) of Hg^{2+} in drinking water. Thus, the overall removal efficiency of mercury ions for the sorbent was found to be $>99.9\%$. All these findings suggested that this POP might be utilized as a benchmark material for selective mercury extraction and could also provide a fresh viewpoint for the removal of other heavy metal ions from contaminated water for environmental rehabilitation. In another work, by utilizing a more facile cost-effective free radical polymerization, the same group developed POP-SH for capture of Hg^{2+} cations, which outperformed PAF-1-SH.[270] The Hg^{2+} extraction kinetics, saturation capacity and all other major capture properties of POP-SH were found to be higher than those of PAF-1-SH (Fig. 14c–f).

Lead is a highly toxic metal which causes serious water pollution when found above the permitted level. Decontamination of water by removing lead metal ions has been reported by Ying and Zhang *et al.*[271] In their work, the team developed a mesoporous POP with a poly-melamine-formaldehyde backbone (mPMF), which exhibited a high surface area, functionalized with highly dense free amine groups and triazine moieties. Owing to the unique characteristic features, this POP was utilized for lead metal ion extraction from water. When tested, the POP was found to demonstrate rapid removal of Pb^{2+} ions from water in the presence of other main group cations (Na^+, K^+, Ca^{2+}). Moreover, the authors performed the flow-through lead ion capture experiment in a dynamic mode with the POP, which resulted in the purification of $\sim$100 mL of water contaminated with 50 ppb Pb^{2+}. The POP was also found to show affinity towards other metal cations such as Cd^{2+}, Pd^{2+} and Cu^{2+} in water. Interestingly, within 5 seconds, more than 99% of Pb^{2+} had been eliminated, bringing the lead concentrations down to PPT levels. The mPMF lead capture study was also determined to be recyclable.

Palladium (Pd) is a different kind of very significant metal that is used extensively in industrial sectors due to its economically desirable characteristics including high melting point, catalytic effectiveness, and corrosion resistance. Therefore, extraction of palladium metal ions has become of particular importance. Ma *et al.* reported selective capture of Pd metal, a platinum group element (PEG), with a series of pyridine-functionalized POPs (POP-Py, POP-pNH_2-Py, and POP-oNH_2-Py).[272] When tested for metal capture, all these POPs were

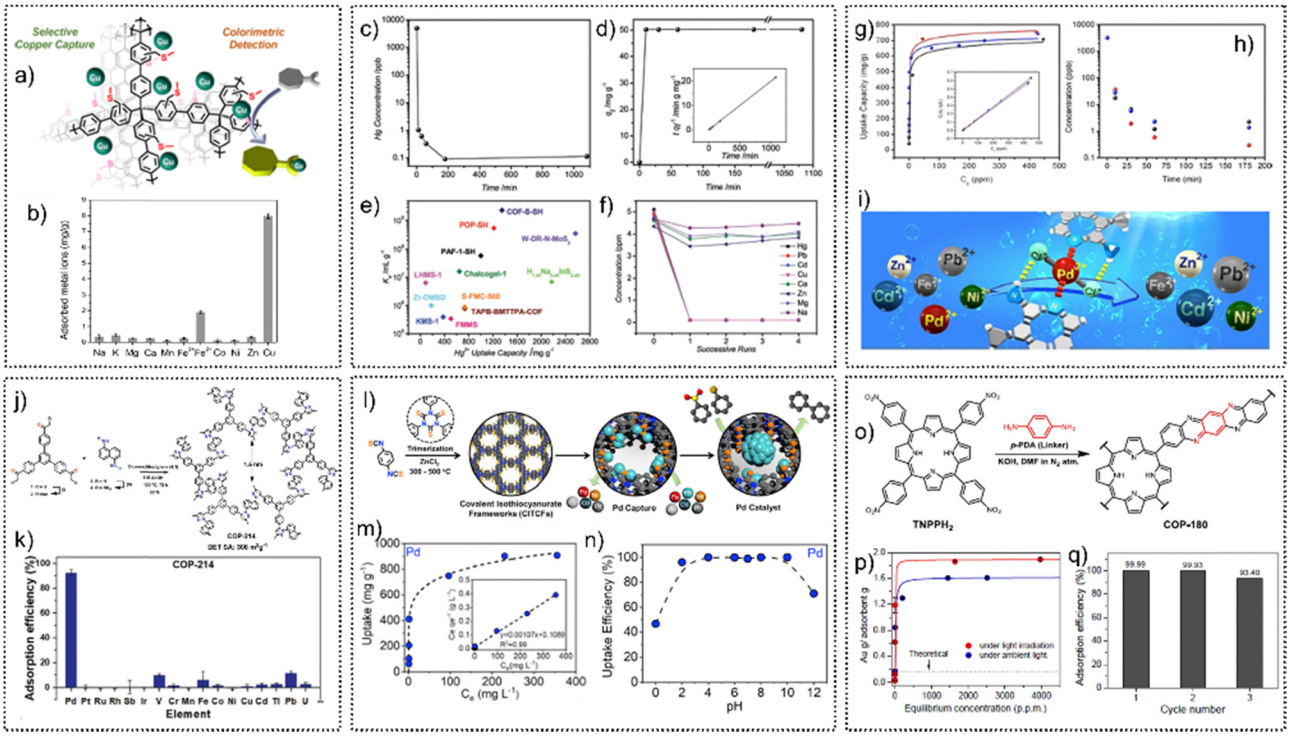

Fig. 14 (a) Schematic representation of colorimetric detection and selective capture of copper with PAF-1-SMe. (b) Capacities of selective capture of Cu-metal along with other physiologically relevant metal ions with PAF-1-SMe. Reproduced with permission from ref. 268. Copyright 2016, American Chemical Society. (c) Hg^{2+} sorption kinetics of POP-SH. (d) Adsorption of Hg^{2+} *versus* contact time using POP-SH. The inset shows the pseudo-second order kinetic plot for adsorption. (e) Comparison of the Hg^{2+} saturation uptake amount and K_d value for POP-SH with other benchmark porous materials. (f) Concentrations of metal ions after the breakthrough experiment with POP-SH. Reproduced with permission from ref. 270. Copyright 2021, Wiley-VCH. (g) and (h) Pd^{2+}adsorption isotherm (inset: Langmuir sorption model) and sorption kinetics, respectively, of POP-Py (black), POP-pNH_2-Py (blue), and POP-oNH_2-Py (red). (i) Illustration of selective Pd^{2+} binding with POP-oNH2-Py. Reproduced with permission from ref. 272. Copyright 2020, Wiley-VCH. (j) Synthetic route to COP-214 from commercially available monomers through the asynchronous double Schiff base strategy. (k) Selective Pd capture of COP-214 in a mixture of various precious and transition metals. Reproduced with permission from ref. 275. Copyright 2021, Wiley-VCH. (l) Synthesis scheme of CITCFs and their selective Pd capture and Pd-based catalyst application. (m) Pd(II) uptake isotherm of CITCF-500 (inset: Langmuir sorption model). (n) pH dependent Pd(II) uptake efficiency of CITCF-500. Reproduced with permission from ref. 273. Copyright 2022, CellPress. (o) Two-step synthesis scheme of COP-180. (p) Adsorption isotherms for gold (Au) capture by COP-180. (q) Gold-capture efficiencies for three consecutive adsorption/desorption cycles. Reproduced with permission from ref. 278. Copyright 2020, United States National Academy of Sciences.

found to selectively and rapidly sequestrate Pd metal with record uptake capacities (Fig. 14g and h). Notably, the authors found that the strategic introduction of amine groups into the polymers triggered the metal capture performance. Moreover, POP-oNH_2-Py exhibited superior sorption capability with high selectivity and regeneration ability towards palladium than the other two POPs (POP-pNH_2-Py and POP-Py). The authors provided the single-crystal X-ray data, which showed that POP-oNH_2-Py exhibited stronger complex formation with $PdCl_2$ compared to POP-pNH_2-Py owing to the intramolecular hydrogen bonding between the amino group and coordinated chlorine molecules (Fig. 14i). In another recent report, Coskun *et al.* demonstrated selective capture of Pd by synthesizing a hierarchical porous polyisothiocyanurate-based polymer (CITCFs) *via* ionothermal trimerization reaction of 1,4-phenyldiisothiocyanate.[273] The synthesized POP exhibited features such as a high surface area and thiourea functionalized porous surface with dense sulfur atoms, which enabled the material to capture Pd(II) (Fig. 14l). The POP showed rapid and selective extraction of Pd(II) from wastewater with an exceptional uptake capacity of 909 mg g^{-1}. Moreover, the POP sequestrated Pd from solutions with a wide range of pH. In addition, the Suzuki–Miyaura cross-coupling process was very effective owing to the reduction of recovered Pd(II) within the polymer network (Fig. 14m and n). In another report, Cai, Feng and coworkers synthesized two cationic CTFs (CTF-S and CTF-L) for the selective extraction of Pd from highly acidic nuclear waste systems.[274] The POP exhibited highly selective and efficient capture of Pd with a maximum sorption capacity of 333 mg g^{-1}, which is the highest at 3 M HNO_3 among all porous adsorbents previously reported. Yavuz *et al.* reported the synthesis of a pyrazole-linked POP *via* the asynchronous double Schiff base reaction and used it for selective recovery of Pd (Fig. 14j).[275] The fabricated pyrazole polymer (COP-214) was found to be highly stable chemically and thermally, and showed fast uptake and quantitative selectivity of Pd(II) over several other interfering metals (especially Pt(II)) in a wide pH range (Fig. 14k). The POP demonstrated reusable capture of Pd metal thanks to a rare mechanistic insight of size-selective strong coordination of Pd onto pyrazole units.

Among metals, gold is a precious metal that has been widely employed in jewellery, electronics, medicine, and catalysis.[276,277]

With the rise in the necessity for producing medical devices, the demand for gold has been rising. Therefore, recovery of gold metal is significantly important. In this domain, a number of pioneering studies have been undertaken by Yavuz *et al.* In a report, a rationally designed POP with porphyrin linkers (COP-180) was synthesized *via* a two step reaction and considered for precious metal recovery (Fig. 14o).[278] The porous porphyrin polymer was employed for the recovery of precious metals, and the POP was found to demonstrate highly selective extraction of gold (Au) from the electronic (PCB) waste leachate even in the presence of 63 elements. The saturation capacity for gold recovery was calculated as a record high of 1.62 g g^{-1} with a swift extraction kinetics as 99% uptake was achieved within 30 min of contact time (Fig. 14p). Additionally, the Au capture study with COP-180 was found to be highly recyclable (Fig. 14q). There are several other reports which demonstrated effective and efficient recovery of precious gold metal by means of POP materials.[279–281]

6.2.2.2 Radioactive waste sequestration. Amorphous porous organic polymers are exclusively reported in the literature for the extraction of various radioactive species such as uranium (^{235}U), iodine ($^{129/131}$I), and others. Among them uranium extraction by POP materials has been documented so far and is thought to be interesting with significant progress.[282–285] Here, a few illustrative examples are discussed briefly. The best uranium chelator is commonly acknowledged to be the amidoxime group (–C(NOH)NH_2, AO).[286] Various POPs have been developed as decorating platforms to anchor AO groups to enhance the effectiveness of selective extraction of uranium.[287,288] Demonstration of POP-based U extraction has been done by Ma *et al.* by synthesizing an amidoxime functionalized PAF material (PAF-1-CH_2AO).[289] The group synthesized PAF-1-CH_2AO by chloromethylation of PAF-1 followed by NaCN treatment to incorporate the cyano groups as well as the amidoximation group (Fig. 15a). The post-synthetic modification of PAF-1 provided abundant binding sites for interaction with U(VI) and the adsorption capacity was found to be 304 mg g^{-1} (Fig. 15b). In a follow-up work, the same group demonstrated the design strategies for developing functional POPs to enhance the U(VI) recovery performance.[290] In this work, they compared the U extraction capacity of two POPs (PAF-1-CH_2NHAO and PAF-1-$NH(CH_2)_2$AO) having different chain lengths and degree of functional groups grafted. When tested for U capture, PAF-1-$NH(CH_2)_2$AO exhibited the adsorption capacity of U(VI) as 385 mg g^{-1}, which was higher than that of PAF-1-CH_2NHAO (Fig. 15c). Porous aromatic polymers (PAFs) were found to be efficient sorbent materials for U extraction. PAFs with amidoxime-modified building units synthesized through the Scholl reaction (PAF-170 to PAF-172) have also been investigated for U(VI) capture from water.[291] Among them, PAF-170 exhibited a highly selective and ultrahigh uranium capacity of 702 mg g^{-1}. In another interesting work, a vinyl linked cyano functionalized series of POPs have been synthesized by radical polymerization reaction (POP1-CN, POP2-CN, and POP3-CN) to show the suitable position based binding activity of the same chelators in POPs.[292] All these POPs were further modified into amidoxime groups called POP1-AO, POP2-AO and POP3-AO, respectively (Fig. 15d). Owing to the high BET surface areas with densely decorated AO groups, these POPs were applied for U(IV) extraction. The U capture result showed the maximum adsorption capacities of U(VI) for POP1-AO, POP2-AO, and POP3-AO to be 857, 504, and 1070 mg g^{-1}, respectively. Also, the result indicated that because of the higher density of amidoxime groups, POP1-AO and POP3-AO had larger adsorption capacities than POP2-AO (Fig. 15e).

Moreover, POP1-AO exhibited highly selective binding affinity towards U(VI) compared to other competitive cations such as Na^+, K^+, Mg^{2+}, Zn^{2+}, Cu^{2+}, Fe^{3+}, Ca^{2+} and V^{5+} even at excess concentration. Further, the authors explained the strong complexation of U(VI) with the AO moieties of the polymer (POP1-AO). Along with this study, the same group created cyano functional vinyl compounds with various amine locations to self-polymerize into polymers, and subsequently the cyano groups were changed into amidoximes.[293] Among the synthesized POPs, POP-AO, POP-pNH_2-AO, and POP-oNH_2-AO had U(VI) adsorption capabilities of 440, 580, and 530 mg g^{-1}, respectively. Moreover, the POPs rapidly reached >90% removal efficiency with a contact time of 1 hour. Interestingly, it was found that due to the inclusion of amino groups and the relative locations of amidoximes, POP-oNH_2-AO had a much higher removal effectiveness under low U(VI) concentrations than POP-AO and POP-pNH_2-AO. Furthermore, the U(VI) capture study of POP-oNH_2-AO was found to be highly selective in the presence of metal cations including transition metals, lanthanides and radioactive elements. Further, for a summary of UO_2^{2+} capture performance of various POP-based materials, see Table S3 (ESI†).

The functional tunability, high porosity with large surface area and excellent physicochemical stability make POPs potential candidates for removal of another radioactive species which is iodine. Due to its mechanism of radioactive decay, iodine poses serious environmental and health risks in nuclear fission products and natural gas production. In the recent few years, extensive studies have been performed for adsorption of iodine by means of various POPs, including CMPs, PAFs, and HCPs (Table S4, ESI†). Among them conjugated porous polymers were found to demonstrate highly efficient sorption of iodine from both vapour phase and aqueous medium, owing to the strong interaction between electronically rich porous surfaces and the electron deficient iodine molecule. Recently, a number of ingenious binding site designs have been invented using a number of N heteroatomic units (such as imine, amine, triazine, pyridine, *etc.*) grafted onto the porous adsorbents for enhanced iodine sorption.[115,294] Based on these aforementioned groups, various POPs were created and their efficiency in removing I_2 from gas and solution phases was examined.[295,296] Feng and co-workers synthesized a series of CMPs (TBTT-CMP@1–3) with identical porosity and similar polymeric structure using different lengths of diamine monomers and TBTT.[297] All these synthesized POPs were applied for the I_2 capture study. Because of its distinct morphology or large pore volume, among all the POPs, TBTT-CMP@1 was shown to have a significantly high iodine adsorption capacity (442 wt%). Zhu *et al.* synthesized a series of PAF materials (PAF-23, PAF-24, and PAF-25) through the Sonogashira–Hagihara coupling reaction

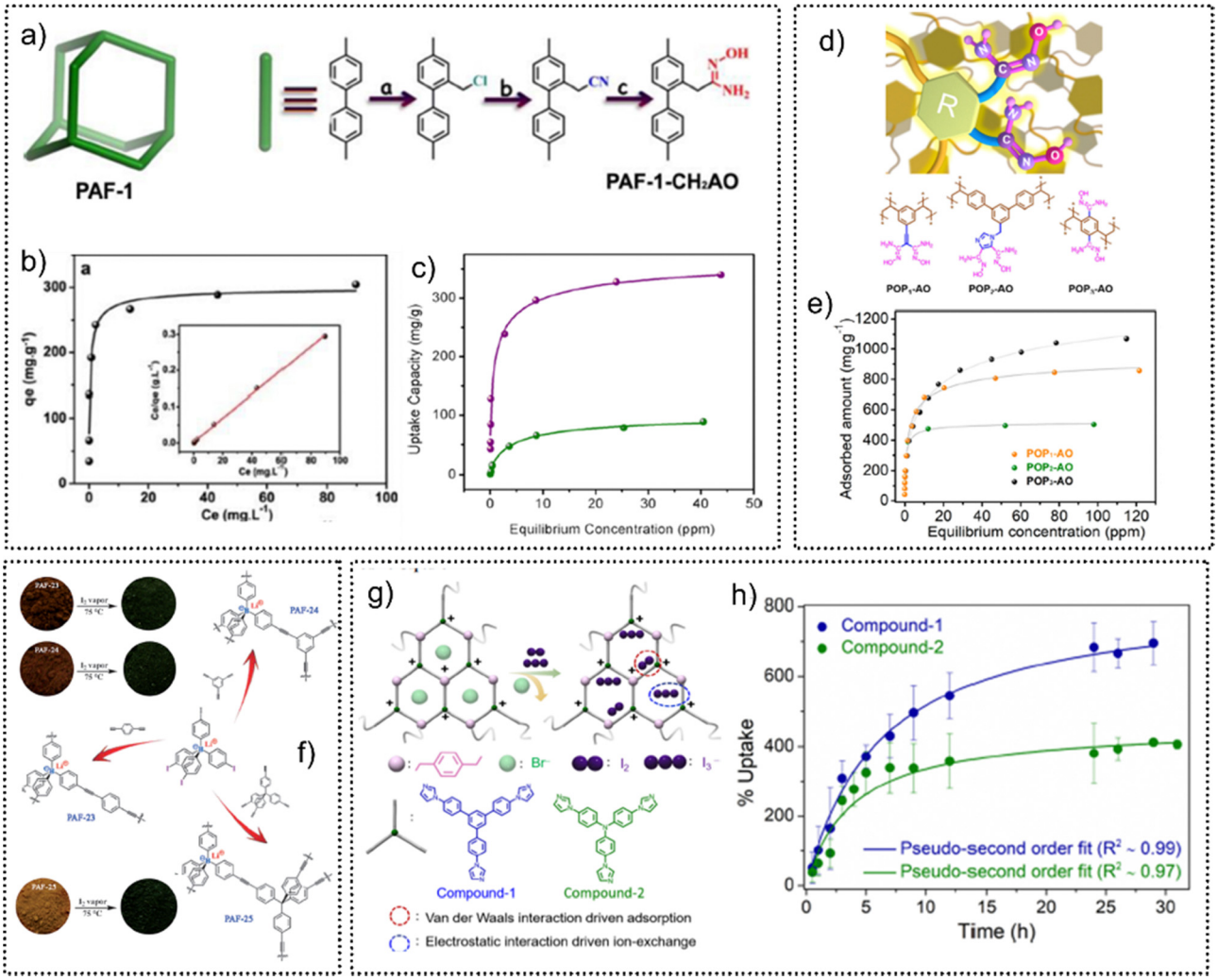

Fig. 15 (a) Schematic representation of synthesis of PAF-1-CH_2AO: [(a) AcOH, H_3PO_4, HCl; (b) NaCN; (c) NH_2·OH]. (b) Uranium (UO_2^{2+}) adsorption isotherm for PAF-1-CH2AO [inset: Langmuir adsorption model fitting]. Reproduced with permission from ref. 289. Copyright 2022, American Chemical Society. (c) Comparison of UO_2^{2+} adsorption performance of PAF-1-$NH(CH_2)_2AO$ (purple) and PAF-1-CH_2NHAO (green). Reproduced with permission from ref. 290. Copyright 2022, American Chemical Society. (d) Schematic illustration of porous frameworks decorated with uranyl-specific ligand "hooks" and the corresponding structures of diamidoxime-functionalized POPs. (e) Sorption isotherm of all the POPs for UO_2^{2+}. Reproduced with permission from ref. 292. Copyright 2022, American Chemical Society. (f) Synthetic procedure for polymers (PAF-23, PAF-24, PAF-25), and their respective images showing the colour change before and after iodine capture. Reproduced with permission from ref. 298. Copyright 2022, Wiley-VCH. (g) Schematic illustration of ionic POPs showing selective iodine capture with van der Waals and electrostatic interaction driven ion-exchange. (h) Gravimetric uptake of I_2 vapour at ~70 °C, 1 bar for compound-1 and -2. Reproduced with permission from ref. 299. Copyright 2022, American Chemical Society.

between a tetrahedral building unit (lithium tetrakis(4-iodophenyl)-borate) and a number of different alkyne monomers (Fig. 15f).[298] All these anionic borate PAFs feature three functional sorption sites – an ionic site, phenyl rings, and triple bonds – which collectively contribute towards a high affinity for iodine. When tested for vapour phase I_2 capture, PAF-23-25 exhibited high iodine adsorption capacities of 2.71, 2.76, and 2.60 g g^{-1}, respectively, at 348 K temperature. The high amount of I_2 uptake by these POPs was visually observed by the sharp color change of these PAFs after I_2 sorption (Fig. 15f). Moreover, using an I_2 solution, the iodine sorption of PAFs was further investigated, and after 24 h of contact, it was evident to see a clear discoloration of the I_2 solution.

In a recent report, our group explored ionic POPs (iPOPs) as a suitable host material for iodine/triiodide anion capture, owing to their exclusive features including high physicochemical stability, a charged surface, and a tunable backbone.[299] For this study, two chemically robust ionic POPs that have several binding sites, such as Lewis basic nitrogen sites with imidazolium cations and free exchangeable bromide anions, and a polarizable surface with phenyl rings have been synthesized (Fig. 15g). These sites work in concert to increase the adsorption of I_2 and I_3^- ions from both vapour and aqueous phase. As a result, under the circumstances of nuclear fuel reprocessing, extraordinary iodine uptake from the vapour phase was observed (Fig. 15h). Moreover, almost >99% I_3^- removal efficiency was found in the case of these POPs within 30 min of contact. For I_3^- anion capture, record uptake capacities and unheard-of selectivity were noted. Owing to the excellent affinity (distribution coefficient,

105 mL g^{-1}) the iPOP was able to extract iodine from samples that had been tainted with seawater. In another report from our group, demonstration of the role of the –OH group in synergy with porosity in the effective capture of iodine from both vapour phase and water medium has been explored by synthesizing three HCPs (HCP-91, HCP-92 and non-functionalized biphenyl HCP).[300] HCP-91 and -92 exhibited 2.99 and 2.49 g. g^{-1} capture capacity toward I_2 in the vapour phase, respectively.

6.2.2.3 Anionic pollutant sequestration from water. An increasing number of harmful contaminants are getting into the freshwater supplies as a result of expanding urbanization and rapid industrialization. The Environmental Protection Agency (EPA) identified a few metal or metalloid-based oxoanions such as chromate (CrO_4^{2-}), pertechnetate (TcO_4^-), perrhenate (ReO_4^-), arsenate (AsO_4^{2-}), *etc.* as potential hazardous inorganic pollutants in wastewater on the priority list.[301] Environmental remediation has drawn a lot of attention for sustainable existence and has recently emerged as a research issue of interest because of the rising demand for clean water and the potential impact of these dangerous oxoanions in contaminated water.[302] Concerns for the environment and for human health are driving attempts to create a variety of effective methods to clean and disinfect wastewater. Adsorption and ion-exchange-based purification techniques using porous materials are among them and are developing as more promising than other traditional procedures.[303,304] In this regard, due to its affordability, simplicity of use, and ability to produce less harmful secondary species, POP-based adsorption (by chelation or ion-exchange) of these toxic oxoanions from wastewater has attracted increasing interest.[138,168,305–307] In some cases, it is also found to be superior to other porous materials towards decontamination application. A few representative examples of POP based oxoanion capture studies are discussed below. In the literature adsorption driven by the ion-exchange process is considered to be effective for POP based oxoanion removal from water. For this, ionic (cationic) porous organic polymers have been explored exclusively for efficient tapping of oxoanions. That being said, owing to the strong electrostatic interaction between the nanoporous structure of cationic POPs with free exchangeable counter anions and anionic oxo-pollutants, various positively charged POPs are reported. Among them, imidazolium based cationic porous organic polymers are one of the promising candidates. By utilizing the Yamamoto reaction between two monomers, namely, 1,3-bis(4-bromophenyl)-imidazolium bromide and tetrakis(4-bromophenyl)ethylene, a series of imidazolium based POPs (POP-Ims) have been prepared to demonstrate capture and sensing of dichromate ($Cr_2O_7^{2-}$) oxoanions.[146] In this work, Wang *et al.* first optimized the porosity, hydrophilicity and water dispersity of an imidazolium backbone containing cationic POP and further applied it for $Cr_2O_7^{2-}$ capture in water. As a result, the polymer exhibited a capture capacity of 171.99 mg g^{-1} along with 87.9% removal efficiency within 5 min of contact time. The anion exchange mechanism was investigated as the principal cause behind this capture study as the nonionic analogue of this POP showed no capture of dichromate anions. Moreover, POP-Im1 exhibited extraordinary selectivity in capturing $Cr_2O_7^{2-}$ and outstanding enrichment capabilities. In another work by the same group, along with the selective detection of $Cr_2O_7^{2-}$, fast capture with high capacity has been achieved by developing another chemically robust luminescent imidazolium-based main-chain ionic polymer (IMIP-Br).[308] The polymer exhibited rapid removal of dichromate anions (92.6% within 30 min) with a high exchange capacity of 318 mg g^{-1}. In this study, for better recycling purpose the POP was integrated with Fe_3O_4 nanoparticles (IMIP-Fe), and applied for repeated oxoanion removal (Fig. 16a). As anticipated, IMIP-Fe was found to exhibit excellent capture of $Cr_2O_7^{2-}$ with superior recyclability from contaminated water systems (Fig. 16b and c). Application of imidazolium-based ionic POPs towards sequestration of oxoanions such as CrO_4^{2-} and ReO_4^- (surrogate anion of TcO_4^-, a radioactive oxo-pollutant) has recently been demonstrated by our group.[39] Two chemically stable iPOPs (iPOP-3 and iPOP-4) have been synthesized which were found to exhibit rapid removal kinetics and very high sorption capacity for CrO_4^{2-} anions (170 and 141 mg g^{-1} for iPOP-3 and iPOP-4 respectively) and ReO_4^- (515.5 and 350.3 mg g^{-1} for iPOP-3 and iPOP-4 respectively). Moreover, even in the presence of numerous other co-existing anions such as Br^-, Cl^-, SO_4^{2-}, NO_3^-, *etc.*, both iPOPs showed extraordinary selectivity towards Cr(VI) and R(VII). In another recent work, we demonstrated the systematic optimization of oxoanion sequestration kinetics towards efficient detoxification of toxic water by adjusting different morphologies of an imidazolium-based cationic polymer (iPOP-5).[76] The POP was found to exhibit a variety of morphologies, including spheres, nanotubes, and flakes, among which the flake-like polymer [iPOP-5(F)] showed rapid capture efficiency ($\sim$99% and $\sim$85% removal within $<$60 s) with high exchange capacities of 301 and 610 mg g^{-1} towards Cr(VI) and Re(VII) oxoanions, respectively, in water (Fig. 16e and f). On the other hand, the spherical morphology-based polymer [iPOP-5(S)] exhibited relatively slow removal kinetics towards both oxoanions. Additionally, even in the presence of overwhelming (100-fold) competing anions from both high and low concentrations of contaminated water, iPOP-5(F) demonstrated quick and selective removal of Cr(vi) and Re(VII). Also, iPOP-5(F) showed excellent regeneration ability and quick removal efficiency across a wide pH range as well as different water systems (potable, lake, river, sea, and tannery) (Fig. 16g and h). More interestingly, the mechanistic analysis revealed that *in situ* exfoliation of flakes of the polymer into thin nanosheets aids in achieving rapid capture efficiency (Fig. 16i).

Rhenium (Re) is one of the rarest and valuable metal elements on Earth, and has found extensive use in aircraft and unleaded gasoline catalysis.[309] Therefore, it is determined to be extremely vital to extract it specifically in its oxoanionic form (ReO_4^-). Li *et al.* produced cationic POPs (SCU-CPN-2) by microwave irradiation of two monomers (TIB and TBB).[310] Owing to the large positive charge densities, SCU-CPN-2 was found to display an ultrahigh adsorption capacity of 1467 mg g^{-1} for ReO_4^-. This maximum adsorption capacity of this polymer was found to be the highest when compared to the previously reported anion exchange materials. In another interesting work, Ma *et al.*

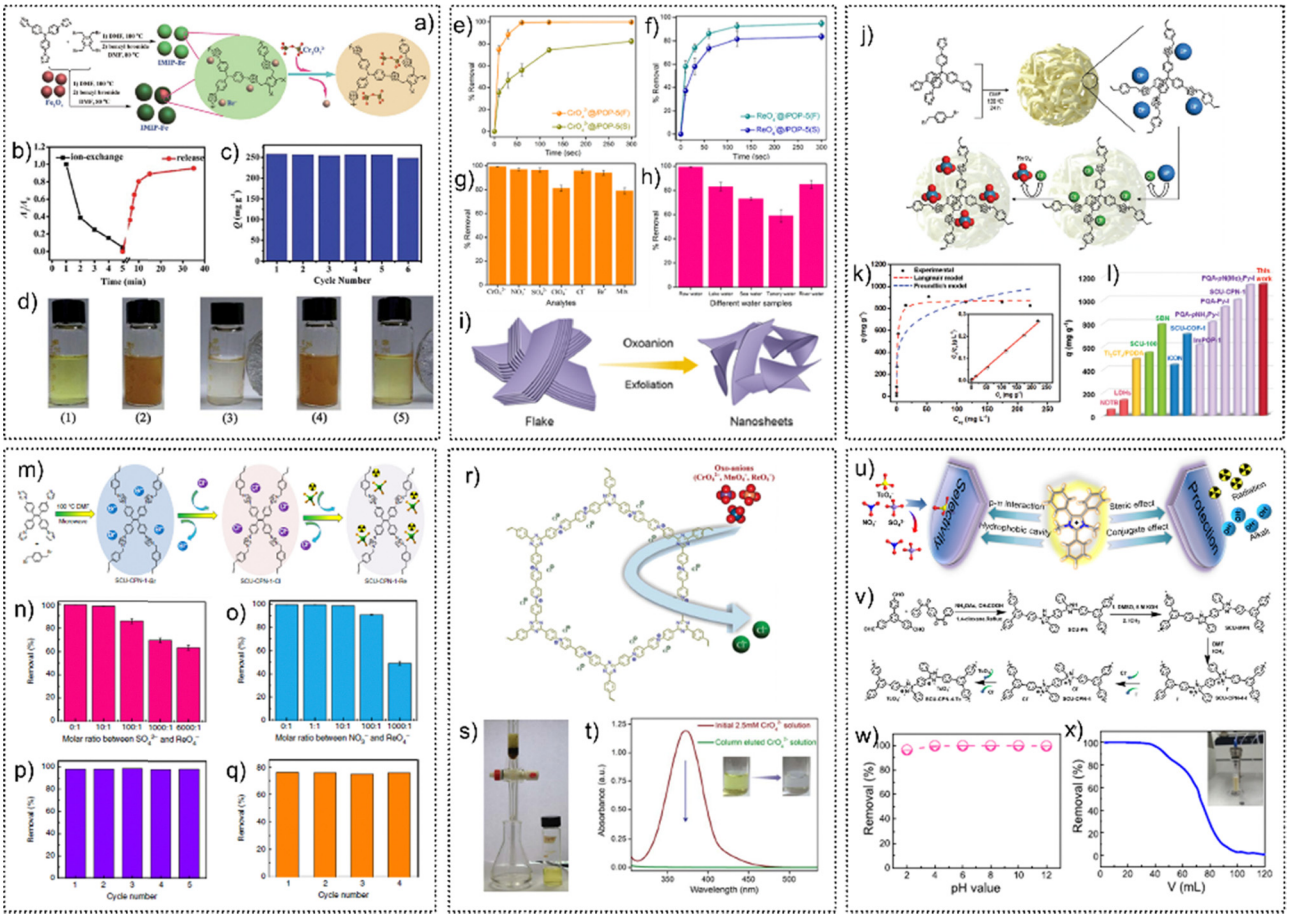

Fig. 16 (a) Schematic illustration of the synthesis and dichromate exchange of IMIP-Br and IMIP-Fe. (b) The ion-exchange and releasing process of $Cr_2O_7^{2-}$. (c) Plot of capture efficiency of IMIP-Fe in the recycling test. (d) Digital images of the recyclable process: (1) $K_2Cr_2O_7$ stock solution (0.55 mmol L^{-1}), (2) IMIP-Fe (8.8 mg) dispersed in $K_2Cr_2O_7$ solution, (3) magnetic separation of IMIP-Fe, (4) releasing of $Cr_2O_7^{2-}$ in KBr solution, (5) magnetic separation of regenerated IMIP-Fe. Reproduced with permission from ref. 313. Copyright 2016, the Royal Society of Chemistry. (e and f) Removal % of CrO_4^{2-} and ReO_4^- anions, respectively, by iPOP-5(F) and iPOP-5(S). (g) Removal % CrO_4^{2-} in the presence of other anions by iPOP-5(F). (h) Removal % of CrO_4^{2-} in different water systems by iPOP-5(F). (i) Schematic illustration of nanosheet formation from flake morphology of iPOP-5(F). Reproduced with permission from ref. 76. Copyright 2022, American Chemical Society. (j) Synthesis scheme of CPN-tpm and its anion-exchange process. (k) Fitted sorption isotherm curves of CPN-tpm-Cl for ReO_4^- capture (inset: Langmuir model). (l) Comparison of ReO_4^- capture capacity with other different materials. Reproduced with permission from ref. 311. Copyright 2022, Wiley-VCH. (m) Synthesis and the ReO_4^--exchange process of SCU-CPN-1. (n) and (o) Percentage removal of ReO_4^- in the presence of different molar concentrations of SO_4^{2-} and NO_3^-, respectively. (p) and (q) Result of the recyclability test of SCU-CPN-1 for ReO_4^- at pH 7 and 3M HNO_3, respectively. Reproduced with permission from ref. 312. Copyright 2016, Nature Publishing Group. (r) Schematic illustration of oxo-anion uptake by compound-1. (s) Digital image and (t) UV-Vis spectra of the CrO_4^{2-} capture test. Reproduced with permission from ref. 137. Copyright 2018, the Royal Society of Chemistry. (u) Schematic representation of designing the cationic key structural feature of SCU-CPN-4. (v) Synthesis and the ion-exchange process of SCU-CPN-4. (w) Effect of pH on ReO_4^- capture by SCU-CPN-4. (x) Result of the dynamic sorption column test of SCU-CPN-4. Reproduced with permission from ref. 314. Copyright 2022, American Chemical Society.

reported a tetraphenylmethane-based 3D cationic polymeric nanotrap (CPN-tpm) synthesized *via* solvothermal reaction of 3D building unit Tipm and 1,4-bis(bromomethyl)benzene (Fig. 16j).[311] The thus synthesized imidazolium salt-based polymers with positive charges exhibited very rapid kinetics with a record maximum uptake capacity of 1133 mg g^{-1} and a k_d value of 8.5 × 10^5 mL g^{-1} for ReO_4^-, which is found to be one of the maximum capacities among the reported adsorbents (Fig. 16k and l). Moreover, high adsorption capacity across a broad pH range and good recyclability for at least five cycles were demonstrated by the polymer CPN-tpm.

As discussed above, ReO_4^- is the nonradioactive surrogate anion of radioactive TcO_4^-. Given the harsh conditions of super acidity, high ionic strength, and intense radiation field, direct sequestration of $^{99}TcO_4^-$ from highly acidic solution is extremely difficult. However, this was demonstrated by Wang *et al.* in a report by developing an excellent radiation-resistant and hydrolytically stable imidazolium-based cationic polymeric network (SCU-CPN-1).[312] At first, the counter bromine anions of the synthesized cationic polymer were exchanged with chlorine anions and further applied for TcO_4^- capture (Fig. 16m). As a result, highly efficient uptake of TcO_4^- from acidic solution with rapid sorption kinetics and highest capture capacity was observed. Moreover, SCU-CPN-1 showed fully recyclable and highly selective uptake of specific oxo-pollutants even in the presence of an excess concentration of competitive anions such

as NO_3^- and SO_4^{2-} (Fig. 16n–q). Again, extraction of TcO_4^- under extreme chemical (acid/base) conditions was reported by Ma and co-workers by developing a series of imidazolium-based cationic POPs (PQA-Py-Cl, PQA-pNH_2Py-Cl, PQA-pN$(Me)_2$Py-Cl).[313] The adsorption capacities of PQA-pN$(Me)_2$Py-Cl, PQA-Py-Cl and PQpNH_2Py-Cl were found to be 997 mg g^{-1}, 849 mg g^{-1} and 642 mg g^{-1}, respectively. Importantly, after being soaked in 12M HCl or 2M NaOH solution for a week, the absorption capability of PQA-PN$(Me)_2$Py-Cl remained unaltered, indicating the stability of the POP for real-time prospective application of TcO_4^- collection from nuclear wastewater. Furthermore, segregation of TcO_4^- under extreme basic conditions was explored by using another cationic imidazolium POP (SCU-CPN-4). Wang *et al.* rationally designed and synthesized an imidazolium-based hydrophobic POP functionalized with the bulky group, which provided protection from attack of OH^- ions because of steric hindrance and hydrophobic interaction for efficient adsorption of TcO_4^- from alkaline waste medium (Fig. 16u and v).[314] SCU-CPN-4 exhibited ultrafast and record high adsorption capacity towards TcO_4^- in the pH range of 2–12. Additionally, almost 98% capture efficiency was calculated in 1 M aqueous NaOH solution (Fig. 16w). Also, the oxoanion removal study was repeatable with six adsorption–desorption cycles. The POP was found to show high sorption efficacy towards TcO_4^- from the simulated high-level waste stream from both the batch experiment and the dynamic column separation test (Fig. 16x).

Owing to the inbuilt cationic nature, viologen unit grafted ionic porous polymers were also found to be promising adsorbents towards sequestration of toxic oxoanions from water.[315] Our group demonstrated successful detoxification of wastewater by selective removal of various metal-based oxoanions by synthesizing a chemically stable viologen-based cationic organic network material (compound-**1**) *via* the Zincke reaction (Fig. 16r).[137] The polymer contained free exchangeable Cl^- ions, which provided an ideal platform for the removal of hazardous anionic oxopollutants from water. When tested, carcinogenic anions, including CrO_4^{2-}, MnO_4^- and ReO_4^-, were found to be selectively and rapidly removed from water with high adsorption capacities. Moreover, to test the real-time aspect, a column exchange based oxoanion capture experiment was performed (Fig. 16s and t). In addition to these examples, the adsorption performance of other POP materials for oxoanion capture is summarized in Table S5 (ESI†).

6.3 Gas-phase pollutant sorption and separation

6.3.1 Pristine POP-based separation

6.3.1.1 Carbon dioxide (CO_2) adsorption. Humankind heavy dependence on fossil fuels as the prime energy source has culminated in the ever-rising concentration of atmospheric CO_2 which is estimated to reach the record high level of 419 ppm (Feb 2022) and expected to increase even further in the future.[316–318] Because of its detrimental effects on global warming, significant research efforts have been devoted towards CO_2 remediation technologies. In this regard, physisorptive separation processes are considered as the most practical solution owing to their lesser energy footprints (enthalpy of adsorption, $Q < 40$ kJ mol^{-1}) in comparison with the chemisorptive methods ($Q > 40$ kJ mol^{-1}). Amongst different techniques of CO_2 capture, adsorptive capture by porous materials is regarded as one of the most energetically adequate and technically achievable methods. To this end, numerous POPs have been studied for the selective adsorption and separation of CO_2 maintaining pre- or post-combustion conditions. The combination of high surface area and ease in tunability of pore surface of POPs is among the prime advantages which render enhancement in molecular interaction with CO_2.[319–322] In an inaugural work, Zhou and co-workers fabricated a series of porous polymer networks (PPNs), namely PNN-3, PNN-4, and PNN-5, *via* the Yamamoto homo-coupling method (Fig. 17a and b).[71] All the PPNs exhibited excellent physiochemical stability as well as a very high BET surface area. Among them, PPN-4 exhibited a BET surface area of 6461 m^2 g^{-1} and a very high CO_2 uptake of 2121 mg^2 g^{-1} at 295 K and 50 bars (Fig. 17c). Both these values were believed to be the highest values reported in the literature for porous materials. The combination of both exceptionally high surface area and excellent stability of PPN-4 was regarded as the dictating factor toward such high uptake performances. In continuation of their effort, the same research group developed novel sulfonic acid and lithium sulfonate based PPNs, namely PPN-6-SO_3H and PPN-6-SO_3Li (Fig. 17d).[323] Following the same Yamamoto homocoupling reaction with chlorosulfonic acid, PPN-6 was synthesized, which was further neutralized to generate PPN-6-SO_3Li. The sulfonate-grafted PPN-6 materials showed significant enhancement in CO_2 uptake capacities as the CO_2 uptake values for PPN-6-SO_3H and PPN-6-SO_3Li were found to be as high as 13.1 and 13.5 wt % respectively at 295 K and 1 bar (Fig. 17e and f). On the other hand, the non-grafted PPN-6 showed a gravimetric CO_2 uptake of 5.1 wt %, clearly indicating the role of –SO_3H and –SO_3Li groups in CO_2 capture. This work potentially opened a new avenue toward exploration of various polar functional moieties in POP synthesis for CO_2 capture. In search of a more efficient material for CO_2 capture with enhanced capacity and selectivity, the same group developed another functional PPN-based system, namely, PPN-6-SO_3NH_4, which was synthesized following the similar protocol mentioned above.[324] The surface area of PPN-6-SO_3NH_4 (593 m^2 g^{-1}) was found to be exactly half of that of PPN-6-SO_3NH_4 which can be attributed to the incorporation of a –NH_4 moiety resulting in partial pore blocking of the material. Further, PPN-6-SO_3NH_4 exhibited a record high adsorption enthalpy of −40 kJ mol^{-1} toward CO_2 at zero loading along with excellent CO_2 uptake in the low pressure range. Furthermore, experimental dynamic breakthrough studies revealed the excellent CO_2 adsorption capacity of 1.7 mmol g^{-1} of PPN-6-SO_3NH_4 at 295 K and 1 bar. In a collaborative pioneering work by Jung, Atilhan, Yavuz and co-workers, the authors presented a unique strategy of utilization of polymeric amidoxime materials for CO_2 capture.[325] Acetamidoxime (AAO-monovalent), having the highest % of amidoxime functionality, showed the best performance toward CO_2 uptake (2.71 mmol g^{-1}) at 70 °C and 180 bar. The other amidoximes,

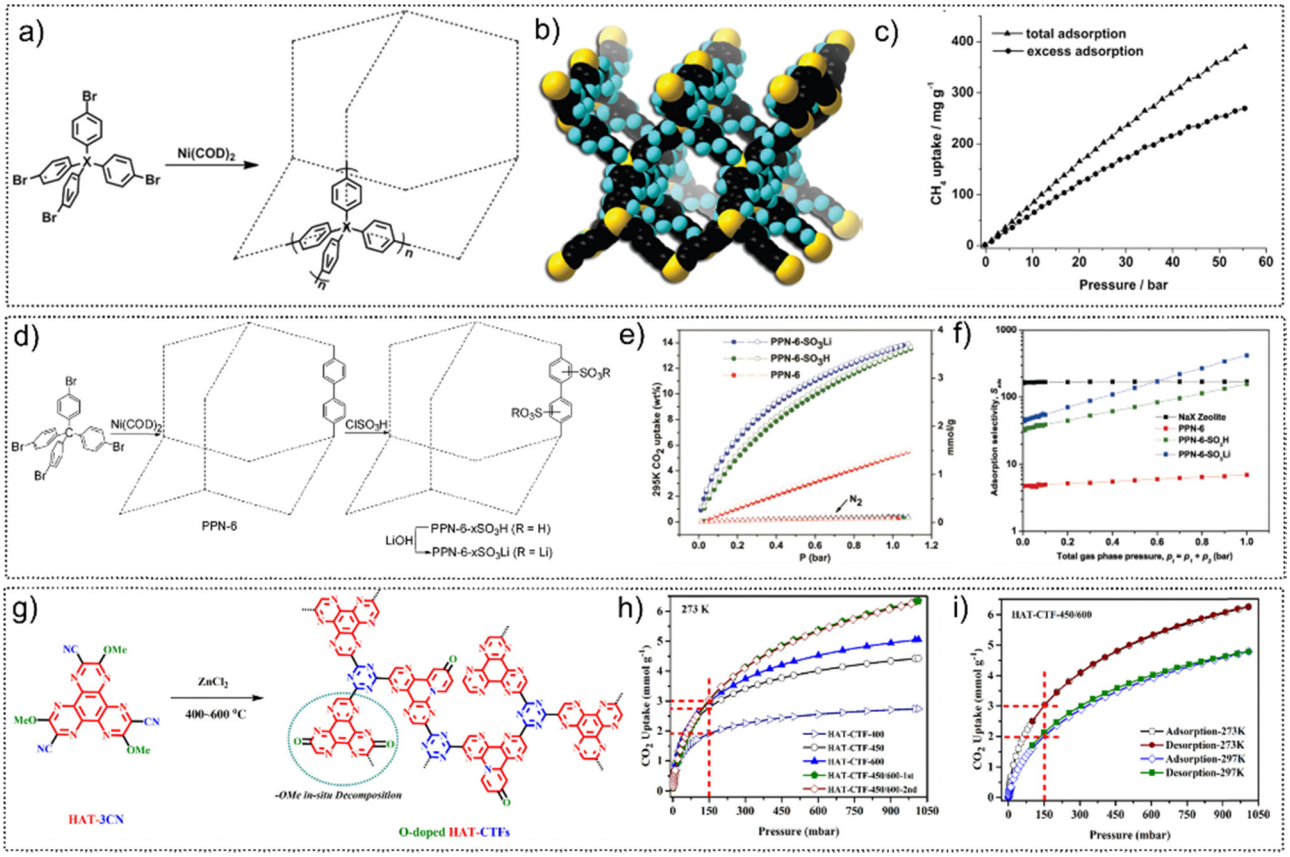

Fig. 17 (a) Synthetic route for PPN-3. (b) The default noninterpenetrated diamondoid network of PPN-4. (c) Excess and total CO_2 adsorption isotherms of PPN-4 at 295 K. Reproduced with permission from ref. 71. Copyright 2011, Wiley-VCH. (d) Schematic representation of synthesis and grafting of PPN-6. (e) Gravimetric CO_2 and N_2 adsorption/desorption isotherms at 295 K of the PPN-6 series. (f) IAST-predicted adsorption selectivities for PPN-6 (red), PPN-6-SO_3H (green), PPN-6-SO_3Li (blue), and NaX zeolite (black). Reproduced with permission from ref. 323. Copyright 2011, American Chemical Society. (g) Synthesis route for O-doped HAT-CTFs. (h) CO_2 uptake of HAT-CTFs at 273 K and 1 bar. (i) CO_2 adsorption–desorption of HAT-CTF-450/600 at 273 and 297 K. Reproduced with permission from ref. 326. Copyright 2016, American Chemical Society.

i.e. terephthalamidoxime (TPAO-divalent) and tetraquinoamidoxime (TQAO-tetravalent), showed lesser uptake of CO_2 than AAO. Furthermore, polyamidoxime (PAO-polyvalent) showed a CO_2 uptake of 0.53 mmol g^{-1} and 0.41 mmol g^{-1} at 43 °C and 70 °C, surpassing activated charcoal Norit RB3 toward CO_2 uptake per unit surface area. An *in situ* doping strategy was demonstrated by Dai and co-workers for the fabrication of a new family of hexaazatriphenylene-based CTFs (HAT-CTFs) for efficient adsorption of CO_2 (Fig. 17g).[326] The resulting task specific material, namely HAT-CTF-450/600, was found to adsorb 6.3 and 4.8 mmol g^{-1} of CO_2 at 273 K and 297 K at 1 bar (Fig. 17h and i). Such high CO_2 uptake was correlated with the synergistic effects of ultrananopores and abundant CO_2-interactive sites (N/O). In another work, strategic design and synthesis of a novel dicyano monomer with the benzimidazole moiety (DCBI) at room temperature were demonstrated by Wang and co-workers (Fig. 18a).[327] Further, by utilizing the DCBIs, a series of benzimidazole functionalized CTFs, namely CTF-BIs, were prepared under ionothermal conditions. The CTF-BI family exhibited very high BET surface areas up to 1549 m2 g^{-1}. Moreover, owing to their suitable chemical pore-environment, they showed selective uptake of CO_2 and the Q_{st} values were found to be between 31.7 kJ mol^{-1} and 34.3 kJ mol^{-1} which is indicative of dipole–quadrupole interactions between the nitrogen-rich polar binding sites and the CO_2 molecules (Fig. 18b and c). Among the CFT-Bis, CTF-BI-11 exhibited a very high CO_2 uptake capacity of 21.68 wt% at 273 K. To check the role of structural diversity in the same class of CFTs, two new CFTs were fabricated with triptycene and fluorene moieties *via* the Friedel–Crafts reaction by Janiak and co-workers (Fig. 18d).[328] The triptycene based CTF, *i.e.* CTF-TPC, was found to show a record high surface area of 1668 m^2 g^{-1}, whereas the surface area of the fluorene based CTF (CTF-FL) was found to be 773 m^2 g^{-1}. Further, the CO_2 adsorption studies revealed a very high uptake of 4.24 mmol g^{-1} for CTF-TPC and 3.26 mmol g^{-1} for CTF-FL at 273 K and 1 bar respectively which in combination with cost-effective synthesis of these CTFs make them promising toward efficient carbon sequestration applications (Fig. 18e and f). In another work, four highly cross-linked polyimide-based microporous networks were prepared using tetraphenyladamantane and tetraphenylmethane as net nodes and (hexafluoroisopropylidene)diphenyl, biphenyl and benzophenone as linking moieties by Wang and co-workers (Fig. 18g).[148] The resultant

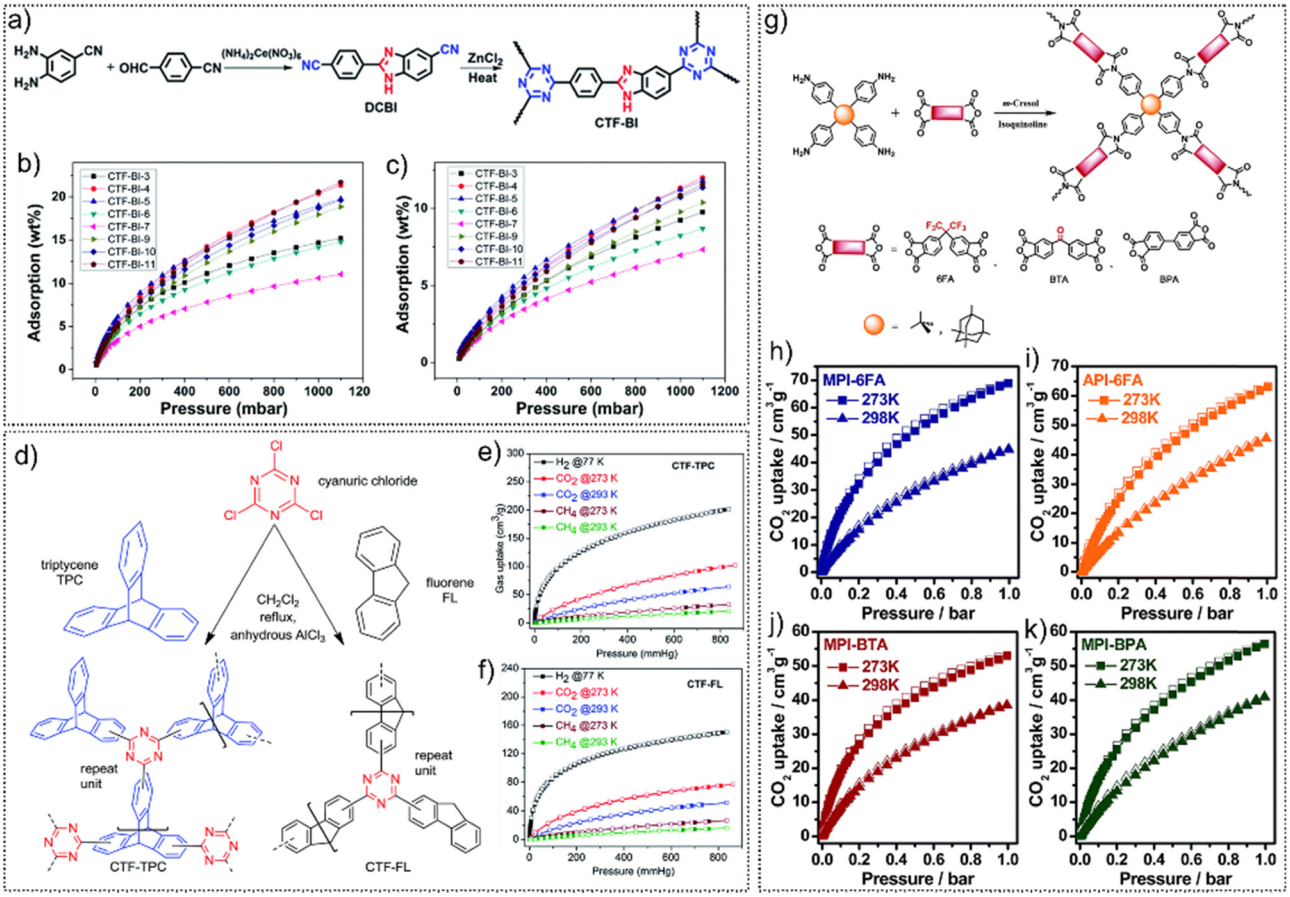

Fig. 18 (a) Schematic representation of the synthesis of CTF-Bis. (b) CO_2 adsorption isotherms at 273 K of CTF-Bis. (c) CO_2 adsorption isotherms at 303 K of CTF-Bis. Reproduced with permission from ref. 327. Copyright 2016, The Royal Society of Chemistry. (d) Synthesis route and model structures for CTF-TPC and CTF-FL. e) Gas sorption isotherms of CTF-TPC. (e) Gas sorption isotherms of CTF-FL. Reproduced with permission from ref. 328. Copyright 2016, The Royal Society of Chemistry. (g) Synthesis routes to the microporous polyimide networks. (h) and (i) Adsorption (filled) and desorption (empty) isotherms of CO_2 at 273 K and 298 K for MPI-6FA, API-6FA, MPI-BPA and MPI-BTA. Reproduced with permission from ref. 148. Copyright 2016, The Royal Society of Chemistry.

polyimide networks, namely MPI-6FA, API-6FA, MPI-BPA and MPI-BTA, showed good thermal stability and BET surface areas up to 781 $m^2\ g^{-1}$ and good CO_2 uptake performances (Fig. 18h–k). The presence of a high density of trifluoromethyls was found to contribute to the very high CO_2 uptake of 13.5 wt% for MPI-6FA at 273 K (1 bar) and resulting in an IAST CO_2/N_2 selectivity value of 53.5. The first study on facile catalyst-free one pot synthesis of three novel nitrogen rich nanoporous amide networks (NANs) was demonstrated by Zulfiqar and co-workers.[329] Fabricated with the tetraphenyladamantane moiety, the NANs, namely NAN-1, NAN-2 and NAN-3, were found to exhibit good CO_2 uptake capacity and NAN-1 in particular showed an excellent selectivity of 74 toward CO_2 over N_2 at 273 K. The combined merits of mesoporous architecture and the presence of CO_2-philic N-containing amide groups were believed to be the prime reason behind such selective sorption properties of NANs. Chang, Yang and co-workers came up with the design and synthesis of a new type of POP, *i.e.* indole-based microporous organic polymer (PINK), fabricated from the condensation polymerization of 3,3′-diindolylmethane and 1,3,5-tris-(4-fluorobenzoyl)benzene.[330] The existing dipole–π interactions between the CO_2 molecules and the adsorbent resulted in a high CO_2 uptake of 16.0 wt% at 273 K (1.0 bar) and also a high selectivity of 15 and 32 toward CO_2/N_2 and CO_2/CH_4 respectively.

Of late, Coskun and co-workers demonstrated the importance of chemical activation of porous materials to enhance the textural properties and high surface areas of porous materials.[331] To rationalise this strategy, they synthesized a microporous CTF, namely, CTF-1, which was further chemically activated with KOH at 700 °C to generate chemically activated CTF-1, *i.e.* caCTF-1-700. Chemical activation was found to affect the porosity of the CTF, resulting in an improved surface area of 2367 $m^2\ g^{-1}$ and also enhanced the gas adsorption properties significantly as the CTF showed very high CO_2 uptake capacities up to 6.0 mmol g^{-1} at 1 bar and 273 K. Such high CO_2 uptake in the low pressure range was directly correlated with the special textural properties of caCTF-1-700 which promote the favourable dipole–quadrupole interactions between CO_2 molecules and the nitrogen atoms inside the ultramicroporous networks.

In quest of low-cost high-performance functional materials, Tan and co-workers developed two hybrid HCPs, namely,

HCP-PN-1 and HCP-PN-2, *via* Friedel–Crafts chemistry with enhanced Lewis base (–P═N) sites.[332] The combined contribution of hierarchical pores, high surface areas and the presence of Lewis base sites resulted in a very high uptake of CO_2 for both the HCPs. The saturation uptake capacities of HCP-PN-1 and HCP-PN-2 were found to be as high as 7.2 and 5.7 wt % at 273 K, and 4.9 and 3.8 wt % at 298 K. In 2019, Wang and co-workers reported a series of four new nitrogen-enriched microporous polymers (MPs), namely, PAN-NH_2, PAN-NH-NH_2, PAN-NH-CH_3, and PAN-N-$(CH_3)_2$. These polymers were synthesized *via* amine-formamide reaction of different primary, secondary and tertiary amine groups such as formohydrazide, formamide, *N*,*N*-dimethylformamide (DMF), and *N*-methylformamide respectively.[333] The resultant four MPs exhibited BET surface areas in the range of 612–748 $m^2\ g^{-1}$. Such high porosity and the systematic tuning of the amine groups result in interesting interfacial interactions between the incoming CO_2 molecules and the porous surfaces. The trend of CO_2 uptake capacity among the MPs was found to be PAN-NH-CH_3 > PAN-N-$(CH_3)_2$ > PAN-NH_2 > PAN-NH-NH_2. Furthermore, PAN-NH-NH_2 was found to show an excellent heat of adsorption value of 40.6 kJ mol^{-1} along with a high CO_2/N_2 selectivity of 151 at 273 K. In another recent report, Das and co-workers have introduced four newly designed triazole functionalized CTFs (TzCTFs), namely, df-TzCTF600, df-TzCTF400, TzCTF600, and TzCTF400, based on 1,2,3-triazole substituted aromatic nitrile building blocks.[334] The combination of high surface area, ultra-micropores, triazine embedded pore surfaces and presence of CO_2-phillic multi-N-containing triazole units resulted in very good adsorption performance toward CO_2. The trend of CO_2 uptake capacity was found to be df-TzCTF600 > df-TzCTF400 > df-TzCTF400 > df-TzCTF600. In addition, transient breakthrough simulation studies were carried out to further access the selective adsorption of CO_2 over N_2 for these polymeric materials. For a summary of CO_2 sorption performance of various POP-based materials, see Table 1 and Table S6 (ESI†).

6.3.1.2 Methane (CH_4) adsorption. Methane gas is one of the prime, widely abundant components of natural gas. It has been the preferred choice because of its lesser environmental impacts upon combustion in comparison with the other hydrocarbon fuels. The ideal value for methane storage estimated by the US Department of Energy (DOE) is 180 cm^3 (STP) at 35 bar (298 K). In this regard, POPs have been considered as the potentially ideal sorbent material for methane storage because of their favourable physiochemical properties.[335,336] To rationalize this, a series of hypercrosslinked polymers were synthesized by Cooper and co-workers to evaluate their methane storage performance.[42]

The hypercrosslinked polymers were synthesized *via* Friedel–Crafts condensation of bischloromethyl monomers such as 4,4′-bis(chloromethyl)-1,10-biphenyl (BCMBP) and dichloroxylene (DCX). Among the synthesized polymers, the BCMBP based network exhibited the highest BET surface area of 1904 $m^2\ g^{-1}$ and a very high uptake of CH_4 (5.2 mmol g^{-1}) at 20 bar and298 K. Furthermore, an easy synthetic strategy to produce continuous monolithic blocks of these polymers was demonstrated, addressing the real-time volumetric issues for the packing of powders. In a more recent work, Yavuz and co-workers reported the highest volumetric working capacity for methane adsorption by an alkane-linked flexible porous aromatic network polymer (COP-150).[337] Fabricated from benzene and 1,2-dichloroethane *via* Friedel–Crafts reactions, COP-150 showed a very high methane working capacity of 0.625 g g^{-1} and 2941 l l^{-1} in between the cyclic pressure range of 5 and 100 bar. These values were found to fall in the permissible range of US DOE of 0.5 g g^{-1} (263 l l^{-1}) for methane storage.

6.3.1.3 Other toxic gas adsorption. Ammonia (NH_3) is one of the most annually produced gases globally because of its utilization in various fertilizer manufacturing, chemical resources, pharmaceutical production, *etc.* However, NH_3 is very harmful and corrosive in nature even at low concentrations which can lead to irritation and burning of the skin, throat, eyes, mouth and lungs. Higher concentration of NH_3 can lead to permanent damage to the lungs and cause death. Hence, immediate and effective removal of NH_3 is of high importance.[338,339] To address this critical issue, a family of diamondoid porous organic polymers featuring isolated as well as cooperative Brønsted acidic functionalities were developed by Long and co-workers.[340] The parent POP material, *i.e.* PAF-1, was further functionalized *via* nitration followed by reduction with sodium dithionite to generate BPP-1 [$(C_6H_4\text{-}C_6H_3NH_2)_2(C)$]. Further another POP, namely BPP-2 [$(C_6H_4\text{-}C_6H_3NH_3Cl)_2(C)$], was produced *via* adding HCl to BPP-1. In addition, the sulfonated derivative of PAF-1, *i.e.* PPN-6-SO_3H, was also prepared to cover the spectrum of functionalities toward NH_3 adsorption. Indeed, the NH_3 uptake performance was found to directly depend upon the acidity of the functional groups and the POP family registered the trend of PPN-6-SO_3H > BPP-2 > BPP-1 > PAF- 1. The excellent NH_3 sorption performance of the lesser acidic functionalized POPs in comparison with PPN-6-SO_3H at both high and low pressure indicates the role of cooperative interaction in the enhancement of NH_3 adsorption capacity. Following a similar polymerization protocol, five different POPs, namely BPP-3, BPP-4, BPP-5, BPP-6, and BPP-7, were synthesized with different monomers. Among them, BPP-5 exhibited a very high NH_3 uptake capacity of 17.7 mmol g^{-1} establishing the role of acidic sites in offering cooperative behaviour within such materials for NH_3 removal application. In the same line, the same research group came up with another Brønsted acidic POP based on poly(amic acid) (PAA) *via* a facile, one-step and catalyst-free synthesis utilizing pyromellitic anhydride and tetrakis(4-aminophenyl)methane.[341] Addition of water as cosolvent was found to be absolutely important to prevent the *in situ* generation of polycyclic imide (PI). PAA showed an excellent uptake capacity of NH_3 (10.7 mmol g^{-1}) at 298 K and 1 bar, outperforming PI (9.0 mmol g^{-1}), despite the smaller pore volume and lesser surface area. Further, dynamic microbreakthrough measurements for NH_3 capture were also performed to check the potential of the material toward practical application. As expected, PAA exhibited a higher NH_3 uptake in both humid (4.4 mmol g^{-1}) and dry (2.4 mmol g^{-1}) conditions compared with PI (3.4 mmol g^{-1} and 1.1 mmol g^{-1}). In 2018, the double

Table 1 Table of POP-based materials for carbon dioxide (CO_2) gas capture

POPs	BET surface area ($m^2\ g^{-1}$)	Temperature (K)	Pressure (bar)	CO_2 uptake (mmol g^{-1})	Q_{st} (kJ mol^{-1})	Ref.
PPN-4	6461	298	50	48.19	NM	81
BILP-2	708	273	1	3.38	28.6	82
BILP-4	1135	273	1	5.34	28.7	
BILP-5	599	273	1	2.9	28.8	
BILP-7	1122	273	1	4.38	27.8	
ALP-1	1235	273	1	5.37	29.2	83
ALP-5	801	273	1	4.46	32.5	84
HCP-BDM	847	273	1	2.87	33.5–25.4	85
HCP-BA	742	273	1	1.92	27.4–24.1	
BILP-6-NH_2	1185	273	1	5.57	29.5	86
p-PDM-DVB	841	273	1	1.25	NM	87
Fe-POP-1	875	273	1	4.30	NM	88
P-PCz	1647	273	1	5.57	30.9	89
PAF-60	1094	273	1	2.53	~34.2	90
PAF-61	793	273	1	1.82	~34.2	
PAF-62	701	273	1	1.69	~34.2	
MOPI-I	206[a]	273	1	3.3	39	91
MOPI-II	644[a]	273	1	2.9	32	
MOPI-III	443[a]	273	1	3.0	32	
MOPI-IV	660[a]	273	1	3.8	31	
MOPI-V	921[a]	273	1	2.9	13	
PINK	2090	273	1	4.11	28.9	92
CTF-TPC	1668	273	1	2.17	32	93
CTF-FL	773	273	1	1.67	35	
TPB	2435	273	1	5.9	NM	94
CTF-BI-4	1025	273	1	2.47	31.7–34.3	95
CTF-BI-11	1549	273	1	2.51	31.7–34.3	
NAN-2	56	273	1	1.49	31.52	96
Ni-Por-1	1711	273	1.08	3.13	24	97
TNP1	1090	273	1	178	37.0	98
TNP4	1348	273	1	196	36.5	
FCDTPA-K-700	2065	273	1.13	6.51	<30.55	99
Network-1	1980	273	1	3.63	23.3	100
BILP-10	787	273	1	4.02	38.2	101
BILP-11	658	273	1	3.09	32.0	
BILP-12	1497	273	1	5.29	27.6	
BILP-13	677	273	1	2.57	26.7	

Table 1 is in continuation of Table S6 in the ESI.

post-synthetic modification strategy was utilized *via* post-oxidation and post-sulfonation to produce an acidified HCP by Hong and co-workers.[342] The parent HCP, namely 1T, was further oxidized to produce the carboxylic acid functionalized HCP, namely 1TC, which was further treated with chlorosulfonic acid to produce sulfonated polymer 1TCS. The NH_3 uptake capacities were found to follow the trend 1TCS (8.52 mmol g^{-1}) > 1TC (6.41 mmol g^{-1}) > 1T (3.8 mmol g^{-1}) at 298 K and 1 bar. The trend for Q_{st} was also found to be the same which clearly highlights the role of high-density acidic functionalization in preferential affinity and enhanced uptake for NH_3. Further to check the role of the hydrophobic polymer in NH_3 uptake, the surface of 1TCS was coated with the PDMS hydrophobic polymer to form 1TCS@PDMS10. 1TCS@PDMS10 exhibited higher NH_3 uptake in the low-pressure range compared to the other HCPs, indicating the role of hydrophobicity in effective NH_3 sorption.

Apart from ammonia, another highly toxic and hazardous gas is hydrogen sulfide (H_2S). H_2S is extremely harmful to human health even at low concentrations causing irritation to the eyes and damage to the respiratory system, and exposure at higher concentration (>700 ppm) can lead to immediate death.[343,344] In addition, while it is released into the air, H_2S can react with water molecules and result in acid, which is detrimental to both the environment and human beings. To address this issue, a new POP, namely KFUPM-5, was prepared *via* the acid catalyzed polycondensation reaction of melamine and pyrrole by Hamouz and co-workers.[345] The strategic choice of these monomers resulted in a high density of nitrogen sites in the POP structure which was further found to be beneficial for H_2S uptake. To check its potential toward selective H_2S sorption, KFUPM-5 was employed in a binary gas mixture of 0.2% H_2S in CH_4 (v/v), in which KFUPM-5 exhibited excellent retention performance toward H_2S (>120 min) over CH_4 and a dynamic capacity of 4.9 $cm^3\ g^{-1}$. Further, KFUPM-5 was found to maintain its performance in up to 5 cycles. Moreover, to mimic the real-world natural gas separation scenario, KFUPM-5 was employed toward a more complex ternary gas mixture of H_2S (0.51% v/v), CO_2 (9.99% v/v), and CH_4 (89.5% v/v) in which KFUPM-5 showed excellent selective retention performance toward H_2S over other gases.

6.3.2 POP-membrane-based separation. Membrane-based separation technologies are of great interest to both scientific research and industries owing to their superior features such as unsuppressed permeability, high selectivity, reduced carbon

footprint, low energy consumption, small capital investment, *etc.*[346] Gas separation membranes are anticipated to selectively permeate specific gas molecules to provide efficient separation. Recent research has revealed that various polymer membranes such as thermally rearranged polymers, polymers of intrinsic microporosity, polyimide polymers, polyethylene glycols, *etc.* can offer dual advantage of low material cost and efficient gas transport. In this regard, POPs are considered as one of the most promising candidates toward fabrication of efficient gas separation polymeric membranes owing to their continuous microporous networks, tunable chemical structure, high surface area, high thermal and chemical stability, and adjustable textural properties.[347] Such control over structural and chemical properties offers advantages in overcoming the long-term existing problem of trade-off between selectivity and permeability of membranes. In 2015, Koros reported a hydroxyl functionalized PIM, namely, PIM-6FDA-OH, for simultaneous adsorption of H_2S and CO_2 from natural gas streams under real-world conditions.[348] The authors further fabricated a membrane derived from PIM-6FDA-OH to validate its potential toward aggressive sour gas separations. Gas permeation experiments were conducted in the gas mixture with 15/15/70% H_2S/CO_2/CH_4 as the feed, and a high separation factor up to 29.9 for H_2S/CH_4 was recorded during the measurement, which was higher than that of many commercial polyimide membranes. The polymer membrane showed an improved plasticization resistance toward both H_2S and CO_2 up to 4.5 and 28 bar respectively compared to only PIM-6FDA-OH. In addition to the single gas adsorption, the PIM6FDA-OH film also exhibited excellent selectivity for both CO_2/CH_4 and H_2S/CH_4 mixed gas permeation studies, highlighting its potential for real-time aggressive sour gas separations. Continuing their effort, in 2019 the same research group demonstrated ultra-selective H_2S separation *via* post-functionalization of PIM-1 with amidoxime, resulting in AO-PIM-1 with enhanced basic groups.[349] Upon applying a ternary mixture feed comprising 20% H_2S/20% CO_2/60% CH_4 under challenging feed pressures (up to 77 bar), AO-PIM-1 exhibited outstanding performance toward purification of sour gas streams. These performances were found to be two to three times better than that of the commercially available glassy polymeric membranes. In a recent pioneering work, Smith, Xia and co-workers reported a library of hydrocarbon ladder polymers fabricated from norbornyl benzocyclobutene moieties.[350] The thus synthesized PIM-based membrane, namely, CANAL-Me-Me$_2$F, was found to exhibit improved gas separation properties owing to its higher ordered structure with compact pore environments compared to that of the fresh PIM membranes having excess free volume. This structural improvement leads to improved selectivity for gas mixtures like CO_2/CH_4, H_2/CH_4, H_2/N_2, O_2/N_2, and H_2/CO_2.

6.4 Heterogeneous catalysis for pollutant degradation

Catalysis is essential for chemical transformations. Catalytic reactions not only play a key role in the production of many industrial chemicals and materials, but also hold paramount importance in diverse applications such as pharmaceutical synthesis, environmental remediation, energy applications, food production, *etc.*[351–353] Depending upon the nature of the catalyst, catalysis can be categorized into two: homogeneous and heterogeneous catalysis. In the case of homogeneous catalysis, the catalyst remains in the same phase with the reactants, whereas in heterogeneous catalysis, the catalyst remains in a different phase from the reactants. Despite the higher activity and selectivity of homogeneous catalysts, several drawbacks like lack of stability and hardship in catalyst/product separation limit their practical applications. To address these issues, significant scientific efforts have been dedicated for development of heterogeneous catalysts with improved features such as easy recyclability, designed active sites, good accessibility, *etc.* In this regard, POPs with high surface areas, tailored porous structures, higher pore volumes, *etc.* are considered as ideal for heterogeneous host materials for the immobilization of molecular catalysts.[15,354] In addition, POPs offer several key superior advantages for any catalytic application. For example, their interconnected hydrophilic or hydrophobic network structures help in enrichment of reactant molecules and hence improving catalytic efficiency. Moreover, the well-defined pore sizes of POPs intrinsically assist in elective transportation of different substrate molecules with different size, resulting in size-selective catalysis. Such features make POPs promising carriers for heterogeneous catalysts. Moreover, the lifetime of a catalyst in industrial reactors is dictated by its thermal, chemical, and mechanical stability. POP-based heterogeneous catalysts render improved stability *via* immobilizing the catalysts on the POP pore surface.[355] Although POP-based heterogeneous catalysis is still in a developing phase, the recent literature indicates that POP-based catalysts are endowed with excellent catalytic properties, like superior stability, high selectivity and catalytic activity, easy recovery and recycling. Typically, two main methods are followed to synthesize POP-based heterogeneous catalysts: (1) pre-synthetic strategies with catalytic monomers and (2) post-synthetic modification of POPs with catalytic units.

6.4.1 Pre-synthetic strategies with catalytic monomers. Incorporation of necessary catalytic moieties as/into the building blocks of POPs is the most well-studied and efficient method to obtain POP-based catalyst materials directly. This strategy enables introduction of various catalytic moieties into the porous networks of POPs *via* polymerization of the functional monomers, allowing the utilization of a vast spectrum of functional units. As a result, tailor made POP-based catalysts for targeted application can be achieved. Based on the chemical nature of the catalytic sites, POP-based catalysts can be divided into two: (1) POPs with metal complexes as catalytic sites and (2) POPs with organic moieties as catalytic sites.

6.4.2 Metal complexes as catalytic sites. Metal complexes of salens and porphyrins are widely explored for their catalytic properties for diverse organic reactions. Such functional heterogeneous catalysts can be synthesized *via* polymerization reaction of metallosalen and metalloporphyrin building blocks.[355] The structural advantage of having rigid macrocycles in porphyrins and salens enables direct inclusion of catalytically active metal

sites in the POPs. For example, the metalloporphyrin catalytic sites are found to be more stabilized inside the POP structure, improving catalytic efficiency because of the higher interactions between catalytic sites and reactant moieties. Moreover, the catalytic efficiency of heterogeneous catalysts can be tuned *via* tuning the porphyrin metal centre and modulating the peripheral pore environments, which have been thoroughly studied.

For example, in 2013, Farha, Hupp, Nguyen and co-workers demonstrated a straightforward strategy for inclusion of catalytically active Al-(porphyrin) moieties inside a POP, namely, Al-PPOP, *via* a cobalt-catalyzed acetylene trimerization method (Fig. 19a).[356] Supercritical CO_2 processing was utilized as the activation method for Al-PPOP which led to improved pore sizes and pore volumes, and significantly enhanced the substrate mobility and catalytic activities.

Al-PPOP was further exploited toward efficient degradation of a nerve agent simulant, *p*-nitrophenyl diphenyl phosphate (PNPDPP), *via* methanolic degradation reaction (Fig. 19b). In 2016, Guo and co-workers established a foam-supported standalone metalloporphyrin-based CMP composite through oxidative homocoupling reaction of terminal alkynes of the Zn(II) complex of 5,10,15,20-tetra(4-ethynylphenyl)porphyrin in the presence of melamine foam (Fig. 19c–e).[357] The resulting metalloporphyrin-CMP organogels equipped with interconnected micropores and macropores also showed very good elastic properties. Further, the CMP foam composite was found to exhibit excellent catalytic activity towards the acyl transfer reaction of *N*-acetylimidazole and 3-pyridylcarbinol (Fig. 19f).

Apart from porphyrins, salens are another class of universal chelating ligands. Salens are the condensation products of diamines and aryl aldehydes which can combine with a variety of metal cations with diverse catalytic properties. Recently, Song, Liang and co-workers have demonstrated a general strategy to synthesize a series of metal–salen-functionalized POPs (M-salen-POPs, M = Mn^{2+}, Co^{2+}, Ni^{2+}) for efficient fixation of CO_2 into cyclic carbonates.[358] Among the M-salen-POPs, Co-salen-POP exhibited excellent catalytic activity toward cycloaddition of both CO_2 and styrene oxide, yielding a selectivity as high as 99% and 96% yield in a CO_2 atmosphere (100 °C, 1 MPa) within just 30 minutes.

In an interesting work, two Anderson-type polyoxometalate (POM) built-in CMPs, namely Bn-Anderson-CMP and Th-Anderson-CMP, were fabricated *via* cross coupling reaction of

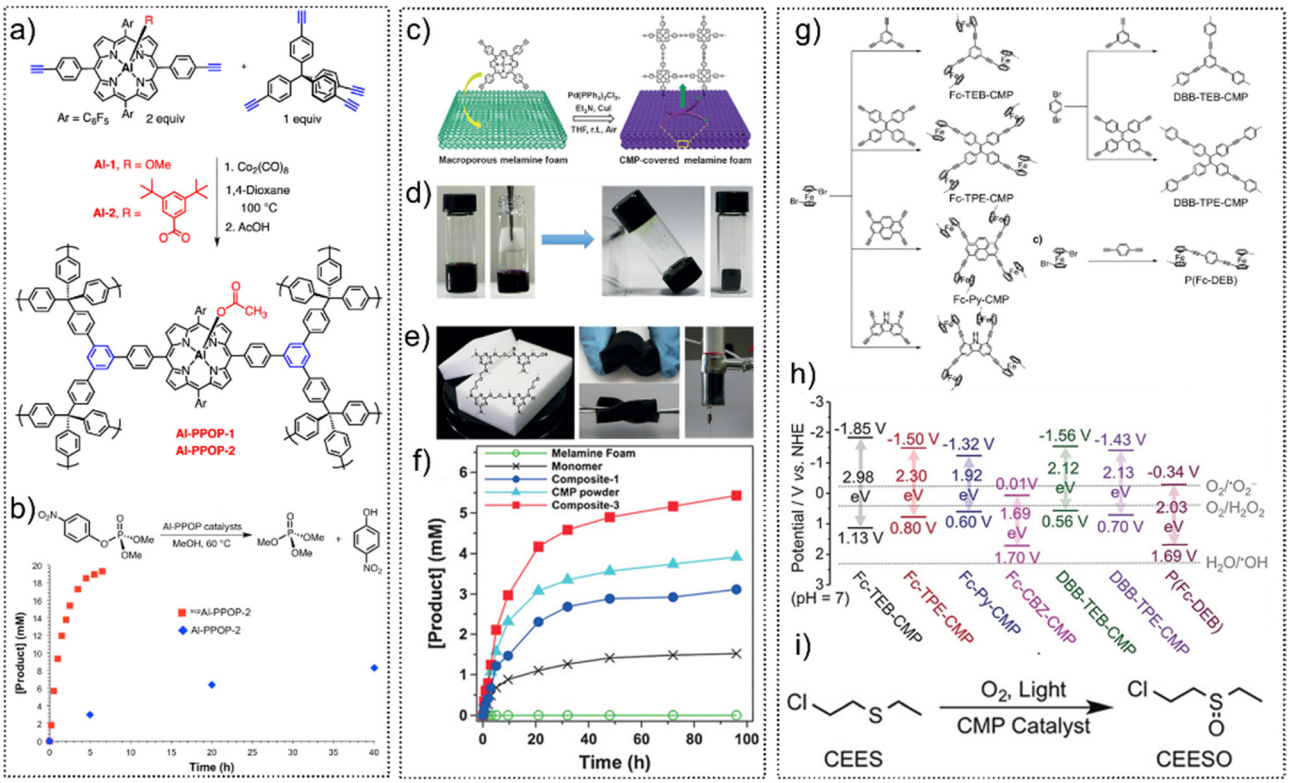

Fig. 19 (a) Synthesis of Al-PPOPs *via* cobalt-catalyzed acetylene trimerization. (b) Reaction profiles for the methanolysis of PNPDPP in the presence of 4 mol % of Al-PPOP-2 and ^{scp}Al-PPOP2. Reproduced with permission from ref. 356. Copyright 2013, American Chemical Society. (c) The CMP-gel-mediated composite strategy for the preparation of the CMP-covered foam composite. (d) The synthetic procedure included: (i) mixing of the foam and reaction solution, (ii) gelation, and (iii) solvent removal and adhesion of CMPs to the foam. (e) Photographs of the melamine foam (left) and as-synthesized CMP foam composites (center, right) that could be compressed and distorted and that fill into the glass syringe. (f) Product concentration *versus* time plots for the formation of 3-(acetoxymethyl)pyridine (3-AMP) from NAI and 3-PC by using composite-3, composite-1, CMP powder, Zn(TEPP) monomer, and melamine foam as catalysts, respectively. Reproduced with permission from ref. 357. Copyright 2016, Wiley-VCH. (g) Syntheses of Fc-based CMPs and controlled polymers. (h) Molecular orbitals of CMPs and P(Fc-DEB) together with ROS redox potentials. (i) Photooxidation reaction of CEES by Fc-based CMPs catalysts. Reproduced with permission from ref. 360. Copyright 2019, Wiley-VCH.

1,3,5-triethynylbenzene and tetrabromo-bifunctionalized POMs by Chen and co-workers.[359] Both of the prepared POM-CMPs were further employed toward photocatalytic degradation of toxic organic dyes, *e.g.* methylene blue (MB) and rhodamine B (RhB). Both Bn-Anderson-CMP and Th-Anderson-CMP showed higher photocatalytic degradation efficiency than that of their parent building units (Anderson POM 1 and 2). Moreover, Bn-Anderson-CMP was found to show 81% degradation efficiency toward RhB in just 30 min and 92% degradation efficiency toward Mb within just 20 mins, which are higher than that of the performance of Th-Anderson-CMP. In addition, conclusive evidence from a series of experiments indicates that H_2O_2 and $^1O_2$ are the two main active species involved in the catalytic degradation of RhB. In another work, incorporation of ferrocene (Fc) inside CMP backbones and systematic tuning of their optical energy gaps were studied by Wang and co-workers (Fig. 19g and h).[360] The Fc-based CMPs, namely, Fc-TPE-CMP, Fc-TEB-CMP, Fc-CBZ-CMP, and Fc-Py-CMP, were prepared through the Sonogashira–Hagihara cross-coupling reaction. Further, the tetrakis(4-ethynylphenyl)ethene derived CMP, *i.e.* Fc-TEB-CMP, was found to exhibit excellent degradation efficiency toward MB and also transform the toxic warfare agent sulfur mustard (CEES) to lesser toxic sulfoxide (CEESO) (Fig. 19i).

6.4.3 Organic moieties as catalytic sites. Organocatalysts are well known for their unique catalytic selectivity and activities in diverse organic transformation reactions. POP-based organocatalysts provide new windows of opportunity in the domain of organocatalysts, since they can potentially solve both the separation and recycling problems associated with the pure organocatalysts. Functional moieties such as various kinds of amines, imines, pyrrolidine, boroxine, pyrene, benzodifuran, benzothiadiazole, and bipyridyl have been used to synthesize organocatalysts. For example, Ahn, Lee, Son and co-workers introduced benzodifuran moieties into a microporous organic network (MON) *via* a tandem synthetic method involving Sonogashira coupling of 2,5-diiodo-1,4-hydroquinone and 1,3,5-triethynylbenzene through intramolecular cyclization.[361] The resultant benzodifuran-introduced MONs exhibited excellent photocatalytic activities toward oxidative transformation of primary amines into imines. In 2015, Cooper and co-workers reported a general approach to synthesize a family of fifteen pyrene-based CMPs using Suzuki–Miyaura polycondensation of 1,4-benzene diboronic acid, and/or 1,2,4,5-tetrabromobenzene, and/or 1,3,6,8-tetraboronic pinacol ester of pyrene and/or 1,3,6,8-tetrabromopyrene.[362] The CMPs were synthesized with tunable optical and electronic properties through statistical copolymerization. Further, these polymer networks were found to show very good performance toward photocatalytic production of hydrogen from water, even without the addition of any photosensitizers or metal cocatalysts. The next year, Yu and co-workers came up with a series of rationally designed porous conjugated polymers (PCPs) featuring various transition metal binding bipyridyl sites and light harvesting chromophores which can exhibit efficient photocatalytic hydrogen generation from water splitting.[363] The combined merits of local ordered structure, improved light absorption and charge separation process, better wettability, *etc.* culminated in enhanced photocatalytic activity. In 2016, Wang and co-workers reported a molecular structure design method of electron donor–acceptor conjugated polymers of polybenzothiadiazoles, having an appropriate energy band and good charge separation and charge transfer abilities for visible light driven H_2 evolution.[364]

In an interesting work, a family of metal-free 9,9′-bifluorenylidene-based CMPs, namely Py-BF-CMP and TPA-BF-CMP, were synthesized *via* Suzuki polycondensation.[365] Extended conjugation and the favourable electron-donation between the bifluorenylidene (BF) and pyrene (Py) moieties resulted in the lowest band gap for Py-BF-CMP. Furthermore, among all the BF-CMPs, Py-BF-CMP exhibited the highest photocatalytic degradation activity toward RhB (81% RhB degradation within 30 mins) which is correlated with the synergistic contribution of the high surface area (1306 $m^2\ g^{-1}$) and the narrowest bandgap (1.55 eV) of Py-BF-CMP. Further, $^{\bullet}O_2^-$ was found to be the main active species responsible for the degradation of RhB. Ma, Vilela, Zhang and co-workers reported a series of well-dispersible CMP NPs, namely B-$FL_{3\text{-a}}$, B-$BPh_{3\text{-a}}$, B-$BT_{3\text{-a}}$, B-$FL_{3\text{-b}}$, B-$BPh_{3\text{-b}}$ and B-$BT_{3\text{-b}}$, featuring different bandgaps.[366] The morphologies of the CMP NPs were found to be tunable (nanorod, nanosphere, nanoring) *via* tuning the donor–acceptor combination. Among the synthesized CMPs, B-$BT_{3\text{-b}}$ fabricated from 1,3,5-triethynylbenzene and 4,7-dibromobenzo[*c*]-1,2,5-thiadiazole exhibited the best catalytic degradation activity toward Rhodamine B (RhB) in water. In an interesting work, Verpoort and co-workers synthesized two low-density hierarchical POPs with semiconducting properties *via* Sonogashira–Hagihara cross-coupling of 1,4-diethynylbenzene with 1,3,5-bromobenzene (POP-1) and 1,2-bis(3,5-dibromophenyl)diazene (POP-2).[367] Further, both the POPs showed excellent photo-degradation activity toward different kinds of organic pollutants such as RhB, MB, azo based dyes (methyl orange and Congo red) and also a mixture of MO and MB. In-depth studies revealed the *in situ* generation of both $^1O_2$ and $O_2^{\bullet-}$ for POP-1 which play a prime role in such catalytic activity. Interestingly, POP-1 was found to maintain its catalytic performance toward RhB, MO, MB and CR even under natural sunlight.

6.4.4 Post-synthetic modification (PSM) of porous polymers with catalytic moieties. Post-synthetic modification methods allow made-to-order synthesis of diverse POP-based catalytically active materials for any desired applications. Considering both the pre-arranged network porosity and the immobilizable catalytic functionality, the pre-synthetic strategy can be restricted in some cases for preparation of POP-based catalysts with different catalytic moieties. Hence, PSM-based methods have emerged as the alternative method for exploration of various POP-based catalysts. The PSM methods allow inclusion of active metal sites *via* modulating the organic linkers with organocatalytic units, the introduction of organic linkers, and encapsulation of the catalytic moieties inside the pore. In 2012, Tan, Li and co-workers presented a ''knitting'' method, in which PPh_3 and benzene were knitted to yield triphenylphosphine functionalized KAPs(Ph-PPh_3) (Fig. 20a).[368] This strategy allowed binding of Pd^{II} with PPh_3 groups to produce palladium-phosphine-based heterogeneous catalysts, namely KAPs(Ph-PPh_3)-Pd. The resultant catalysts were found

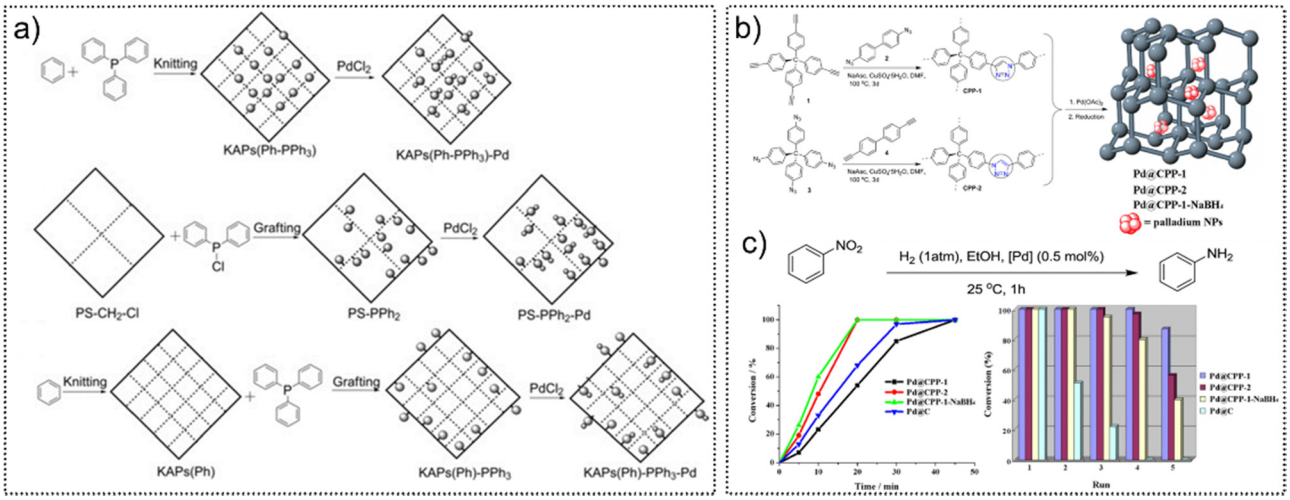

Fig. 20 (a) Synthetic route to KAPs(Ph-PPh 3)-Pd, PS-PPh 2-Pd and, KAPs(Ph)-PPh 3-Pd. Reproduced with permission from ref. 368. Copyright 2012, Wiley-VCH. (b) Synthesis of CPP-1 and CPP-2 and the schematic illustration of Pd@CPP. (c) Conversion of nitrobenzene as a function of time in hydrogenation reactions and reusability of Pd@CPP-1, Pd@CPP-2, Pd@CPP-1-NaBH4, and Pd@C. Reproduced with permission from ref. 370. Copyright 2014, American Chemical Society.

to show excellent selective activity toward the Suzuki–Miyaura cross-coupling reaction of aryl chlorides. In 2016, Xiao and co-workers presented a facile and general strategy to fabricate a family of insoluble porous organic ligands through free radical polymerization of vinyl-functionalized diphosphine monomers followed by synthesis of diphosphine-based POPs.[369] Furthermore, metalation of these polymers with Rh resulted in the formation of Rh/POLs catalysts. The Rh/POLs catalysts were found to show high catalytic activity as well as chemo/regio-selectivity toward hydroformylation of olefins with enhanced stability and recyclability. In an early work, Wang and co-workers demonstrated the design and synthesis of two POPs, namely CPP-1 and CPP-2, based on "click chemistry" (Fig. 20b).[370] Further, CPP-1 and CPP-2 were utilized as hosts for post-synthesis metalation of ultrafine Pd-nanoparticles with uniform distributions. The prepared Pd@CPP catalysts exhibited excellent catalytic activity toward hydrogenation of nitroarenes at 25 °C under 1 atm (Fig. 20c). A novel class of yolk–shell structured periodic mesoporous polymer nanoparticles were successfully developed by Wu and co-workers in 2016.[371] The Au yolks were found to be homogeneously encapsulated in the ordered polymeric mesoporous shells *via* a reactive interface-guided co-assembly. Owing to their ordered mesoporous channels, they allowed fast mobilization of the reactants and revealed excellent catalytic reduction performance toward nitroaromatic compounds such as 4-nitrophenol and nitrobenzene. The hydrophobic polymeric shells allowed favourable diffusion of hydrophobic nitrobenzene molecules, imparting selectivity in catalytic reaction over 4-nitrophenol. For a summary of cycloaddition of epoxides with CO_2 by POP-based materials see Table S7 (ESI†).

7. Concluding remarks and future outlook

Porous organic polymers are an excellent example of materials having the combined merits of tunable porous structures and controlled surface chemistry. These materials have been found to offer diverse admirable properties and have received a great deal of attention for use in environmental remediation applications, including toxic gas adsorption/separation, chemical sensing, wastewater treatment, and heterogeneous catalysis. The incorporation of functional groups within POPs enhances their selectivity and affinity towards specific contaminants, facilitating targeted remediation strategies. Recent scientific advancements have demonstrated that amorphous porous organic polymers that can be synthesized *via* relatively easy, facile and scalable synthetic methods can be used as versatile platforms for task-specific real-world applications with distinctive characteristics and excellent performances. These innovative insights into POP-based environmental remediation provide a viable means of tackling pollution-related problems and opening the door to a more sustainable future. As an outcome, various POPs with tunable porosity, diverse topologies and morphologies, as well as adaptable compositions and functions have been successfully produced (Scheme 5). In this Review, we have provided an overview of current developments in POP materials from the standpoint of material design, synthetic methods, and chemical reactions involved in the creation of POPs, and state-of-the-art characterization for potential application in the field of environmental remediation, which may be primarily summarized as follows.

(i) For effective gas adsorption/separation/storage applications, POPs with tunable pore architectures, controllable components and suitable functionality have been designed and tailored. (ii) In the case of environmentally toxic chemical sensing application, as hosts for the designability and inclusion of highly active components, POPs with built-in open nanopores and voids enable the transit of active analytes. Moreover, the added advantage of heterogeneous nature of POPs provide easy recyclable detection of targeted pollutants in water and convenient recovery of the material. (iii) The development of task-specific POPs by utilizing versatile covalent chemistry *via*

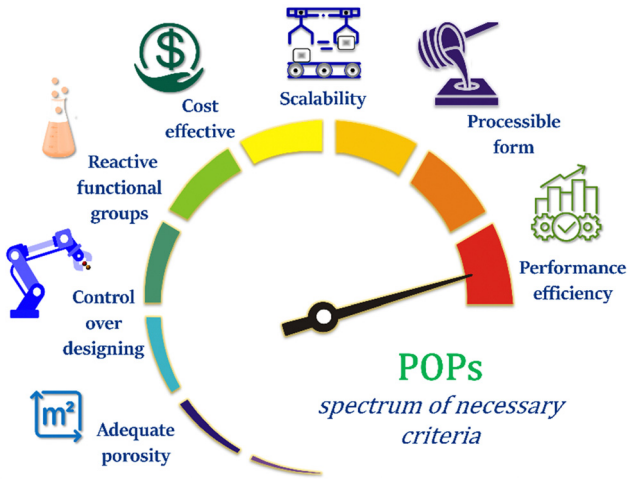

Scheme 5 Spectrum of qualifying criteria in POPs, paving routes to environmental remediation. The mark indicated refers to an ideal situation where all seven standards are met by the POPs, through various environmental remediation applications.

post- or pre-synthetic modification of the functional elements in POPs. The tailored pore structures combined with greatly increased affinities toward guest molecules produce synergistic effects for improved performances in environmental remediation such as toxic gas or pollutant separation and identification. (iv) For successful use in pollutant separation, POPs with customized pore architectures, controlled surface functions, and altered structural stiffness have been investigated. The targeted molecules can enter and pass through the apertures due to the size sieving effect, dynamic surface hydrophilic or hydrophobic effects, and distinctive stiff architectures, which endows them with exceptional pollutant separation performances. (v) For environment related heterogeneous catalysts, the two major methods for creating POP-based highly efficient catalysts are thought to be pre-synthetic modification using building blocks integrated with catalytic sites and post-synthetic modification of polymers with catalytic moieties. The numerous environmental applications of POPs have significantly advanced the field of their use.

Despite the exceptional accomplishments that have been made in the field of POP development and their promising utility in environmental remediation, there are still many challenges that need to be addressed. These issues associated with insight chemistry of POPs are described below: (i) In the case of developing functional POPs *via* post-synthetic modification, POPs invariably experience compromised surface areas as a result of pore blockage. The distribution of active sites with good porosity while keeping several particular components is still a significant problem in the exploration of multifunctional POPs. In this context, when specific applications are required, porous polymer structures can be strategically designed using the knowledge amassed by examining the relationships between porous structure, functionality, and performance. (ii) The chemical and physical stability of POPs under extreme conditions is another challenge that remains to be clarified. High stability may be bequeathed by the high friction of the POP-producing reactants. (iii) The molecular level fine design of POPs is an evolving process, and the computational prediction for the creation of novel POPs is an ongoing issue. (iv) While talking about POP-based environmental remediation application, parameters such as diffusion kinetics, sorption capacity, recognition sensitivity, molecular sieving, and heterogeneous catalysis efficiency are highly related with enthalpy of adsorption, a significant thermodynamic parameter, which should be properly investigated. (v) The system testing circumstances for porous polymers are not representative of real-world application environments, which could be a severe obstacle to the development of their significant capability. (vi) Most importantly, the industrial application of laboratory-tested high-performance POP materials should be pursued with continuing diligence. The commercial achievements of numerous well-known polymer materials, including polymeric separation membranes, and ion exchange and adsorption resins, provide a wealth of experience and knowledge in this area.

Future industrial applications should give careful consideration to low-cost sustainable raw materials including monomers, cross-linkers, solvents, catalysts, simple reaction processes that enable large scale production, and effective material processing techniques. It is important to highlight the value of successfully utilizing the special synthesis and processability aspects of POPs. Interface polymerization of monomers on porous supports is one of the solutions as it provides easy and scale-up development of nano-filtration membranes. Many required macroscopic forms, including membranes, fibres, and monoliths, can be easily manufactured from certain particular soluble porous polymers, such as PIMs. On the other hand, POPs such as HCPs, CMPs, and PAFs are frequently found as intrinsically brittle and powder forms, which restrict their processability into various aforementioned robust devices. This seriously limits their large-scale real-time applications. In this context, significant efforts may be undertaken to build processable composites of these porous polymers.

The facts discussed in this review only scratch the surface of chemistry involved in porous organic polymers and their potential applications in environmental remediation. With the contributions of scientists and researchers from several disciplines, including chemistry, materials science, physics, engineering and environmental science, this demanding sector is becoming more multidisciplinary. Constructive interactions between such diverse disciplines are indeed to facilitate the further advancement in the domain of POPs.

Conflicts of interest

There are no conflicts to declare.

Acknowledgements

S. F. acknowledges the DST-Inspire fellowship (DST/INSPIRE/03/2016/001694). S. D. is thankful to IISER Pune for the fellowships. S. K. G. thanks SERB (Project No. CRG/2022/001090) for funding.

Notes and references

1 Resolution A/RES/64/292; United Nations General Assembly, July 2010.
2 World Population Prospects: The 2015 Revision, Methodology of the United Nations Population Estimates and Projections; Working Paper No. ESA/P/WP.242; Department of Economic and Social Affairs, Population Division, United Nations, 2015.
3 P. J. J. Alvarez, C. K. Chan, M. Elimelech, N. J. Halas and D. Villagrán, *Nat. Nanotechnol.*, 2018, **13**, 634–641.
4 D.-H. Yang, Y. Tao, X. Ding and B.-H. Han, *Chem. Soc. Rev.*, 2022, **51**, 761–791.
5 M. K. Debe, *Nature*, 2012, **486**, 43–51.
6 J. Wu, F. Xu, S. Li, P. Ma, X. Zhang, Q. Liu, R. Fu and D. Wu, *Adv. Mater.*, 2019, **31**, 1802922.
7 D. Wu, F. Xu, B. Sun, R. Fu, H. He and K. Matyjaszewski, *Chem. Rev.*, 2012, **112**, 3959–4015.
8 *Metal–organic frameworks (MOFs) for environmental applications*, ed. S. K. Ghosh, Elsevier, 1st edn, 2019, DOI: **10.1016/C2017-0-01721-4**.
9 J. K. Sun and Q. Xu, *Energy Environ. Sci.*, 2014, **7**, 2071–2100.
10 A. G. Slater and A. I. Cooper, *Science*, 2015, **348**, aaa8075.
11 S. R. Batten, N. R. Champness, X.-M. Chen, J. Garcia-Martinez, S. Kitagawa, L. Ohrstrom, M. O'Keeffe, M. Paik Suh and J. Reedijk, *Pure Appl. Chem.*, 2013, **85**, 1715–1724.
12 S. Dutta, Y. D. More, S. Fajal, W. Mandal, G. K. Dam and S. K. Ghosh, *Chem. Commun.*, 2022, **58**, 13676–13698.
13 H. Furukawa, K. E. Cordova, M. O'Keeffe and O. M. Yaghi, *Science*, 2013, **341**, 1230444.
14 M. S. Lohse and T. Bein, *Adv. Funct. Mater.*, 2018, **28**, 1705553.
15 P. Kaur, J. T. Hupp and S. T. Nguyen, *ACS Catal.*, 2011, **1**, 819–835.
16 M. G. Mohamed, A. F. M. EL-Mahdy, M. G. Kotp and S.-W. Kuo, *Mater. Adv.*, 2022, **3**, 707–733.
17 S. Das, P. Heasman, T. Ben and S. Qiu, *Chem. Rev.*, 2017, **117**, 1515–1563.
18 A. Trewin and A. I. Cooper, *Angew. Chem., Int. Ed.*, 2010, **49**, 1533–1535.
19 Q. Sun, Z. Dai, X. Meng and F.-S. Xiao, *Chem. Soc. Rev.*, 2015, **44**, 6018–6034.
20 D. Luo, M. Li, Q. Ma, G. Wen, H. Dou, B. Ren, Y. Liu, X. Wang, L. Shui and Z. Chen, *Chem. Soc. Rev.*, 2022, **51**, 2917–2938.
21 J. H. Kim, D. W. Kang, H. Yun, M. Kang, N. Singh, J. S. Kim and C. S. Hong, *Chem. Soc. Rev.*, 2022, **51**, 43–56.
22 T. Zhou, X. Huang, N. Ding, Z. Lin, Y. Yao and J. Guo, *Chem. Soc. Rev.*, 2022, **51**, 237–267.
23 L. Tan and B. Tan, *Chem. Soc. Rev.*, 2017, **46**, 3322–3356.
24 A. B. Soliman, M. H. Hassan, A. A. Abugable, S. G. Karakalos and M. H. Alkordi, *ChemCatChem*, 2017, **9**, 2946–2951.
25 P. Samanta, A. V. Desai, S. Let and S. K. Ghosh, *ACS Sustainable Chem. Eng.*, 2019, **7**, 7456–7478.
26 N. Singh, S. Son, J. An, I. Kim, M. Choi, N. Kong, W. Tao and J. S. Kim, *Chem. Soc. Rev.*, 2021, **50**, 12883–12896.
27 Y. Tang, A. Varyambath, Y. Ding, B. Chen, X. Huang, Y. Zhang, D.-G. Yu, I. Kim and W. Song, *Biomater. Sci.*, 2022, **10**, 5369–5390.
28 S. Let, G. K. Dam, P. Samanta, S. Fajal, S. Dutta and S. K. Ghosh, *J. Org. Chem.*, 2022, **87**(24), 16655–16664.
29 K. S. Song, P. W. Fritz and A. Coskun, *Chem. Soc. Rev.*, 2022, **51**, 9831–9852.
30 L. Zou, Y. Sun, S. Che, X. Yang, X. Wang, M. Bosch, Q. Wang, H. Li, M. Smith, S. Yuan, Z. Perry and H.-C. Zhou, *Adv. Mater.*, 2017, **29**, 1700229.
31 J. S. M. Lee and A. I. Cooper, *Chem. Rev.*, 2020, **120**, 2171–2214.
32 J.-X. Jiang, F. Su, A. Trewin, C. D. Wood, N. L. Campbell, H. Niu, C. Dickinson, A. Y. Ganin, M. J. Rosseinsky, Y. Z. Khimyak and A. I. Cooper, *Angew. Chem., Int. Ed.*, 2007, **46**, 8574–8578.
33 S. Xu, Y. Luo and B. Tan, *Macromol. Rapid Commun.*, 2013, **34**, 471–484.
34 K. Konstas, J. W. Taylor, A. W. Thornton, C. M. Doherty, W. X. Lim, T. J. Bastow, D. F. Kennedy, C. D. Wood, B. J. Cox, J. M. Hill, A. J. Hill and M. R. Hill, *Angew. Chem., Int. Ed.*, 2012, **51**, 6639–6642.
35 Q. Sun, B. Aguila, J. Perman, L. D. Earl, C. W. Abney, Y. Cheng, H. WeiII, N. Nguyen, L. Wojtas and S. Ma, *J. Am. Chem. Soc.*, 2017, **139**(7), 2786–2793.
36 P. Kuhn, M. Antonietti and A. Thomas, *Angew. Chem., Int. Ed.*, 2008, **47**, 3450–3453.
37 S. Ren, M. J. Bojdys, R. Dawson, A. Laybourn, Y. Z. Khimyak, D. J. Adams and A. I. Cooper, *Adv. Mater.*, 2012, **24**, 2357–2361.
38 T. Ben, H. Ren, S. Ma, D. Cao, J. Lan, X. Jing, W. Wang, J. Xu, F. Deng and J. M. Simmons, *Angew. Chem., Int. Ed.*, 2009, **48**, 9457–9460.
39 A. Sen, S. Dutta, G. K. Dam, P. Samanta, S. Let, S. Sharma, M. M. Shirolkar and S. K. Ghosh, *Chem. – Eur. J.*, 2021, **27**, 13442–13449.
40 Y. Xu, S. Jin, H. Xu, A. Nagai and D. Jiang, *Chem. Soc. Rev.*, 2013, **42**, 8012–8031.
41 R. T. Woodward, L. A. Stevens, R. Dawson, M. Vijayaraghavan, T. Hasell, I. P. Silverwood, A. V. Ewing, T. Ratvijitvech, J. D. Exley, S. Y. Chong, F. Blanc, D. J. Adams, S. G. Kazarian, C. E. Snape, T. C. Drage and A. I. Cooper, *J. Am. Chem. Soc.*, 2014, **136**, 9028–9035.
42 C. D. Wood, B. Tan, A. Trewin, F. Su, M. J. Rosseinsky, D. Bradshaw, Y. Sun, L. Zhou and A. I. Cooper, *Adv. Mater.*, 2008, **20**, 1916–1921.
43 V. A. Davankov, S. V. Rogozhin and M. P. Tsyurupa, *USSR Pat.*, 299165, 1969, *US Pat.*, 3729457, 1971; *Chem. Abstr.*, 1971, **75**, 6841B.
44 V. A. Davankov, S. V. Rogoshin and M. P. Tsyurupa, *J. Polym. Sci., Polym. Symp.*, 1974, **47**, 95–101.
45 V. A. Davankov, M. M. Ilyin, M. P. Tsyurupa, G. I. Timofeeva and L. V. Dubrovina, *Macromolecules*, 1996, **29**, 8398–8403.
46 R. Joseph, W. T. Ford, S. Zhang, M. P. Tsyurupa, A. V. Pastukhov and V. A. Davankov, *J. Polym. Sci., Part A: Polym. Chem.*, 1997, **35**, 695–701.

47 J.-H. Ahn, J.-E. Jang, C.-G. Oh, S.-K. Ihm, J. Cortez and D. C. Sherrington, *Macromolecules*, 2006, **39**, 627–632.
48 B. Li, R. Gong, Y. Luo and B. Tan, *Soft Matter*, 2011, **7**, 10910–10916.
49 B. Li, X. Huang, R. Gong, M. Ma, X. Yang, L. Liang and B. Tan, *Int. J. Hydrogen Energy*, 2012, **37**, 12813–12820.
50 N. B. McKeown, H. Li and S. Makhseed, *In Supported Catalysts and Their Applications*, ed. D. C. Sherrington and A. P. Kybett, RSC Publishing, Cambridge, UK, 2001, pp. 214–217.
51 N. B. McKeown, *ISRN Mater. Sci.*, 2012, **2012**, 1.
52 N. B. McKeown, S. Makhseed and P. M. Budd, *Chem. Commun.*, 2002, 2780–2781.
53 N. B. McKeown, S. Hanif, K. Msayib, C. E. Tattershall and P. M. Budd, *Chem. Commun.*, 2002, 2782–2783.
54 P. M. Budd, B. S. Ghanem, S. Makhseed, N. B. McKeown, K. J. Msayib and C. E. Tattershall, *Chem. Commun.*, 2004, 230–231.
55 B. S. Ghanem, K. Msayib, N. B. McKeown, K. D. M. Harris, Z. Pan, P. M. Budd, A. Butler, J. Selbie, D. Book and A. Walton, *Chem. Commun.*, 2007, 67–69.
56 P. Zhang, X. Jiang, S. Wan and S. Dai, *J. Mater. Chem. A*, 2015, **3**, 6739–6741.
57 P. Zhang, X. Jiang, S. Wan and S. Dai, *Chem. – Eur. J.*, 2015, **21**, 12866–12870.
58 J.-X. Jiang, F. Su, A. Trewin, C. D. Wood, H. Niu, J. T. A. Jones, Y. Z. Khimyak and A. I. Cooper, *J. Am. Chem. Soc.*, 2008, **130**, 7710–7720.
59 A. I. Cooper, *Adv. Mater.*, 2009, **21**, 1291–1295.
60 J.-X. Jiang, A. Trewin, D. J. Adams and A. I. Cooper, *Chem. Sci.*, 2011, **2**, 1777–1781.
61 J. R. Holst, E. Stöckel, D. J. Adams and A. I. Cooper, *Macromolecules*, 2010, **43**, 8531–8538.
62 W. Chaikittisilp, A. Sugawara, A. Shimojima and T. Okubo, *Chem. – Eur. J.*, 2010, **16**, 6006–6014.
63 Q. Chen, M. Luo, T. Wang, J.-X. Wang, D. Zhou, Y. Han, C.-S. Zhang, C.-G. Yan and B.-H. Han, *Macromolecules*, 2011, **44**, 5573–5577.
64 A. Li, R.-F. Lu, Y. Wang, X. Wang, K.-L. Han and W.-Q. Deng, *Angew. Chem., Int. Ed.*, 2010, **49**, 3330–3333.
65 R. Dawson, D. J. Adams and A. I. Cooper, *Chem. Sci.*, 2011, **2**, 1173–1177.
66 T. J. Mooibroek and P. Gamez, *Inorg. Chim. Acta*, 2007, **360**, 381–404.
67 P. Katekomol, J. Roeser, M. Bojdys, J. Weber and A. Thomas, *Chem. Mater.*, 2013, **25**, 1542–1548.
68 T. Ben and S. Qiu, *CrystEngComm*, 2013, **15**, 17–26.
69 Y. Tian and G. Zhu, *Chem. Rev.*, 2020, **120**, 8934–8986.
70 T. Ben, C. Pei, D. Zhang, J. Xu, F. Deng, X. Jing and S. Qiu, *Energy Environ. Sci.*, 2011, **4**, 3991–3999.
71 D. Yuan, W. Lu, D. Zhao and H.-C. Zhou, *Adv. Mater.*, 2011, **23**, 3723–3725.
72 C. Baerlocher, L. B. McCusker and D. H. Olson, *Atlas of Zeolite Framework Types*, Elsevier, The Netherlands, 2007, pp. 194–195.
73 Y. Yuan, P. Cui, Y. Tian, X. Zou, Y. Zhou, F. Sun and G. Zhu, *Chem. Sci.*, 2016, **7**, 3751–3756.
74 X. Zhuang, F. Zhang, D. Wu, N. Forler, H. Liang, M. Wagner, D. Gehrig, M. R. Hansen, F. Laquai and X. Feng, *Angew. Chem., Int. Ed.*, 2013, **52**, 9668–9672.
75 N. Wan, Q. Chang, F. Hou, J. Li, X. Zang, S. Zhang, C. Wang and Z. Wang, *Anal. Chim. Acta*, 2022, **1195**, 339458.
76 W. Mandal, S. Fajal, S. Mollick, M. M. Shirolkar, Y. D. More, S. Saurabh, D. Mahato and S. K. Ghosh, *ACS Appl. Mater. Interfaces*, 2022, **14**(17), 20042–20052.
77 P. Samanta, A. V. Desai, B. Anothumakkool, M. M. Shirolkar, A. Karmakar, S. Kurungot and S. K. Ghosh, *J. Mater. Chem. A*, 2017, **5**, 13659–13664.
78 N. Wan, Q. Chang, F. Hou, S. Zhang, X. Zang, X. Zhao, C. Wang, Z. Wang and Y. Yamauchi, *Chem. Mater.*, 2022, **34**, 7598–7619.
79 M. S. Lohse and T. Bein, *Adv. Funct. Mater.*, 2018, **28**, 1705553.
80 O. Buyukcakir, S. H. Je, S. N. Talapaneni, D. Kim and A. Coskun, *ACS Appl. Mater. Interfaces*, 2017, **9**, 7209–7216.
81 J. Kim, C. M. Moisanu, C. N. Gannett, A. Halder, J. J. Fuentes-Rivera, S. H. Majer, K. M. Lancaster, A. C. Forse, H. D. Abruna and P. J. Milner, *Chem. Mater.*, 2021, **33**(21), 8334–8342.
82 E. Troschke, S. Gratz, T. Lubken and L. Borchardt, *Angew. Chem., Int. Ed.*, 2017, **56**, 6859–6863.
83 G. Das, Ti Skorjanc, S. K. Sharma, F. Gandara, M. Lusi, D. S. Rao, S. Vimala, S. K. Prasad, J. Raya, D. S. Han, R. Jagannathan, J. Olsen and A. Trabolsi, *J. Am. Chem. Soc.*, 2017, **139**, 9558–9565.
84 S. Chai, N. Hu, Y. Han, X. Zhang, Z. Yang, L. Wei and H. Wei, *RSC Adv.*, 2016, **6**, 49425–49428.
85 X. Cui, Y. Li, W. Dong, D. Liu and Q. Duan, *React. Funct. Polym.*, 2020, **154**, 104633.
86 F.-Y. Zhang, M. Hong, Z. Liu, H.-Y. Yu, C.-Y. Qin, B.-B. Liu and Y.-X. Li, *ChemistrySelect*, 2019, **4**, 12719–12725.
87 H. Zhang, Y. Zhang, C. Gu and Y. Ma, *Adv. Energy Mater.*, 2015, **5**, 1402075.
88 H. Liu, Y. Wang, W. Mo, H. Tang, Z. Cheng, Y. Chen, S. Zhang, H. Ma, B. Li and X. Li, *Adv. Funct. Mater.*, 2020, **30**, 1910275.
89 Z. Zhou, D. Guo, D. B. Shinde, L. Cao, Z. Li, X. Li, D. Lu and Z. Lai, *ACS Nano*, 2021, **15**, 11970–11980.
90 Y. Tao, T.-X. Wang, X. Ding and B.-H. Han, *Macromolecules*, 2022, **55**(18), 8365–8371.
91 F. Vilela, K. Zhang and M. Antonietti, *Energy Environ. Sci.*, 2012, **5**, 7819–7832.
92 Z. Li, H. Li, H. Xia, X. Ding, X. Luo, X. Liu and Y. Mu, *Chem. – Eur. J.*, 2015, **21**, 17355–17362.
93 M. Xu, X. Han, T. Wang, S. Li and D. Hua, *J. Mater. Chem. A*, 2018, **6**, 13894–13900.
94 G. Cheng, T. Hasell, A. Trewin, D. J. Adams and A. I. Cooper, *Angew. Chem., Int. Ed.*, 2012, **51**, 12727–12731.
95 K. Sonogashira, Y. Tohda and N. Hagihara, *Tetrahedron Lett.*, 1975, **16**, 4467–4470.
96 H. Li, B. Xu, X. Liu, A. Sigen, C. He, H. Xia and Y. Mu, *J. Mater. Chem. A*, 2013, **1**, 14108–14114.
97 G. Ji, Z. Yang, Y. Zhao, H. Zhang, B. Yu, J. Xu, H. Xu and Z. Liu, *Chem. Commun.*, 2015, **51**, 7352–7355.

98 M. Xu, T. Wang, P. Gao, L. Zhao, L. Zhou and D. Hua, *J. Mater. Chem. A*, 2019, **7**, 11214–11222.
99 H. P. Ma, H. Ren, X. Q. Zou, F. X. Sun, Z. J. Yan, K. Cai, D. Y. Wang and G. S. Zhu, *J. Mater. Chem. A*, 2013, **1**, 752–758.
100 J.-X. Jiang, F. Su, H. Niu, C. D. Wood, N. L. Campbell, Y. Z. Khimyak and A. I. Cooper, *Chem. Commun.*, 2008, 486–488.
101 J. Schmidt, M. Werner and A. Thomas, *Macromolecules*, 2009, **42**, 4426–4429.
102 K. Yuan, P. Guo-Wang, T. Hu, L. Shi, R. Zeng, M. Förster, T. Pichler, Y. Chen and U. Scherf, *Chem. Mater.*, 2015, **27**, 7403–7411.
103 L. Li, H. Ren, Y. Yuan, G. Yu and G. Zhu, *J. Mater. Chem. A*, 2014, **2**, 11091–11098.
104 S. Zhang, Q. Yang, C. Wang, X. Luo, J. Kim, Z. Wang and Y. Yamauchi, *Adv. Sci.*, 2018, **5**, 1801116.
105 Y. Guo, R. Ma, W. Liu, L. Hao, Q. Wu and Z. Wang, *J. Chromatogr. A*, 2020, **1622**, 461131.
106 R. Yu, L. Liu, L. Yin, Y. Jing, N. Zhang, H. Bian and G. Zhu, *Chem. Sci.*, 2023, **14**, 3782–3788.
107 Y. Yuan and G. Zhu, *ACS Cent. Sci.*, 2019, **5**, 409–418.
108 Y. Liu, Z. Liao, X. Ma and Z. Xiang, *ACS Appl. Mater. Interfaces*, 2018, **10**(36), 30698–30705.
109 L. Sun, Z. Liang, J. Yu and R. Xu, *Polym. Chem.*, 2013, **4**, 1932–1938.
110 J.-J. Chen, T.-L. Zhai, Y.-F. Chen, S. Geng, C. Yu, J.-M. Liu, L. Wang, B. Tan and C. Zhang, *Polym. Chem.*, 2017, **8**, 5533–5538.
111 R. N. Kumar, P. Das, R. A. Agrawal, K. S. Mandal and S. S. Zade, *Mater. Adv.*, 2021, **2**, 7473–7481.
112 Z. Xie, Y. Wei, X. Zhao, Y. Li, S. Ding and L. Chen, *Mater. Chem. Front.*, 2017, **1**, 867–872.
113 Y. Liao, Z. Cheng, W. Zuo, A. Thomas and C. F. J. Faul, *ACS Appl. Mater. Interfaces*, 2017, **9**, 38390–38400.
114 Y. Zhang, S. A. Y. Zou, X. Luo, Z. Li, H. Xia, X. Liu and Y. Mu, *J. Mater. Chem. A*, 2014, **2**, 13422–13430.
115 T. Geng, S. Ye, Z. Zhu and W. Zhang, *J. Mater. Chem. A*, 2018, **6**, 2808–2816.
116 T. Geng, W. Zhang, Z. Zhu and X. Kai, *Microporous Mesoporous Mater.*, 2019, **273**, 163–170.
117 X. Jing, D. Zou, P. Cui, H. Ren and G. Zhu, *J. Mater. Chem. A*, 2013, **1**, 13926–13931.
118 Y. Liao, H. Wang, M. Zhu and A. Thomas, *Adv. Mater.*, 2018, **30**, 1705710.
119 X. Qian, B. Wang, Z.-Q. Zhu, H.-X. Sun, F. Ren, P. Mu, C. Ma, W.-D. Liang and A. Li, *J. Hazard. Mater.*, 2017, **338**, 224–232.
120 M. Rose, N. Klein, I. Senkovska, C. Schrage, P. Wollmann, W. Bohlmann, B. Bohringer, S. Fichtner and S. Kaskel, *J. Mater. Chem.*, 2011, **21**, 711–716.
121 H. Bohra, P. Z. Li, C. J. Yang, Y. L. Zhao and M. F. Wang, *Polym. Chem.*, 2018, **9**, 1972–1982.
122 S.-Y. Yu, J. Mahmood, H.-J. Noh, J.-M. Seo, S.-M. Jung, S.-H. Shin, Y.-K. Im, I.-Y. Jeon and J.-B. Baek, *Angew. Chem., Int. Ed.*, 2018, **57**, 8438–8442.
123 P. Pandey, A. P. Katsoulidis, I. Eryazici, Y. Wu, M. G. Kanatzidis and S. B. T. Nguyen, *Chem. Mater.*, 2010, **22**(17), 4974–4979.
124 M. A. Sabri, M. H. Al-Sayah, S. Sen, T. H. Ibrahim and O. M. El-Kadri, *Sci. Rep.*, 2020, **10**, 15943.
125 M. Shunmughanathan, N. Madankumar and K. Pitchumani, *ChemistrySelect*, 2018, **3**, 13743–13750.
126 X. Ding and B.-H. Han, *Angew. Chem., Int. Ed.*, 2015, **54**, 6536–6539.
127 Z.-H. Guo, C. Wang, Q. Zhang, S. Che, H.-C. Zhou and L. Fang, *Mater. Chem. Front.*, 2018, **2**, 396–401.
128 Y.-C. Zhao, D. Zhou, Q. Chen, X.-J. Zhang, N. Bian, A.-D. Qi and B.-H. Han, *Macromolecules*, 2011, **44**(16), 6382–6388.
129 H. Lyu, C. S. Diercks, C. Zhu and O. M. Yaghi, *J. Am. Chem. Soc.*, 2019, **1**, 6848–6852.
130 X. Li, Y. Zou, Z. Jia, J. Zhang, Y. Li, X. Guo, M. Zhang, K. Li, J. Li and L. Ma, *J. Hazard. Mater.*, 2021, **401**, 123802.
131 X. Zhuang, W. Zhao, F. Zhang, Y. Cao, F. Liu, S. Bi and X. Feng, *Polym. Chem.*, 2016, **7**, 4176–4181.
132 R. Hu, M. Hassan, L. Liu, S. Zhang and W. Gong, *Chin. Chem. Lett.*, 2023, **34**, 107541.
133 A. B. Marco, D. Cortizo-Lacalle, I. Perez-Miqueo, G. Valenti, A. Boni, J. Plas, K. Strutynski, S. D. Feyter, F. Paolucci, M. Montes, A. N. Khlobystov, M. Melle-Franco and A. Mateo-Alonso, *Angew. Chem., Int. Ed.*, 2017, **56**, 6946–6951.
134 M. G. Rabbani and H. M. El-Kaderi, *Chem. Mater.*, 2011, **23**, 1650–1653.
135 H. Zhou, B. Zhou, C. Fu, Z. Wu, C. Wang, Y. Ding, B.-H. Han and A. Hu, *Macromolecules*, 2019, **52**, 3935–3941.
136 G. Lu, H. Yang, Y. Zhu, T. Huggins, Z. J. Ren, Z. Liu and W. Zhang, *J. Mater. Chem. A*, 2015, **3**, 4954–4959.
137 P. Samanta, P. Chandra, S. Dutta, A. Desai and S. K. Ghosh, *Chem. Sci.*, 2018, **9**, 7874–7881.
138 Z.-J. Li, H.-D. Xue, Y.-X. Ma, Q. Zhang, Y.-C. Li, M. Xie, H.-L. Qi and X.-D. Zheng, *ACS Appl. Mater. Interfaces*, 2019, **11**(49), 46197–46204.
139 R. Dawson, F. Su, H. Niu, C. D. Wood, J. T. A. Jones, Y. Z. Khimyak and A. I. Cooper, *Macromolecules*, 2008, **41**, 1591–1593.
140 J. Germain, J. M. J. Fréchet and F. Svec, *J. Mater. Chem.*, 2007, **17**, 4989–4997.
141 J. Germain, J. M. J. Frechet and F. Svec, *Chem. Commun.*, 2009, 1526–1528.
142 Y. He, Z. Cheng, H. Zuo, C. Yan and Y. Liao, *ChemElectroChem*, 2020, **7**, 959–966.
143 H. A. Patel, S. H. Je, J. Park, D. P. Chen, Y. Jung, C. T. Yavuz and A. Coskun, *Nat. Commun.*, 2013, **4**, 1357.
144 Q. Q. Dang, X. M. Wang, Y. F. Zhan and X. M. Zhang, *Polym. Chem.*, 2016, **7**, 643–647.
145 K. Thiel, R. Zehbe, J. Roeser, P. Strauch, S. Enthaler and A. Thomas, *Polym. Chem.*, 2013, **4**, 1848–1856.
146 Y. Su, Y. Wang, X. Li, X. Li and R. Wang, *ACS Appl. Mater. Interfaces*, 2016, **8**, 18904–18911.
147 O. K. Farha, A. M. Spokoyny, B. G. Hauser, Y.-S. Bae, S. E. Brown, R. Q. Snurr, C. A. Mirkin and J. T. Hupp, *Chem. Mater.*, 2009, **21**(14), 3033–3035.
148 G. Li, B. Zhang, J. Yan and Z. Wang, *J. Mater. Chem. A*, 2016, **4**, 11453–11461.

149 P. Pandey, O. K. Farha, A. M. Spokoyny, C. A. Mirkin, M. G. Kanatzidis, J. T. Hupp and S. T. Nguyen, *J. Mater. Chem.*, 2011, **21**, 1700–1703.
150 H. Lee, H. Kim, T. J. Choi, H. W. Park and J. Y. Chang, *Chem. Commun.*, 2015, **51**, 9805–9808.
151 Y. Zhang, B. Li and S. Ma, *Chem. Commun.*, 2014, **50**, 8507–8510.
152 X. Wang, L. Xie, K. Lin, W. Ma, T. Zhao, X. Ji, M. Alyami, N. M. Khashab, H. Wang and J. L. Sessler, *Angew. Chem., Int. Ed.*, 2021, **60**, 7188–7196.
153 H. Ma, H. Ren, X. Zou, S. Meng, F. Sun and G. Zhu, *Polym. Chem.*, 2014, **5**, 144–152.
154 A. Marchetti, J. Chen, Z. Pang, S. Li, D. Ling, F. Deng and X. Kong, *Adv. Mater.*, 2017, **29**, 1605895.
155 B. Li, R. Gong, W. Wang, X. Huang, W. Zhang, H. Li, C. Hu and B. Tan, *Macromolecules*, 2011, **44**, 2410–2414.
156 L. P. Skala, A. Yang, M. J. Klemes, L. Xiao and W. R. Dichtel, *J. Am. Chem. Soc.*, 2019, **141**, 13315–13319.
157 L. Xie, Z. Zheng, Q. Lin, H. Zhou, X. Ji and J. L. Sessler, *Angew. Chem., Int. Ed.*, 2022, **61**, e202113724.
158 A. Y. Zhi, K. Li, H. Xia, M. Xue, Y. Mu and X. Liu, *J. Mater. Chem. A*, 2017, **5**, 8697–8704.
159 H. Bhambri, S. Khullar, Sakshi and S. K. Mandal, *Mater. Adv.*, 2022, **3**, 19–124.
160 T. Zhu, B. Shi, H. Wu, X. You, X. Wang, C. Fan, Q. Peng and Z. Jiang, *Ind. Eng. Chem. Res.*, 2021, **60**(17), 6337–6343.
161 S. Bandyopadhyay, A. G. Anil, A. James and A. Patra, *ACS Appl. Mater. Interfaces*, 2016, **8**(41), 27669–27678.
162 Q. Chen, M. Luo, P. Hammershoj, D. Zhou, Y. Han, B. W. Laursen, C.-G. Yan and B.-H. Han, *J. Am. Chem. Soc.*, 2012, **134**, 6084–6087.
163 Y. Liu, S. Wang, X. Meng, Y. Ye, X. Song, Z. Liang and Y. Zhao, *Angew. Chem., Int. Ed.*, 2020, **59**, 19487–19493.
164 M. Li, H. Ren, F. Sun, Y. Tian, Y. Zhu, J. Li, X. Mu, J. Xu, F. Deng and G. Zhu, *Adv. Mater.*, 2018, **30**, 1804169.
165 S. K. Das, P. Bhanja, S. K. Kundu, S. Mondal and A. Bhaumik, *ACS Appl. Mater. Interfaces*, 2018, **10**, 23813–23824.
166 K. Wang, L. Huang, S. Razzaque, S. Jin and B. Tan, *Small*, 2016, **12**(23), 3134–3142.
167 Y. Yang, B. Tan and C. D. Wood, *J. Mater. Chem. A*, 2016, **4**, 15072–15080.
168 Z.-J. Li, Q. Zhang, H.-D. Xue, X.-D. Zheng, H.-L. Qi and H.-C. Li, *Adv. Mater. Interfaces*, 2021, 2100016.
169 G. Das, T. Skorjanc, S. K. Sharma, T. Prakasam, C. Platas-Lglesias, D. S. Han, J. Raya, J.-C. Olsen, R. Jagannathan and A. Trabolsi, *ChemNanoMat*, 2018, **4**(1), 61–65.
170 A. Giri, S. Biswas, M. D. W. Hussain, T. K. Dutta and A. Patra, *ACS Appl. Mater. Interfaces*, 2022, **14**(5), 7369–7381.
171 S. Fajal, A. Hassan, W. Mandal, M. M. Shirolkar, S. Let, N. Das and S. K. Ghosh, *Angew. Chem., Int. Ed.*, 2023, **62**, e202214095.
172 Z. Wang, H. Ma, T.-L. Zhai, G. Cheng, Q. Xu, J.-M. Liu, J. Yang, Q.-M. Zhang, Q.-P. Zhang, Y.-S. Zheng, B. Tan and C. Zhang, *Adv. Sci.*, 2018, **5**, 1800141.
173 M. K. Goshisht and N. Tripathi, *J. Mater. Chem. C*, 2021, **9**, 9820–9850.
174 S. Wang, H. Li, H. Huang, X. Cao, X. Chen and D. Cao, *Chem. Soc. Rev.*, 2022, **51**, 2031–2080.
175 T. Skorjanc, D. Shetty and M. Valant, *ACS Sens.*, 2021, **6**, 1461–1481.
176 X. Sun, Y. Wang and Y. Lei, *Chem. Soc. Rev.*, 2015, **44**, 8019–8061.
177 H. S. Jung, P. Verwilst, W. Y. Kim and J. S. Kim, *Chem. Soc. Rev.*, 2016, **45**, 1242–1256.
178 B. Bonillo, R. S. Sprick and A. I. Cooper, *Chem. Mater.*, 2016, **28**, 3469–3480.
179 M. E. Germain and M. J. Knapp, *Chem. Soc. Rev.*, 2009, **38**, 2543–2555.
180 Z. Xiang and D. Cao, *Macromol. Rapid Commun.*, 2012, **33**, 1184–1190.
181 N. Sang, C. Zhan and D. Cao, *J. Mater. Chem. A*, 2015, **3**, 92–96.
182 M. Wang, H. Zhang, L. Guo and D. Cao, *Sens. Actuators, B*, 2018, **274**, 102–109.
183 A. Karmakar, A. Kumar, A. K. Chaudhari, P. Samanta, A. V. Desai, R. Krishna and S. K. Ghosh, *Chem. – Eur. J.*, 2016, **22**, 4931–4937.
184 T. Geng, W. Zhang, Z. Zhu, G. Chen, L. Ma, S. Ye and Q. Niu, *Polym. Chem.*, 2018, **9**, 777–784.
185 H. Ma, B. Li, L. Zhang, D. Han and G. Zhu, *J. Mater. Chem. A*, 2015, **3**, 19346–19352.
186 X. Liu, Y. Xu and D. Jiang, *J. Am. Chem. Soc.*, 2012, **134**, 8738–8741.
187 C. Gu, N. Huang, J. Gao, F. Xu, Y. Xu and D. Jiang, *Angew. Chem., Int. Ed.*, 2014, **53**, 4850–4855.
188 C. Gu, N. Huang, Y. Wu, H. Xu and D. Jiang, *Angew. Chem., Int. Ed.*, 2015, **54**, 11540–11544.
189 A. Palma-Cando, D. Woitassek, G. Brunklaus and U. Scherf, *Mater. Chem. Front.*, 2017, **1**, 1118–1124.
190 A. Raupke, A. Palma-Cando, E. Shkura, P. Teckhausen, A. Polywka, P. Gorrn, U. Scherf and T. Riedl, *Sci. Rep.*, 2016, **6**, 29118.
191 Y. Fan, S. Liu, Y. Yi, H. Rong and J. Zhang, *ACS Nano*, 2021, **15**, 2005–2037.
192 S. Wang, Q. Hu, Y. Liu, X. Meng, Y. Ye, X. Liu, X. Song and Z. Liang, *J. Hazard. Mater.*, 2020, **387**, 121949.
193 S. Bhunia, N. Dey, A. Pradhan and S. Bhattacharya, *Chem. Commun.*, 2018, **54**, 7495–7498.
194 W. Mandal, S. Fajal, P. Samanta, S. Dutta, M. M. Shirolkar, Y. D. More and S. K. Ghosh, *ACS Appl. Polym. Mater.*, 2022, **4**(11), 8633–8644.
195 B. Zhang, J. Yan, Y. Shang and Z. Wang, *Macromolecules*, 2018, **51**, 1769–1776.
196 S. Qu, N. Song, G. Xu and Q. Jia, *Sens. Actuators, B*, 2019, **290**, 9–14.
197 P. Wang, F. Zhou, C. Zhang, S. Y. Yin, L. Teng, L. Chen, X. X. Hu, H. W. Liu, X. Yin and X. B. Zhang, *Chem. Sci.*, 2018, **9**, 8402–8408.
198 Y. Shi, Q. Fu, J. Li, H. Liu, Z. Zhang, T. Liu and Z. Liu, *ACS Appl. Mater. Interfaces*, 2020, **12**, 55564–55573.
199 S. Fajal, W. Mandal, D. Majumder, M. M. Shirolkar, Y. D. More and S. K. Ghosh, *Chem. – Eur. J.*, 2022, **28**, e202104175.

200 J. Li, S. Wang, X. Cao, H. Huang and D. Cao, *Mater. Chem. Front.*, 2021, **5**, 3428–3435.
201 Y. Fu, W. Yu, W. Zhang, Q. Huang, J. Yan, C. Pan and G. Yu, *Polym. Chem.*, 2018, **9**, 4125–4131.
202 Y. Li, Y. He, F. Guo, S. Zhang, Y. Liu, W. P. Lustig, S. Bi, L. J. Williams, J. Hu and J. Li, *ACS Appl. Mater. Interfaces*, 2019, **11**, 27394–27401.
203 S. Fajal, P. Samanta, S. Dutta and S. K. Ghosh, *Inorg. Chim. Acta*, 2020, **502**, 119359.
204 D. Ma, B. Li, Z. Cui, K. Liu, C. Chen, G. Li, J. Hua, B. Ma, Z. Shi and S. Feng, *ACS Appl. Mater. Interfaces*, 2016, **8**, 24097–24103.
205 T. Ma, X. Zhao, Y. Matsuo, J. Song, R. Zhao, M. Faheem, M. Chen, Y. Zhang, Y. Tian and G. Zhu, *J. Mater. Chem. C*, 2019, **7**, 2327–2332.
206 E. Ö. Zdemir, D. Thirion and C. T. Yavuz, *RSC Adv.*, 2015, **5**, 69010–69015.
207 H. Liu and H. Liu, *J. Mater. Chem. A*, 2017, **5**, 9156–9162.
208 L. Guo, X. Zeng, J. Lan, J. Yun and D. Cao, *ChemistrySelect*, 2017, **2**, 1041–1047.
209 Z. Li, Y. Zhang, H. Xia, Y. Mu and X. Liu, *Chem. Commun.*, 2016, **52**, 6613–6616.
210 P. Jagadesan, G. Eder and P. L. McGrier, *J. Mater. Chem. C*, 2017, **5**, 5676–5679.
211 R. Shen, Y. Liu, W. Yang, Y. Hou, X. Zhao and H. Liu, *Chem. – Eur. J.*, 2017, **23**, 13465–13473.
212 N. Tang, J. Liang, C. Niu, H. Wang, Y. Luo, W. Xing, S. Ye, C. Liang, H. Guo, J. Guo, Y. Zhang and G. Zeng, *J. Mater. Chem. A*, 2020, **8**, 7588–7625.
213 P. Ju, Q. Su, Z. Liu, X. Li, B. Guo, W. Liu, G. Li and Q. Wu, *J. Mater. Sci.*, 2018, **54**, 851–861.
214 H. Wang, X. Ji, M. Ahmed, F. Huang and J. L. Sessler, *J. Mater. Chem. A*, 2019, **7**, 1394–1403.
215 D. Mahato, S. Fajal, P. Samanta, W. Mandal and S. K. Ghosh, *ChemPlusChem*, 2022, **87**, e202100426.
216 J. Fawell, K. Bailey, J. Chilton, E. Dahi, L. Fewtrell and Y. Magara, World Health Organization (WHO), *Fluoride in Drinking Water*, IWA Publishing, London, 2006.
217 D. Xu, L. Chen, X. Dai, B. Li, Y. Wang, W. Liu, J. Li, Y. Tao, Y. Wang, Y. Liu, G. Peng, R. Zhou, Z. Chai and S. Wang, *ACS Appl. Mater. Interfaces*, 2020, **12**, 15288–15297.
218 H. Li, X. Wu, Y. Xu, H. Tong and L. Wang, *Polym. Chem.*, 2014, **5**, 5949–5956.
219 W. Zhao, X. Zhuang, D. Wu, F. Zhang, D. Gehrig, F. Laquai and X. Feng, *J. Mater. Chem. A*, 2013, **1**, 13878–13884.
220 V. M. Suresh, A. Bandyopadhyay, S. Roy, S. K. Pati and T. K. Maji, *Chem. – Eur. J.*, 2015, **21**, 10799–10804.
221 Q. Dang, H. Wan and X. Zhang, *ACS Appl. Mater. Interfaces*, 2017, **9**, 21438–21446.
222 L. Guo, M. Wang, X. Zeng and D. Cao, *Mater. Chem. Front.*, 2017, **1**, 2643–2650.
223 S. Gu, J. Guo, Q. Huang, J. He, Y. Fu, G. Kuang, C. Pan and G. Yu, *Macromolecules*, 2017, **50**, 8512–8520.
224 H. Zuo, Y. Li and Y. Liao, *ACS Appl. Mater. Interfaces*, 2019, **11**, 39201–39208.
225 J. Dong, A. K. Tummanapelli, X. Li, S. Ying, H. Hirao and D. Zhao, *Chem. Mater.*, 2016, **28**, 7889–7897.
226 Y. Tang, H. Huang, B. Peng, Y. Chang, Y. Li and C. Zhong, *J. Mater. Chem. A*, 2020, **8**, 16542–16550.
227 J. Yu and C. Zhang, *J. Mater. Chem. C*, 2020, **8**, 16463–16469.
228 T. Geng, C. Zhang, G. Chen, L. Ma, W. Zhang and H. Xia, *Microporous Mesoporous Mater.*, 2019, **284**, 468–475.
229 T. Geng, L. Ma, G. Chen, C. Zhang, W. Zhang, H. Xia and H. Zhu, *J. Polym. Res.*, 2019, **26**, 113.
230 T. Geng, M. Liu, C. Zhang, C. Hu and H. Xia, *Polym. Adv. Technol.*, 2020, **31**, 1388–1394.
231 J. Liu, K. K. Yee, K. K. Lo, K. Y. Zhang, W. P. To, C. M. Che and Z. Xu, *J. Am. Chem. Soc.*, 2014, **136**, 2818–2824.
232 S. Maiti, B. Mandal, M. Sharma, S. Mukherjee and A. K. Das, *Chem. Commun.*, 2020, **56**, 9348–9351.
233 R. Sun, S. Feng, B. Zhou, Z. Chen, D. Wang and H. Liu, *ACS Macro Lett.*, 2019, **9**, 43–48.
234 W. Yang, X. Jiang and H. Liu, *RSC Adv.*, 2015, **5**, 12800–12806.
235 N. Xu, R. Wang, D. Li, Z. Zhou, T. Zhang, Y. Xie and Z. Su, *New J. Chem.*, 2018, **42**, 13367–13374.
236 J. R. Werber, C. O. Osuji and M. Elimelech, *Nat. Rev. Mater.*, 2016, **1**, 1–15.
237 M. A. Shannon, P. W. Bohn, M. Elimelech, J. G. Georgiadis, B. J. Marinas and A. M. Mayes, *Nature*, 2008, **452**, 301–310.
238 S. Bolisetty, M. Peydayesh and R. Mezzenga, *Chem. Soc. Rev.*, 2019, **48**, 463–487.
239 I. Ali, *Chem. Rev.*, 2012, **112**, 5073–5091.
240 M. M. Mekonnen and A. Y. Hoekstra, *Sci. Adv.*, 2016, **2**, e1500323.
241 Y. Zhang, X. Hong, X.-M. Cao, X.-Q. Huang, B. Hu, S.-Y. Ding and H. Lin, *ACS Appl. Mater. Interfaces*, 2021, **13**, 6359–6366.
242 S. Rojas and P. Horcajada, *Chem. Rev.*, 2020, **120**, 8378–8415.
243 Q. Sun, B. Aguila and S. Ma, *Trends Chem.*, 2019, **1**, 292–303.
244 R. Dawson, A. Laybourn, R. Clowes, Y. Z. Khimyak, D. J. Adams and A. I. Cooper, *Macromolecules*, 2009, **42**, 8809–8816.
245 P. Samanta, P. Chandra, A. V. Desai and S. K. Ghosh, *Mater. Chem. Front.*, 2017, **1**, 1384–1388.
246 S. Let, S. Dutta, P. Samanta, S. Sharma and S. K. Ghosh, *ACS Appl. Mater. Interfaces*, 2021, **13**, 51474–51484.
247 T. Skorjanc, D. Shetty and A. Trabolshi, *Chem*, 2021, **7**, 882–918.
248 Z. Li and Y.-W. Yang, *Adv. Mater.*, 2022, **34**, 2107401.
249 L.-P. Yang, H. Ke, H. Yao and W. Jiang, *Angew. Chem., Int. Ed.*, 2021, **60**, 21404–21411.
250 D. Shetty, I. Jahovic, J. Raya, Z. Asfari, J.-C. Olsen and A. Trabolsi, *ACS Appl. Mater. Interfaces*, 2018, **10**(3), 2976–2981.
251 X. Ji, R.-T. Wu, L. Long, C. Guo, N. M. Khashab, F. Huang and J. L. Sessler, *J. Am. Chem. Soc.*, 2018, **140**, 2777–2780.
252 Z. Wang, I. T. Cousins, U. Berger, K. Hungerbuhler and M. Scheringer, *Environ. Int.*, 2016, 235–247.
253 E. M. Sunderland, X. C. Hu, C. Dassuncao, A. K. Tokranov, C. C. Wagner and J. G. Allen, *J. Exposure Sci. Environ. Epidemiol.*, 2019, **29**, 131–147.
254 S. E. Fenton, A. Ducatman, A. Boobis, J. C. DeWitt, C. Lau, C. Ng, J. S. Smith and S. M. Roberts, *Environ. Toxicol. Chem.*, 2021, **40**, 606–630.

255 Y. Song, J. Phipps, C. Zhu and S. Ma, *Angew. Chem., Int. Ed.*, 2023, e202216724.
256 M. J. Klemes, L. P. Skala, M. Ateia, B. Trang, D. E. Helbling and W. R. Dichtel, *Acc. Chem. Res.*, 2020, **53**, 2314–2324.
257 L. Xiao, Y. Ling, A. Alsbaiee, C. Li, D. E. Helbling and W. R. Dichtel, *J. Am. Chem. Soc.*, 2017, **139**, 7689–7692.
258 A. Alsbaiee, B. J. Smith, L. Xiao, Y. Ling, D. E. Helbling and W. R. Dichtel, *Nature*, 2016, **529**, 190–194.
259 M. J. Klemes, Y. Ling, C. Ching, C. Wu, L. Xiao, D. E. Helbling and W. R. Dichtel, *Angew. Chem., Int. Ed.*, 2019, **58**, 12049–12053.
260 R. Wang, Z.-W. Lin, M. J. Klemes, M. Ateia, B. Trang, J. Wang, C. Ching, D. E. Helbling and W. R. Dichtel, *ACS Cent. Sci.*, 2022, **8**, 663–669.
261 A. Yang, C. Ching, M. Easler, D. E. Helbling and W. R. Dichtel, ACS, *Mater. Lett.*, 2020, **2**, 1240–1245.
262 X. Liu, C. Zhu, J. Yin, J. Li, Z. Zhang, J. Li, F. Shui, Z. You, Z. Shi, B. Li, X.-H. Bu, A. Nafady and S. Ma, *Nat. Commun.*, 2022, **13**, 2132.
263 A. Li, H.-X. Sun, D.-Z. Tan, W.-J. Fan, S.-H. Wen, X.-J. Qing, G.-X. Li, S.-Y. Li and W.-Q. Deng, *Energy Environ. Sci.*, 2011, **4**, 2062–2065.
264 X. S. Wang, J. Liu, J. M. Bonefont, D. Q. Yuan, P. K. Thallapally and S. Q. Ma, *Chem. Commun.*, 2013, **49**, 1533–1535.
265 B. Li, Y. Zhang, D. Ma, Z. Xing, T. Ma, Z. Shi, X. Ji and S. Ma, *Chem. Sci.*, 2016, **7**, 2138–2144.
266 S. Dutta, S. Let, S. Sharma, D. Mahato and S. K. Ghosh, *Chem. Rec.*, 2021, **21**, 1666–1680.
267 Q. Sun, B. Aguila, Y. Song and S. Ma, *Acc. Chem. Res.*, 2020, **53**(4), 812–821.
268 S. Lee, G. Barin, C. M. Ackerman, A. Muchenditsi, J. Xu, J. A. Reimer, S. Lutsenko, J. R. Long and C. J. Chang, *J. Am. Chem. Soc.*, 2016, **138**, 7603–7609.
269 B. Li, Y. Zhang, D. Ma, Z. Shi and S. Ma, *Nat. Commun.*, 2014, **5**, 5537.
270 B. Aguila, Q. Sun, J. A. Perman, L. D. Earl, C. W. Abney, R. Elzein, R. Schlaf and S. Ma, *Adv. Mater.*, 2017, **29**, 1700665.
271 M. X. Tan, Y. N. Sum, J. Y. Ying and Y. Zhang, *Energy Environ. Sci.*, 2013, **6**, 3254–3259.
272 B. Aguila, Q. Sun, H. C. Cassady, C. Shan, Z. Liang, A. M. Al-Enizic, A. Nafadyc, J. T. Wright, R. W. Meulenberg and S. Ma, *Angew. Chem., Int. Ed.*, 2020, **59**, 19618–19622.
273 K. S. Song, T. Ashirov, S. N. Talapaneni, A. H. Clark, A. V. Yakimov, M. Nachtegaal, C. Coperet and A. Coskun, *Chem*, 2022, **8**, 2043–2059.
274 P. Wu, H. Liu, M. Sun, Y. Zeng, J. Ye, S. Qin, Y. Cai, W. Feng and L. Yuan, *J. Mater. Chem. A*, 2021, **9**, 27320–27331.
275 M. Garai, M. Mahato, Y. Hong, V. Rozyyev, U. Jeong, Z. Ullah and C. T. Yavuz, *Adv. Sci.*, 2021, **8**, 2001676.
276 J. R. Dodson, H. L. Parker, A. Muñoz García, A. Hicken, K. Asemave, T. J. Farmer, H. He, J. H. Clark and A. J. Hunt, *Green Chem.*, 2015, **17**, 1951–1965.
277 S. J. Berners-Price and A. Filipovska, *Metallomics*, 2011, **3**, 863–873.
278 Y. Hong, D. Thirion, S. Subramanian, M. Yoo, H. Choi, H. Y. Kim, J. F. Stoddart and C. T. Yavuz, *PNAS*, 2020, **117**, 16174–16180.
279 Y. Hong, V. Rozyyev and C. T. Yavuz, *Small Sci.*, 2021, **1**, 2000078.
280 T. S. Nguyen, Y. Hong, N. A. Dogan and C. T. Yavuz, *Chem. Mater.*, 2020, **32**, 5343–5349.
281 N. A. Dogan, Y. Hong, E. Ozdemir and C. T. Yavuz, *ACS Sustainable Chem. Eng.*, 2019, **7**, 123–128.
282 Z. Wang, Q. Meng, R. Ma, Z. Wang, Y. Yang, H. Sha, X. Ma, X. Ruan, X. Zou, Y. Yuan and G. Zhu, *Chem*, 2020, **6**, 1683–1691.
283 M. Ahmad, J. Chen, K. Yang, T. Shah, M. Naik, Q. Zhang and B. Zhang, *Chem. Eng. J.*, 2021, **418**, 129370.
284 R.-H. Yan, W.-R. Cui, C.-R. Zhang, X.-J. Li, J. Huang, W. Jiang, R.-P. Liang and J.-D. Qiu, *Chem. Eng. J.*, 2021, **420**, 129658.
285 Y. Li, L. Wang, B. Li, M. Zhang, R. Wen, X. Guo, X. Li, J. Zhang, S. Li and L. Ma, *ACS Appl. Mater. Interfaces*, 2016, **8**, 28853–28861.
286 C. W. Abney, R. T. Mayes, T. Saito and S. Dai, *Chem. Rev.*, 2017, **117**, 13935–14013.
287 Q. Sun, Y. Song, B. Aguila, A. S. Lvanov, V. S. Bryantsev and S. Ma, *Adv. Sci.*, 2021, **8**, 2001573.
288 L. Zhang, N. Pu, B. Yu, G. Ye, J. Chen, S. Xu and S. Ma, *ACS Appl. Mater. Interfaces*, 2020, **12**, 3688–3696.
289 B. Li, Q. Sun, Y. Zhang, C. W. Abney, B. Aguila, W. Lin and S. Ma, *ACS Appl. Mater. Interfaces*, 2017, **9**, 12511–12517.
290 B. Aguila, Q. Sun, H. Cassady, C. W. Abney, B. Li and S. Ma, *ACS Appl. Mater. Interfaces*, 2019, **11**, 30919–30926.
291 Z. Li, Q. Meng, Y. Yang, X. Zou, Y. Yuan and G. Zhu, *Chem. Sci.*, 2020, **11**, 4747–4752.
292 Y. Song, C. Zhu, Q. Sun, B. Aguila, C. W. Abney, L. Wojtas and S. Ma, *ACS Cent. Sci.*, 2021, **7**, 1650–1656.
293 Q. Sun, B. Aguila, J. Perman, A. S. Lvanov, V. S. Bryantsev, L. D. Earl, C. W. Abney, L. Wojtas and S. Ma, *Nat. Commun.*, 2018, **9**, 1644.
294 F. Ren, Z. Q. Zhu, X. Qian, W. D. Liang, P. Mu, H. X. Sun, J. H. Liu and A. Li, *Chem. Commun.*, 2016, **52**, 9797–9800.
295 T. M. Geng, Z. M. Zhu, W. Y. Zhang and Y. Wang, *J. Mater. Chem. A*, 2017, **5**, 7612–7617.
296 Q. Zhang, T. Zhai, Z. Wang, G. Cheng, H. Ma, Q. Zhang, Y. Zhao, B. Tan and C. Zhang, *Adv. Mater. Interfaces*, 2019, **6**, 1900249.
297 C. Feng, G. Xu, W. Xie, S. Zhang, C. Yao and Y. Xu, *Polym. Chem.*, 2020, **11**, 2786–2790.
298 Z. Yan, Y. Yuan, Y. Tian, D. Zhang and G. Zhu, *Angew. Chem., Int. Ed.*, 2015, **54**, 12733–12737.
299 A. Sen, S. Sharma, S. Dutta, M. M. Shirolkar, G. K. Dam, S. Let and S. K. Ghosh, *ACS Appl. Mater. Interfaces*, 2021, **13**, 34188–34196.
300 P. Samanta, S. Dutta, S. Let, A. Sen, M. M. Shirolkar and S. K. Ghosh, *ChemPlusChem*, 2022, **87**, e202200212.
301 S. Fajal, W. Mandal, S. Mollick, Y. D. More, A. Torris, S. Saurabh, M. M. Shirolkar and S. K. Ghosh, *Angew. Chem., Int. Ed.*, 2022, e202203385.

302 S. Dutta, P. Samanta, B. Joarder, S. Let, D. Mahato, R. Babarao and S. K. Ghosh, *ACS Appl. Mater. Interfaces*, 2020, **12**(37), 41810–41818.
303 S. Mollick, S. Fajal, S. Saurabh, D. Mahato and S. K. Ghosh, *ACS Cent. Sci.*, 2020, **6**(9), 1534–1541.
304 S. Sharma, A. V. Desai, B. Joarder and S. K. Ghosh, *Angew. Chem., Int. Ed.*, 2020, **59**, 7788–7792.
305 Z.-J. Li, J.-Y. Liu, Y. Yu, K.-J. Chang, H. Wang, Y.-J. Li and K. Gai, *ACS Appl. Mater. Interfaces*, 2022, **14**, 23868–23876.
306 S. Jiao, L. Deng, X. Zhang, Y. Zhang, K. Liu, S. Li, L. Wang and D. Ma, *ACS Appl. Mater. Interfaces*, 2021, **13**, 39404–39413.
307 A. Hassan, C. Saritha, V. K. Rajana, D. Mandal and N. Das, *ACS Macro Lett.*, 2023, **12**(3), 376–381.
308 Y. Wang, H. Zhao, X. Li and R. Wang, *J. Mater. Chem. A*, 2016, **4**, 12554–12560.
309 A. N. Zagorodnyaya, Z. S. Abisheva, L. Y. Agapova and A. S. Sharipova, *Theor. Found. Chem. Eng.*, 2019, **53**, 841.
310 J. Li, L. Chen, N. Shen, R. Xie, M. V. Sheridan, X. Chen, D. Sheng, D. Zhang, Z. Chai and S. Wang, *Sci. China Chem.*, 2021, **64**, 1251–1260.
311 X. Li, Y. Li, H. Wang, Z. Niu, Y. He, L. Jin, M. Wu, H. Wang, L. Chai, A. M. Al-Enizi, A. Nafady, S. F. Shaikh and S. Ma, *Small*, 2021, **17**, e2007994.
312 J. Li, X. Dai, L. Zhu, C. Xu, D. Zhang, M. A. Silver, P. Li, L. Chen, Y. Li, D. Zuo, H. Zhang, C. Xiao, J. Chen, J. Diwu, O. K. Farha, T. E. Albrecht-Schmitt, Z. Chai and S. Wang, *Nat. Comm.*, 2018, **9**, 3007.
313 Q. Sun, L. Zhu, B. Aguila, P. K. Thallapally, C. Xu, J. Chen, S. Wang, D. Rogers and S. Ma, *Nat. Commun.*, 2019, **10**, 1646.
314 J. Li, B. Li, N. Shen, L. Chen, Q. Guo, L. Chen, L. He, X. Dai, Z. Chai and S. Wang, *ACS Cent. Sci.*, 2021, **7**(8), 1441–1450.
315 G. Das, T. Prakasam, S. Nuryyeva, D. S. Han, A. Abdel-Wahab, J. C. Olsen, K. Polychronopoulou, C. PlatasIglesias, F. Ravaux, M. Jouiad and A. Trabolsi, *J. Mater. Chem. A*, 2016, **4**, 15361–15369.
316 N. MacDowell, N. Florin, A. Buchard, J. Hallett, A. Galindo, G. Jackson, C. S. Adjiman, C. K. Williams, N. Shah and P. Fennell, *Energy Environ. Sci.*, 2010, **3**, 1645–1669.
317 M. Ding, R. W. Flaig, H.-L. Jiang and O. M. Yaghi, *Chem. Soc. Rev.*, 2019, **48**, 2783–2828.
318 M. Mikkelsen, M. Jørgensen and F. C. Krebs, *Energy Environ. Sci.*, 2010, **3**, 43–81.
319 W. Lu, D. Yuan, D. Zhao, C. I. Schilling, O. Plietzsch, T. Muller, S. Bräse, J. Guenther, J. Blümel, R. Krishna, Z. LiII and H.-C. Zhou, *Chem. Mater.*, 2010, **22**(21), 5964–5972.
320 W. Wang, M. Zhou and D. Yuan, *J. Mater. Chem. A*, 2017, **5**, 1334–1347.
321 A. K. Sekizkardes, P. Wang, J. Hoffman, S. Budhathoki and D. Hopkinson, *Mater. Adv.*, 2022, **3**, 6668–6686.
322 P. Bhanja, A. Modak and A. Bhaumik, *ChemCatChem*, 2019, **11**, 244–257.
323 W. Lu, D. Yuan, J. Sculley, D. Zhao, R. Krishna and H.-C. Zhou, *J. Am. Chem. Soc.*, 2011, **133**, 18126–18129.
324 W. Lu, W. M. Verdegaal, J. Yu, P. B. Balbuena, H.-K. Jeong and H.-C. Zhou, *Energy Environ. Sci.*, 2013, **6**, 3559–3564.
325 S. Zulfiqar, F. Karadas, J. Park, E. Deniz, G. D. Stucky, Y. Jung, M. Atilhan and C. T. Yavuz, *Energy Environ. Sci.*, 2011, **4**, 4528–4531.
326 X. Zhu, C. Tian, G. M. Veith, C. W. Abney, J. Dehaudt and S. Dai, *J. Am. Chem. Soc.*, 2016, **138**, 11497–11500.
327 L. Tao, F. Niu, C. Wang, J. Liu, T. Wang and Q. Wang, *J. Mater. Chem. A*, 2016, **4**, 11812–11820.
328 S. Dey, A. Bhunia, D. Esquivel and C. Janiak, *J. Mater. Chem. A*, 2016, **4**, 6259–6263.
329 S. Zulfiqar, D. Mantione, O. E. Tall, M. Ilyas Sarwar, F. Ruipérez, A. Rothenberger and D. Mecerreyes, *J. Mater. Chem. A*, 2016, **4**, 8190–8197.
330 G. Chang, Z. Shang, T. Yu and L. Yang, *J. Mater. Chem. A*, 2016, **4**, 2517–2523.
331 Y. J. Lee, S. N. Talapaneni and A. Coskun, *ACS Appl. Mater. Interfaces*, 2017, **9**, 30679–30685.
332 A. Abid, S. Razzaque, I. Hussain and B. Tan, *Macromolecules*, 2021, **54**, 5848–5855.
333 B. Zhang, J. Yan, G. Li and Z. Wang, *Polym. Chem.*, 2019, **10**, 3371–3379.
334 S. Mukherjee, M. Das, A. Manna, R. Krishna and S. Das, *J. Mater. Chem. A*, 2019, **7**, 1055–1068.
335 S. Ma and H.-C. Zhou, *Chem. Commun.*, 2010, **46**, 44–53.
336 B. Li, H.-M. Wen, W. Zhou, J. Q. Xu and B. Chen, *Chem*, 2016, **1**, 557–580.
337 V. Rozyyev, D. Thirion, R. Ullah, J. Lee, M. Jung, H. Oh, M. Atilhan and C. T. Yavuz, *Nat. Energy*, 2019, **4**, 604–611.
338 F. Schuth, R. Palkovits, R. Schlogl and D. S. Su, *Energy Environ. Sci.*, 2012, **5**, 6278–6289.
339 J. W. Erisman, M. A. Sutton, J. Galloway, Z. Klimont and W. Winiwarter, *Nat. Geosci.*, 2008, **1**, 636–639.
340 J. F. Van Humbeck, T. M. McDonald, X. Jing, B. M. Wiers, G. Zhu and J. R. Long, *J. Am. Chem. Soc.*, 2014, **136**, 2432–2440.
341 J. W. Lee, G. Barin, G. W. Peterson, J. Xu, K. A. Colwell and J. R. Long, *ACS Appl. Mater. Interfaces*, 2017, **9**, 33504–33510.
342 D. W. Kang, M. Kang, M. Moon, H. Kim, S. Eom, J. H. Choe, W. R. Lee and C. S. Hong, *Chem. Sci.*, 2018, **9**, 6871–6877.
343 J. Kazmierczak-Razna, B. Gralak-Podemska, P. Nowicki and R. Pietrzak, *Chem. Eng. J.*, 2015, **269**, 352–358.
344 A. G. De Crisci, A. Moniri and Y. Xu, *Int. J. Hydrogen Energy*, 2019, **44**, 1299–1327.
345 M. M. Abdelnaby, K. E. Cordova, I. Abdulazeez, A. M. Alloush, B. A. Al-Maythalony, Y. Mankour, K. Alhooshani, T. A. Saleh and O. C. S. A. Hamouz, *ACS Appl. Mater. Interfaces*, 2020, **12**, 47984–47992.
346 G. Dong, H. Li and V. Chen, *J. Mater. Chem. A*, 2013, **1**, 4610.
347 Y. Song, C. Zhu and S. Ma, *Energy Chem.*, 2022, **4**, 100079.
348 S. Yi, X. Ma, I. Pinnau and W. J. Koros, *J. Mater. Chem. A*, 2015, **3**, 22794–22806.
349 S. Yi, B. Ghanem, Y. Liu, I. Pinnau and W. J. Koros, *Sci. Adv.*, 2019, **5**, eaaw5459.
350 H. W. H. Lai, F. M. Benedetti, J. M. Ahn, A. M. Robinson, Y. Wang, I. Pinnau, Z. P. Smith and Y. Xia, *Science*, 2022, **375**, 1390–1392.

351 J. Chakraborty, I. Nath and F. Verpoort, *Chem. Soc. Rev.*, 2022, **51**, 1124–1138.
352 T. Zhang, V. G. Gregoriou, N. Gasparini and C. L. Chochos, *Chem. Soc. Rev.*, 2022, **51**, 4465–4483.
353 Z. Zhang, J. Jia, Y. Zhi, S. Ma and X. Liu, *Chem. Soc. Rev.*, 2022, **51**, 2444–2490.
354 Y. Zhang and S. N. Riduan, *Chem. Soc. Rev.*, 2012, **41**, 2083–2094.
355 P. Zhang, S. Wang, S. Ma, F.-S. Xiao and Q. Sun, *Chem. Commun.*, 2020, **56**, 10631–10641.
356 R. K. Totten, Y. S. Kim, M. H. Weston, O. K. Farha, J. T. Hupp and S. T. Nguyen, *J. Am. Chem. Soc.*, 2013, **135**, 11720.
357 K. Wu, J. Guo and C. Wang, *Angew. Chem., Int. Ed.*, 2016, **55**, 6013–6017.
358 G. Yuan, Y. Lei, X. Meng, B. Ge, Y. Ye, X. Song and Z. Liang, *Inorg. Chem. Front.*, 2022, **9**, 1208–1216.
359 Y. Li, M. Liu and L. Chen, *J. Mater. Chem. A*, 2017, **5**, 13757–13762.
360 L. Ma, Y. Liu, Y. Liu, S. Jiang, P. Li, Y. Hao, P. Shao, A. Yin, X. Feng and B. Wang, *Angew. Chem., Int. Ed.*, 2019, **58**, 4221–4226.
361 N. Kang, J. H. Park, K. C. Ko, J. Chun, E. Kim, H. W. Shin, S. M. Lee, H. J. Kim, T. K. Ahn, J. Y. Lee and S. U. Son, *Angew. Chem., Int. Ed.*, 2013, **52**, 6228.
362 R. S. Sprick, J. X. Jiang, B. Bonillo, S. Ren, T. Ratvijitvech, P. Guiglion, M. A. Zwijnenburg, D. J. Adams and A. I. Cooper, *J. Am. Chem. Soc.*, 2015, **137**, 3265.
363 L. Li, Z. Cai, Q. Wu, W. Y. Lo, N. Zhang, L. X. Chen and L. Yu, *J. Am. Chem. Soc.*, 2016, **138**, 7681.
364 C. Yang, B. C. Ma, L. Zhang, S. Lin, S. Ghasimi, K. Landfester, K. A. I. Zhang and X. Wang, *Angew. Chem., Int. Ed.*, 2016, **55**, 9202.
365 B. Wang, Z. Xie, Y. Li, Z. Yang and L. Chen, *Macromolecules*, 2018, **51**, 3443–3449.
366 B. C. Ma, S. Ghasimi, K. Landfester, F. Vilela and K. A. I. Zhang, *J. Mater. Chem. A*, 2015, **3**, 16064–16071.
367 I. Nath, J. Chakraborty, P. M. Heynderickx and F. Verpoort, *Appl. Catal., B*, 2018, **227**, 102–113.
368 B. Li, Z. Guan, W. Wang, X. Yang, J. Hu, B. Tan and T. Li, *Adv. Mater.*, 2012, **24**, 3390.
369 Q. Sun, Z. Dai, X. Liu, N. Sheng, F. Deng, X. Meng and F. S. Xiao, *J. Am. Chem. Soc.*, 2015, **137**, 5204.
370 L. Li, H. Zhao, J. Wang and R. Wang, *ACS Nano*, 2014, **8**, 5352–5364.
371 Y. Liang, W. Mai, J. Huang, Z. Huang, R. Fu, M. Zhang, D. Wu and K. Matyjaszewski, *Chem. Commun.*, 2016, **52**, 2489.
372 O. Buyukcakir, Y. Seo and A. Coskun, *Chem. Mater.*, 2015, **27**, 4149–4155.
373 S. N. Talapaneni, D. Kim, G. Barin, O. Buyukcakir, S. H. Je and A. Coskun, *Chem. Mater.*, 2016, **28**, 4460–4466.
374 D. Shetty, I. Jahovic, J. Raya, F. Ravaux, M. Jouiad, J. Olsen and A. Trabolsi, *J. Mater. Chem. A*, 2017, **5**, 62–66.
375 A. Giri, W. M. Hussain, B. Sk and A. Patra, *Chem. Mater.*, 2019, **31**, 8440–8450.

